AD-A172 140 ALLOY DEVELOPMENT PROCESSING AND CHARACTERIZATION OF DEVITRIFIED TITANIUM..(U) NORTHEASTERN UNIV BOSTON MA BARNETT INST OF CHEMICAL ANALYSIS.. S H WHANG JAN 86 1\2

UNCLASSIFIED N00014-82-K-0597 F/G 11/6 NL

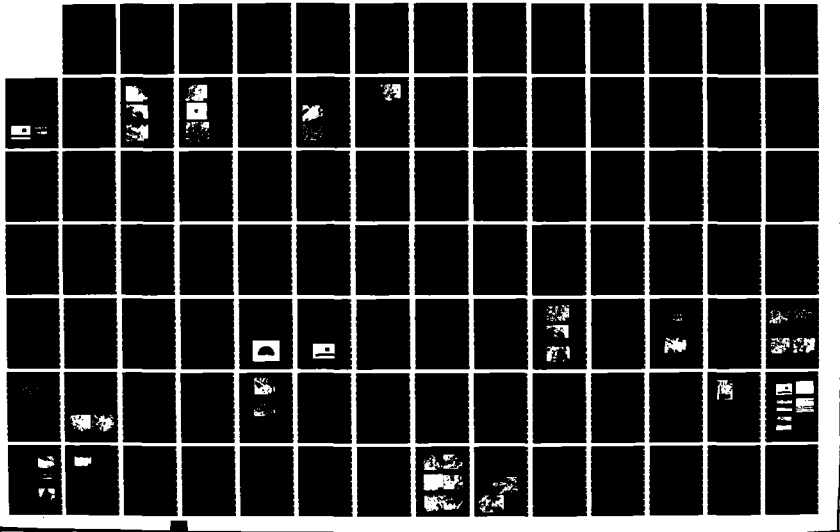

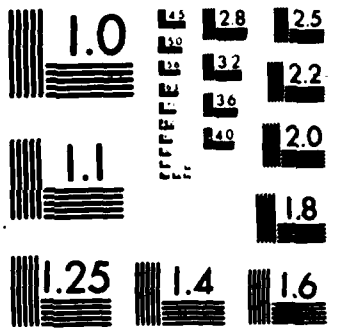
1.0
1.1
1.25
1.4
1.6
1.8
2.0
2.2
2.5
2.8
3.2
3.6
4.0

ALLOY DEVELOPMENT, PROCESSING AND CHARACTERIZATION OF DEVITRIFIED TITANIUM BASE MICROCRYSTALLINE ALLOYS

ANNUAL REPORT

CONTRACT - N00014-82-K-0597

(1984 - 1985)

FOR

OFFICE OF NAVAL RESEARCH

ARLINGTON, VA 22217

JANUARY 18, 1986

BY

S. H. WHANG

DEPARTMENT OF METALLURGY AND MATERIALS SCIENCE

POLYTECHNIC UNIVERSITY, 333 JAY STREET, BROOKLYN, NY 11201

(THIS WORK HAS BEEN PERFORMED AT BARNETT INSTITUTE

NORTHEASTERN UNIVERSITY, BOSTON, MA 02115)

ALLOY DEVELOPMENT, PROCESSING AND CHARACTERIZATION OF DEVITRIFIED TITANIUM BASE MICROCRYSTALLINE ALLOYS

ANNUAL REPORT

CONTRACT - N00014-82-K-0597

(1984 - 1985)

FOR

OFFICE OF NAVAL RESEARCH

ARLINGTON, VA 22217

JANUARY 18, 1986

BY

S. H. WHANG

DEPARTMENT OF METALLURGY AND MATERIALS SCIENCE

POLYTECHNIC UNIVERSITY, 333 JAY STREET, BROOKLYN, NY 11201

(THIS WORK HAS BEEN PERFORMED AT BARNETT INSTITUTE

NORTHEASTERN UNIVERSITY, BOSTON, MA 02115)

SECURITY CLASSIFICATION OF THIS PAGE (When Data Entered)

REPORT DOCUMENTATION PAGE		READ INSTRUCTIONS BEFORE COMPLETING FORM
1. REPORT NUMBER	2. GOVT ACCESSION NO. ADA172140	3. RECIPIENT'S CATALOG NUMBER
4. TITLE (and Subtitle) ALLOY DEVELOPMENT, PROCESSING AND CHARACTERIZATION OF DEVITRIFIED TITANIUM BASE MICROCRYSTALLINE ALLOYS		5. TYPE OF REPORT & PERIOD COVERED Annual Report Sept. 1984-Aug. 1985 6. PERFORMING ORG. REPORT NUMBER
7. AUTHOR(s) Sung H. Whang		8. CONTRACT OR GRANT NUMBER(s) N00014-82-K-0597
9. PERFORMING ORGANIZATION NAME AND ADDRESS Polytechnic University 333 Jay Street Brooklyn, New York 11201		10. PROGRAM ELEMENT, PROJECT, TASK AREA & WORK UNIT NUMBERS 650-003
11. CONTROLLING OFFICE NAME AND ADDRESS Office of Naval Research 800 N. Quincy Street Arlington, VA 22217		12. REPORT DATE January 1986 13. NUMBER OF PAGES 110
14. MONITORING AGENCY NAME & ADDRESS(if different from Controlling Office)		15. SECURITY CLASS. (of this report) Unclassified 15a. DECLASSIFICATION/DOWNGRADING SCHEDULE

16. DISTRIBUTION STATEMENT (of this Report)

This document has been approved for public release and its distribution is unlimited. Reproduction in whole or in part is permitted by the U.S. Government.

17. DISTRIBUTION STATEMENT (of the abstract entered in Block 20, if different from Report)

18. SUPPLEMENTARY NOTES

19. KEY WORDS (Continue on reverse side if necessary and identify by block number)

Rapidly solidified Ti alloy, arc melt spinning, rare earth dispersoid, Ostwald ripening of rare earth dispersoids, age hardening in rapidly solidified Ti alloy, alpha Ti alloys, high temperature Ti alloys.

20. ABSTRACT (Continue on reverse side if necessary and identify by block number)

Effect of rapid solidification on solid solubility, microstructural refinement and phase transformation in binary and ternary Ti alloys was studied.
The stability of the refined microstructures produced by rapid quenching were investigated under the isothermal and isochronal conditions. In particular, Ostwald ripening of rare earth (Y, La,Er) and Th dispersoids in Ti-Sn-X (Y,La,Er,Th) systems at

DD FORM 1 JAN 73 1473 EDITION OF 1 NOV 65 IS OBSOLETE

Unclassified

SECURITY CLASSIFICATION OF THIS PAGE (When Data Entered)

elevated temperatures (700-900°C, phase) was investigated by TEM and image analyzer.
The grain growth rate at the presence of the rare earth and Th dispersoids was investigated and determined as a function of time. The deterioration of microhardness in the ternary alloys containing rare earth dispersion upon high temperature annealing was studied in relation to microstructural coarsening.

ABSTRACT

titanium

Effect of rapid solidification on solid solubility, microstructural refinement and phase transformation in binary and ternary Ti alloys was studied.

The stability of the refined microstructures produced by rapid quenching were investigated under the isothermal and isochronal conditions. In particular, Ostwald ripening of rare earth (Y, La, Er) and Thorium dispersoids in Ti-Sn-X (Y, La, Er, Th) systems at elevated temperatures (700-900°C, α phase) was investigated by transmission electron microscopy and image analyzer.

The grain growth rate at the presence of the rare earth and Th dispersoids was investigated and determined as a function of time.

The deterioration of microhardness in the ternary alloys containing rare earth dispersions upon high temperature annealing was studied in relation to microstructural coarsening.

Keywords: [illegible]; Binary [illegible] Titanium [illegible]; Microstructure, [illegible] A)

TABLE OF CONTENTS

SUMMARY OF PRINCIPAL RESULTS

During 1984/85 fisical year, general microstructure, microstructural coarsening and its influence on mechanical properties were focused.

A) EXTENDED SOLUBILITY AND OCCURRENCE OF METASTABLE PHASES

Although it is well known that rapid quenching of the molten alloy drastically increase solid solubility of solute in Al based alloys, such extensive solubility increase in Ti is less dramatic and varies significantly depending upon the equilibrium phase diagram features of binary Ti systems.

These phase diagram features may be conveniently divided into four categories depending upon β-α transformation mode : 1. β-isomorphous 2. eutectoid type 3. peritectoid type 4. monotectic-peritectic type. Moderate increase in solid solubility of solute by rapid quenching was observed in the first two types whereas no increase in the solubility for the monotectic-peritectic type.

Another effect of rapid solidification is that high temperature phase, β can be stabilized against the low temperature phases: α as well as compound phases. Also, the decomposition at invarient points can be suppresed by rapid quenching. As a result, the terminal solid solubility of α phase increase at the expense of α + compound phase. The occurrence of metastable phases by rapid quenching is strongly dictated by kinetical conditions during rapid solidification. In binary Ti alloy systems, entropy stabilized phases such as glassy phase and β phase can be stabilized down to room temperature by rapid quenching against close packed structures such as FCC and HCP.

The terminal solid solubility of α phase can be correlated with relative atomic size and electronegativity of solute. In other word, the solid solubility of α can be predicted in an expanded version of Darken and Gurry type map.

Besides, martensite initiation and ω phase formation in the binary systems can be suppressed by rapid cooling, indicating that the martensite and the ω phase is no longer purely athermal.

B) OSTWALD RIPENING

The slow growth of these rare earth dispersoids has been characterized quantitatively in the last two years. The results show that 1. particle coarsening occurs by the volume diffusion of rare earth metals in Ti; 2. the coarsening rate is very low, which is attributed to the low solubility of rare earth metals in Ti and more importantly to the low diffusion coefficient of these metals in Ti.

Also, preliminary results show that Th dispersoids in Ti matrix coarsen

at the slowest rate at 900°C among the investigated dispersoids. This low coarsening of Th dispersoids appears to stem from the low diffusion coefficient of Th in Ti.

The hierarchy of the estimated coefficient of R.E. is accidently related to the atomic size of rare earth metals, i.e., Y : 1.78 A, (12 n.n.) $D=4.4\times10^{-13}cm^2/sec$; La: 1.87 A , $D=7.5\times10^{-14}cm^2/sec$. Nevertheless, it is premature to make any conclusion regarding the atomic size effect without knowing diffusion coefficients of many rare earth metals in Ti.

The quantitative measurements on the dispersoid coarsening conducted in the last one year are compared with those of previously determined values, as shown in table 1.

TABLE 1

alloy system	Temp. °C	f(k,T) (m^3/s)	Vol. Frc. %	k*	C_s	V_m (m^3/g-mol)	D (cm^2/s)
Ti-5Sn-3Y	760	0.9×10^{-28}	1.05	1.12	0.0042	1.67×10^{-5}	1.0×10^{-13}
	800	3.7×10^{-28}					4.4×10^{-13}
	840	1.52×10^{-27}					2.0×10^{-12}
Ti-5Sn-4.5La (La_2Sn)	760	1.23×10^{-29}	1.4	1.16	0.0046	2.33×10^{-5}	9.4×10^{-15}
	800	9.39×10^{-29}					7.5×10^{-14}
Ti-5Sn-5.4Er	800	1.8×10^{-28}	1.8				
Ti-5Al-7.5Th	900	6.4×10^{-27}					

$$\text{Where } f(K,T) = \frac{\bar{r}^3 - \bar{r}_o^3}{t - t_o}$$

C) GRAIN GROWTH

In rapidly solidified Ti alloys, the grain growth is another important parameter determining alloy stability at high temperatures.

The study shows that the growth of the grains containing rare earth dispersoids (Er, La) and Th dispersoids deviates significantly from the parabolic law ($D = Kt^n$, $n=0.5$), indicating a strong interaction between the grain boundary and the particles.

The results are summarized in table 2.

TABLE 2.

Alloy System wt. %	Annealing Temperature ^{o}C	Time Exponent n
Ti-5Al-7.5Th	900	0.15
Ti - 5Al - 4.5La	900	0.25
Ti - 0.03 Er (at. %)	900	0.38 *
Ti - 0.3 Er (at. %)	900	0.13 *

* extrapolated from the data in ref. 1

D) MECHANICAL PROPERTIES (microhardness)

Effects of microstructural coarsening on mechanical responses are primary subjects in these investigations. Microstructural coarsening: grain growth and dispersion coarsening in Ti-5Al-2.9Y, Ti-5Al-4.5La, Ti-5Al-5.4Er and Ti-5Al-7.5Th were studied and their effects on hardness were evaluated.

The results show that a combination of grain growth and dispersion coarsening during isothermal annealing is the prime cause of the softening of these ternary alloys tested at room temperature. However, the Ti matrix softening at elevated temperatures is a result of dislocation climb and high diffusion coefficient of Ti at these temperatures. Hence, at these temperatures, the role of dispersoids as dislocation blocker in these ternary alloys appears minimal.

REFERENCE

1. B.B. Rath, B.A. MacDonald, S.M.L. Sastry, R.J. Lederich, J.E. O'Neal, C.R. Whitsett, Proc. Fourth Int. Conf. on Ti , " Titanium '80 - Science and Technology." edited by Kimura and Isumi, Kyoto, Japan, May 19-22, 1980, pp. 1185-1196.

MICROSTRUCTURES AND MECHANICAL PROPERTIES OF RAPIDLY SOLIDIFIED Ti-5Al-4.5La AND Ti-5Al-5.4Er ALLOYS.

C. S. Chi and S. H. WHANG

Proc. Sym. Rapidly Solidified Materials, S.M.L. Sastry and B. MacDonald eds., pp. 231-245, The Metallurgical Society of AIME., 1986.

MICROSTRUCTURES AND MECHANICAL PROPERTY OF RAPIDLY-SOLIDIFIED Ti-5Al-4.5La AND Ti-5Al-5.4Er Alloys*

C. S. Chi and S. H. Whang

Barnett Institute
Northeastern University
Boston, Massachusetts 02115

Rapidly-solidified alloy ribbons (Ti-5Al-4.5La and Ti-5Al-5.4Er), processed by the arc melt-spinning technique, were consolidated by HIPing. The microstructures and hardness of the precursor as well as the HIPed alloys were studied by TEM, electron microprobe, and hardness testers.

* Research supported by the Office of Naval Research.

Introduction

Although research on rapidly-solidified Ti alloy was initiated a decade ago, the initial approach for strengthening materials was primarily based on microstructural refinement of Si-and B-containing Ti-alloys (1,2). As a result, the improvement in strength and creep resistance at elevated temperatures was not anticipated, though a substantial increase in room temperature strength as well as intermediate temperature strength resulting from such microstructural refinements has been demonstrated. Recently, the addition of rare-earth elements to conventional-casting Ti alloy reportedly improved mechanical properties (3-6). Nevertheless, a large quantity of rare-earth addition results in coarse particles (several micron diameter), as well as serious segregation through conventional ingot metallurgy (6). Recent rapid-solidification technologies allow compound-forming additives — metalloids or rare-earth metals — to dissolve in the Ti matrix without segregation.

Such flexibility in alloy processing stimulates development of high-temperature Ti alloys containing various rare-earth metals (7-9). Preliminary studies of rare-earth dispersion in Ti alloys show significant improvement in mechanical properties at both room and elevated temperatures (10-13), and, among the alloys investigated, the La- (13) and the Er-containing alloys (14) in particular exhibit exceptionally high mechanical strength at both temperatures. Since the investigation of mechanical properties in these two alloy systems (Ti-Al-La and Ti-Al-Er) has been carried out independently by different research groups, the differentiation between the properties of the two alloy systems is not known. Such differentiation is discussed in this paper.

Experiments

Rapidly-solidified Ti alloy ribbons of nominal compositions (Ti-5Al-5.4 Er and Ti-5Al-4.5La) were produced by the following manner: Alloy buttons weighing 20g each were prepared in a pilot scale arc-melt furnace from pure metals: Ti (99.9 at %) and Al (99.99 at %), and rare-earth metals: La and Er (99.9 at %). Subsequently, each button was remelted in the cold copper crucible of the pilot melt spinner (Fig. 1) and cast into thin ribbon ~40μm thick and ~1.5mm wide by injecting the molten alloy onto a rotating copper disk through the orifice at the bottom of the copper crucible under inert gas atmosphere (Ar) (Fig. 2a). This ribbon was initially chopped into segments ~1.5 mm long by a rotary chopper and re-fed into the chopper until they were less than 1mm long. The flakes were cold compacted and HIPed in a small mild steel can at 850°/2.1GPa/3h. The fully-densified HIPed alloy was subjected to hardness testing and microstructural study. Hot hardness was measured on HIPed alloys using a 1000g load at the temperature range of 500-900°C. The measurements at each temperature take 15 minutes. Also, other HIPed specimens were isothermally annealed at 900°C for various duration and subjected to room temperature hardness measurements.

Prior to heat treatment, foil or consolidated alloy was wrapped in a Ta foil and sealed in quartz tubing under high vacuum (10^{-3} torr). TEM specimens of thin foil and carbon extraction replica were prepared either by electropolishing the foil in 5% H_2SO_4 acid or by etching in $5HF-6HNO_3-89H_2O$ solution (Vol. %). Subsequently, carbon was deposited onto the etched surface of the foil in a vacuum evaporator, followed by the detachment of the film in a $8HF-8HNO_3-84H_2O$ solution (Vol. %). These electropolished foils and carbon extraction replica were studied by TEM, STEM, EDX and electron microprobe.

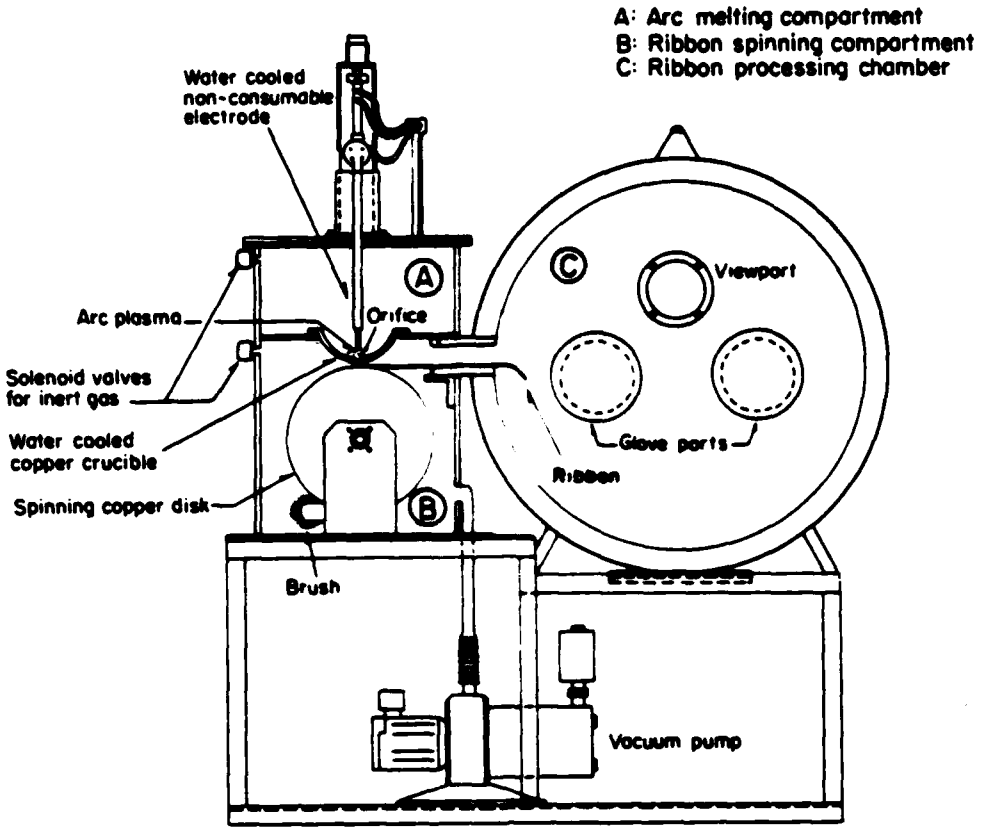

Figure 1 - Schematic diagram of pilot arc melt spinning unit

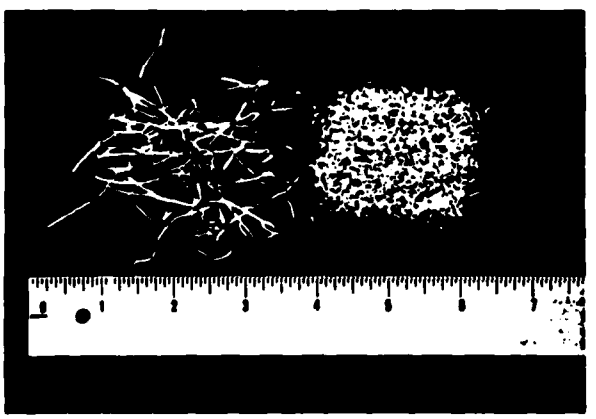

Figure 2a - Melt-spun alloy ribbons and chopped flakes by a rotary chopper.

Figure 2b - HIPed alloy consolidated from the chopped flakes using a small mild steel can.

Results

Microstrucures

Microstructural study of alloys Ti-5Al-4.5La and Ti-5Al-5.4Er were primarily focused on the identification of dispersoids and the microstructural changes before and after HIPing or associated with other heat treatments. As-spun alloy ribbons, by pilot arc melt-spinning technique, were electropolished into thin foils and studied by TEM. The microstructures of the two as-spun alloys (Figs. 3a and 3b) show spherical dispersoids of a size range 0.05 - 0.2 μm diameter embedded uniformly in the matrices. The Er-containing alloy ribbon annealed at 900°C/2h revealed little coarsening of the dispersoids (Fig. 3c) compared with those in the as-quenched alloys. Also, no distinctive grain growth was noticed between the as-quenched and the annealed alloys. In order to identify those dispersoids in the Ti-5Al-5.4Er alloy, carbon extraction replica was prepared from the splat-quenched foils by the hammer-and-anvil technique and subsequently annealed at 760°C/2h (Fig. 4a). The corresponding diffraction patterns (Fig. 4b) contain a large number of rings exceeding the diffraction patterns of any single compound known between Al and Er or of Er_2O_3. Although the replica was checked by EDX spectroscopy, the Al peak can't be identified since the weak Al peak is superimposed on the strong Er peak.

Another carbon extracion replica of the Ti-10Al-9Er splat alloy, annealed at 930°C/36h, was prepared, as shown in Fig. 5a. Electron microprobe spectra (Fig. 5b) obtained from the circled area of Fig. 5a indicate that the particles in the circled area contain Er as well as Al. In contrast, other spectra obtained from this replica show only an Er peak (Fig. 5c). Clearly, there are two different types of dispersoids co-existing in this alloy. The analysis of composition as well as the identification of oxygen by the microprobe, however, is not possible with this replica since the particle size is not large enough to provide the appreciable intensity of the oxygen spectra. Copper spectra in Figs. 5a and c come from the copper grids holding the extraction replicas.

The as-HIPed alloy containing La shows large grains 10-20μm in diameter and, in addition, many fine grains of several microns at the triple junctions between the large grains (Fig. 6a). The same alloy shows dispersoids as fine as those in the as-spun ribbon under TEM (Fig. 6b). The detailed micrograph (Fig. 6c) shows many chains of dispersoids lined up along dislocations. This characteristic arrangement of dispersoids is seen only in the La-containing alloy. The HIPed and annealed alloy at 900°C/100h (Fig. 6d) yields an average grain size larger than the mean size in the as-HIPed alloy by a factor of two, indicating slow growth in this alloy. Similarly, the HIPed alloy containing Er under the same conditions shows a similar average dispersoid size, but lacks such a chain arrangement.

Hardness

Age-hardening behavior and both room- and high-temperature strength of the ribbon, as well as HIPed alloys, were studied by hardness measurements. First, the Ti-5Al-4.5La alloy ribbon annealed isothermally at 700°C was checked by microhardness testing (Fig. 8) in order to identify age hardening. Although aging occurs in both alloys, full aging occurs within 10h in the Er-containing alloy, while it takes 25h for the La-containing alloy to reach full strength. In other words, slow aging is a characteristic of the La-containing alloy. Also, hardness was measured on the alloy ribbon, isochronally

Figure 3a - As-spun Ti-5Al-4.5La alloy ribbon (~40μm thick).

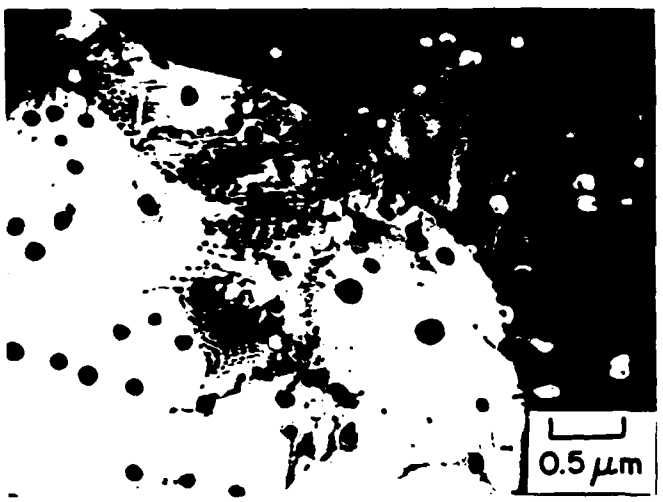

Figure 3b - As-spun Ti-5Al-5.4Er alloy ribbon (~40μm thick).

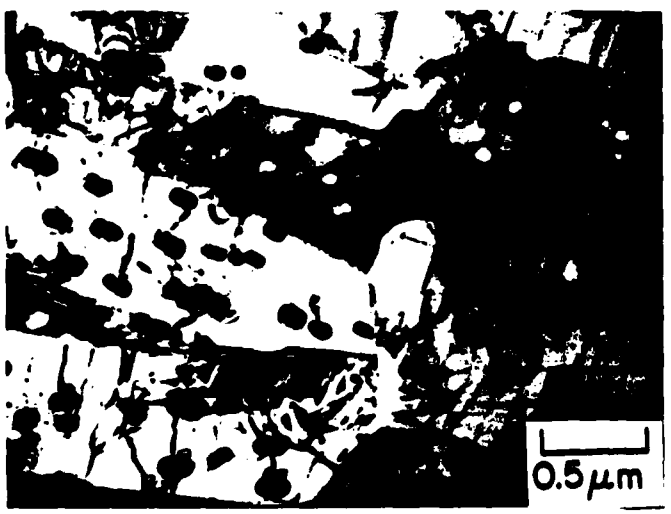

Figure 3c - Annealed Ti-5Al-5.4Er alloy ribbon at 900°C/2h.

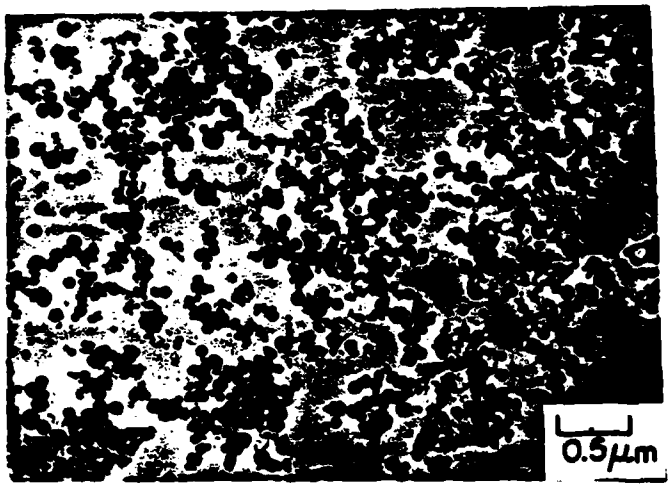

Figure 4a - Carbon extraction replica from annealed Ti-5Al-5.4Er alloy at 760°C/2h.

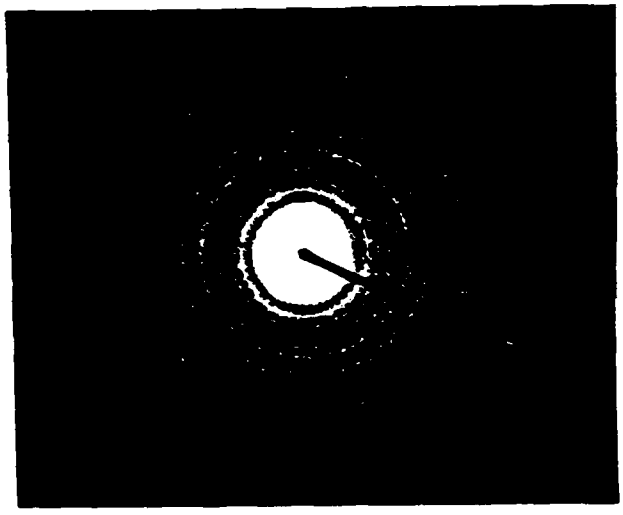

Figure 4b - Diffraction ring patterns from 4a.

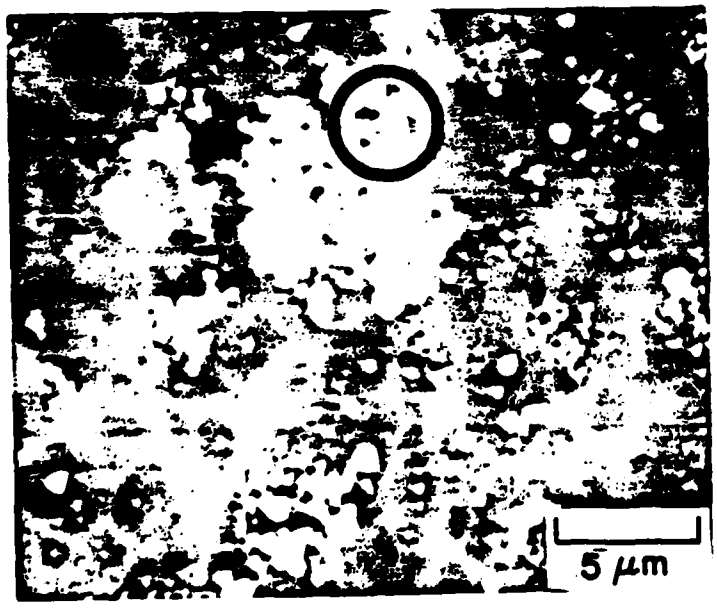

Figure 5a - Carbon extraction replica from annealed Ti-10Al-9Er alloy at 930°C/36h.

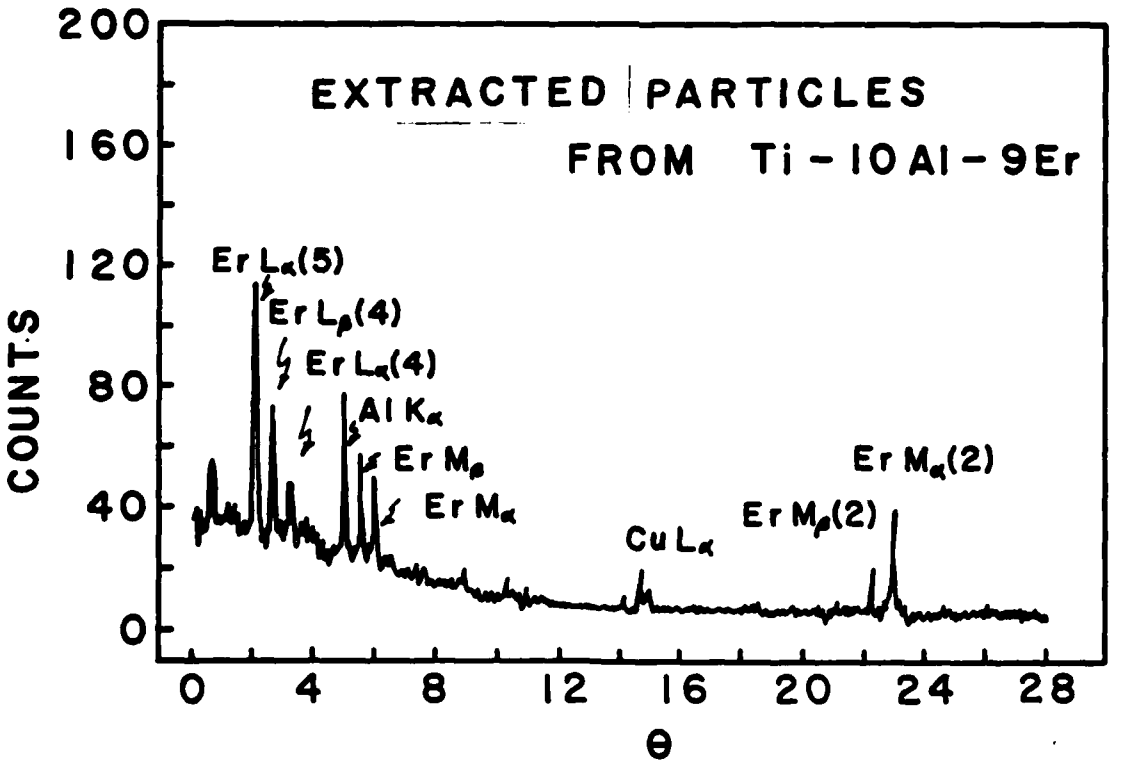

Figure 5b - Electron microprobe spectra from the dispersoids of the circled area in Fig. 5a.

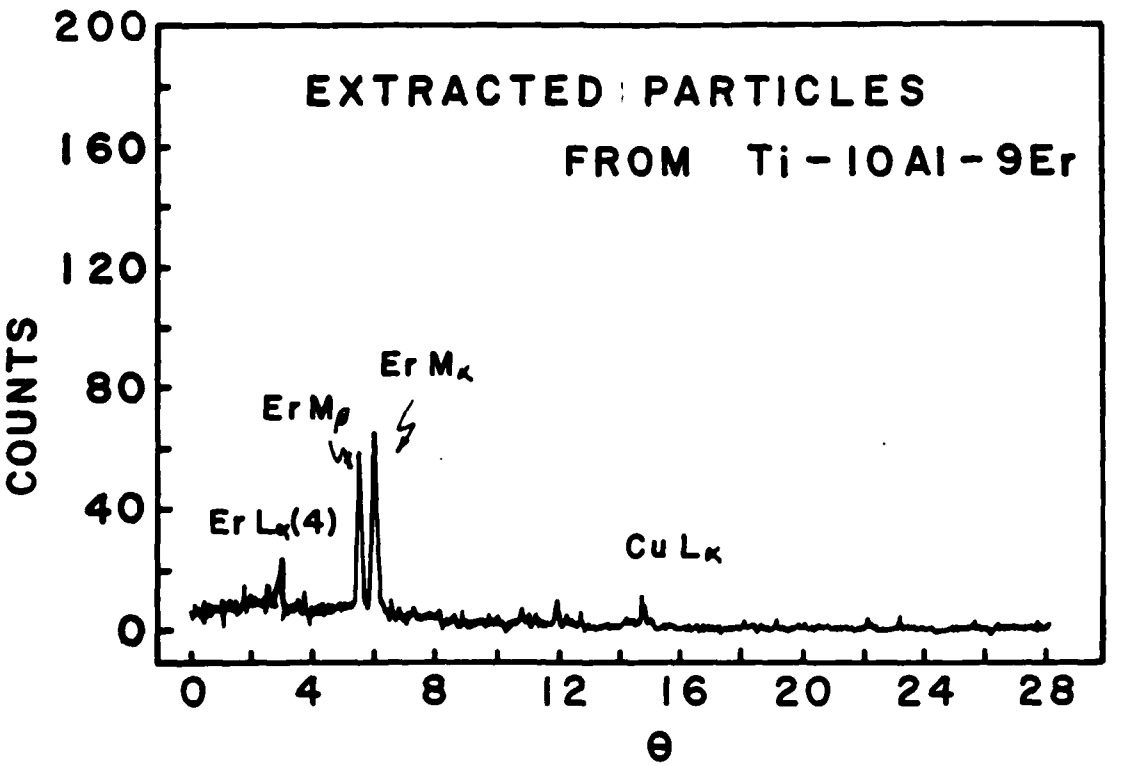

Figure 5c - Electron microprobe spectra from the dispersoids of other area (not shown in Fig. 5a).

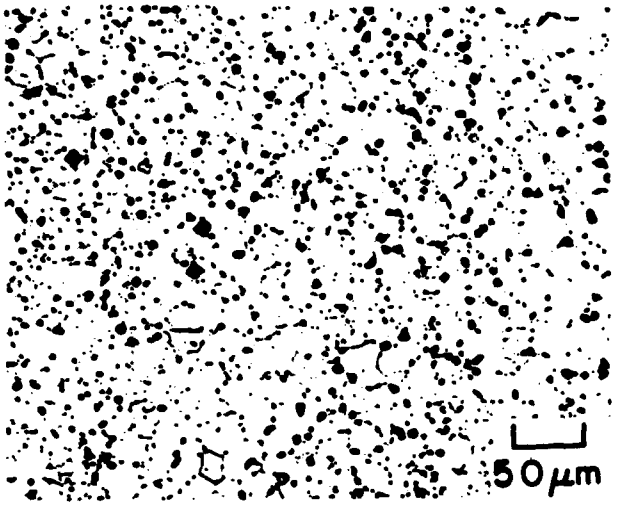

Figure 6a - Optical micrograph of as-HIPED Ti-5Al-4.5La alloy (850°C/2.1GPa/3h).

Figure 6b - TEM micrograph of as-HIPed Ti-5Al-4.5La alloy.

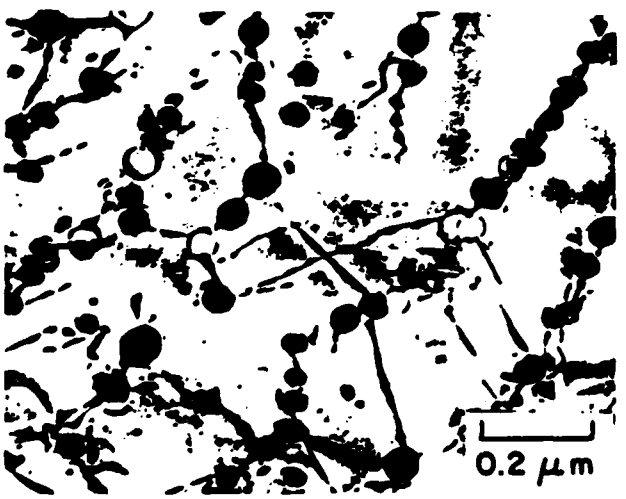

Figure 6c - Characteristic dispersoid chains in the TEM micrograph of the HIPed Ti-5Al-4.5La alloy.

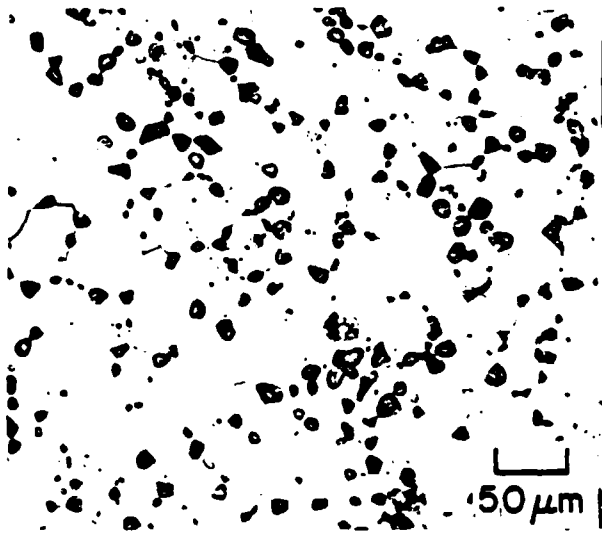

Figure 6d - Optical micrograph of HIPed and heat treated Ti-5Al-4.5La alloy (900°C/100h).

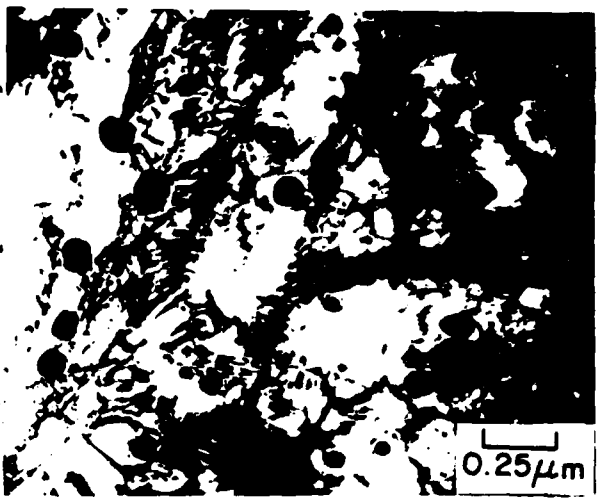

Figure 7 - TEM micrograph of HIPed Ti-5Al-5.4Er alloy (850°C/2.1GPa/3h).

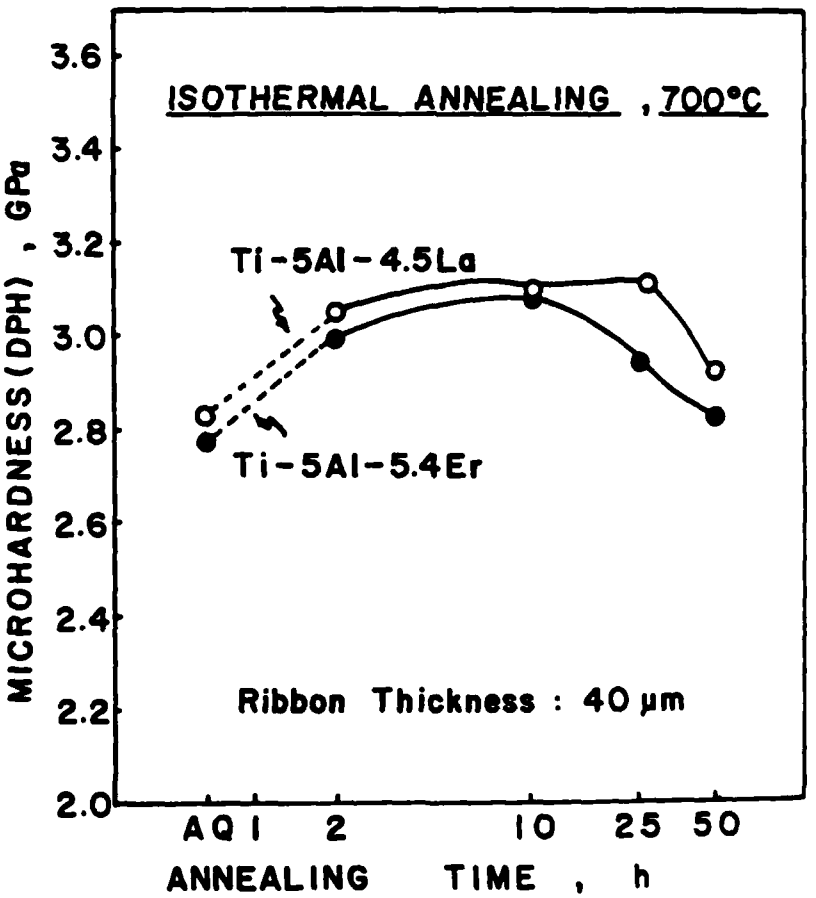

Figure 8 - Hardness response as a function of annealing time at 700°C in Ti-5Al-4.5La and -5.4Er alloy ribbons.

annealed for two hours from 500°C to 900°C with 100°C increment (Fig. 9). The maximum strength resulting from the aging occurs at 700°C, followed by rapid softening above 700°C. The rapid softening of the Er-containing alloys contrasts with the relatively slow softening of the La-containing alloy. The softening of the HIPed alloy, depending upon temperature, was investigated by hot hardness measurements in a range from room temperature to 900°C (Fig. 10). The hardness of the two alloys decreases linearly with increasing temperature from room temperature up to 700°C. Above 700°C, the Er-containing alloy continues to soften linearly up to 900°C while the La-containing alloy starts to lose its strength more rapidly above 600°C than predictable by the temperature increase. This is a manifestation of microstructure coarsening in the La-containing alloy above 600°C. It becomes clear that the softening in the La-containing alloy levels off at 900°C, joining the Er-containing alloy.

The room temperature hardness measured on the HIPed Ti-5Al-4.5La alloy annealed at 900°C is plotted against the annealing time shown in Fig. 11. The calculated Hall-Petch stress and Orowan-Ashby stress (15) are given in the plot, which will be discussed in the next section. Overall, hardness falls rapidly as a function of time at this temperature, consistent with microstructural coarsening such as grain growth and dispersoid coarsening. The measured values of the grain size and dispersoid diameter are tabulated in Table I.

Table I - Hardness, grain and dispersoid diameter of HIPed and heat treated Ti-5Al-4.5La alloy.

Annealing condition (900°C)	grain diameter(D) μm	Dispersoid diameter (d) μm	micro-hardness (DPH),GPa
As-HIPed	13.3	0.09	3.28
25h	21.4	0.15	2.94
50h	30.6	0.35	2.82
100h	44.6	0.65	2.55

Based on the data in Table I, the grain growth fairly well obeys the parabolic law $D^2 \propto kt$, where k and t are constant and annealing time. Nevertheless, the interaction between the grain growth and dispersoid coarsening as suggested by Zener (16) and Gladman (17) can't be confirmed because of a lack of sufficient data.

Discussion

In the past, rare-earth dispersoids in rapidly quenched ternary Ti alloys have been identified as binary intermetallic compounds or rare-earth sesquioxide. Examples are: Al_3La (Hex., DO_{19}) and Al_4La (Orth., $D1_3$) in Ti-5Al-3La alloy (13); La_2Sn (Hex., $B8_2$) in Ti-9.5Sn-5.3La alloy (13); Y_5Sn_3 (Hex., $B8_2$) in Ti-5Sn-3Y alloy (18) and also Y_2O_3 in laser surface melted Ti-8Al-4Y alloy (at. %) (19). For all ternary alloy systems studied, neither ternary compound nor line compound has been found so far. The rare-earth sesquioxide is widely discovered in binary (7) as well as ternary Ti alloy systems, since oxygen concentration larger than 800 ppm is available as impurity in pure titanium. In most cases, a mixture of these two types of compounds is found to co-exist in rapidly solidified and heat treated Ti alloys. Nevertheless, the precise fraction of the two types of compounds

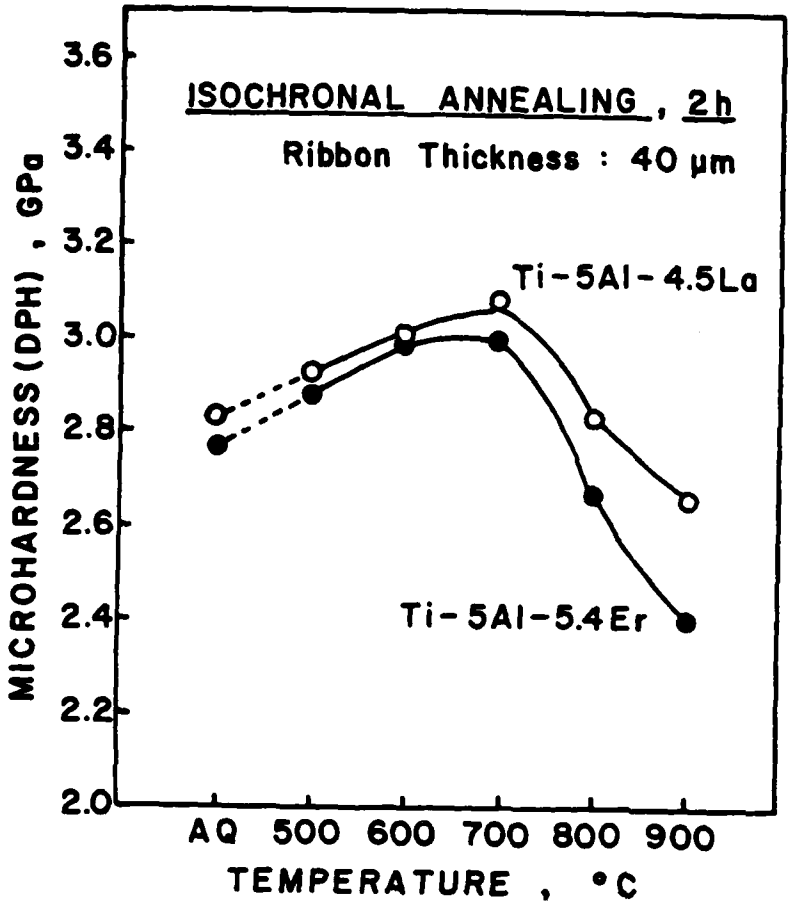

Figure 9 - Room temperature hardness in isochronally annealed Ti-5Al-4.5La and -5.4Er alloy ribbons.

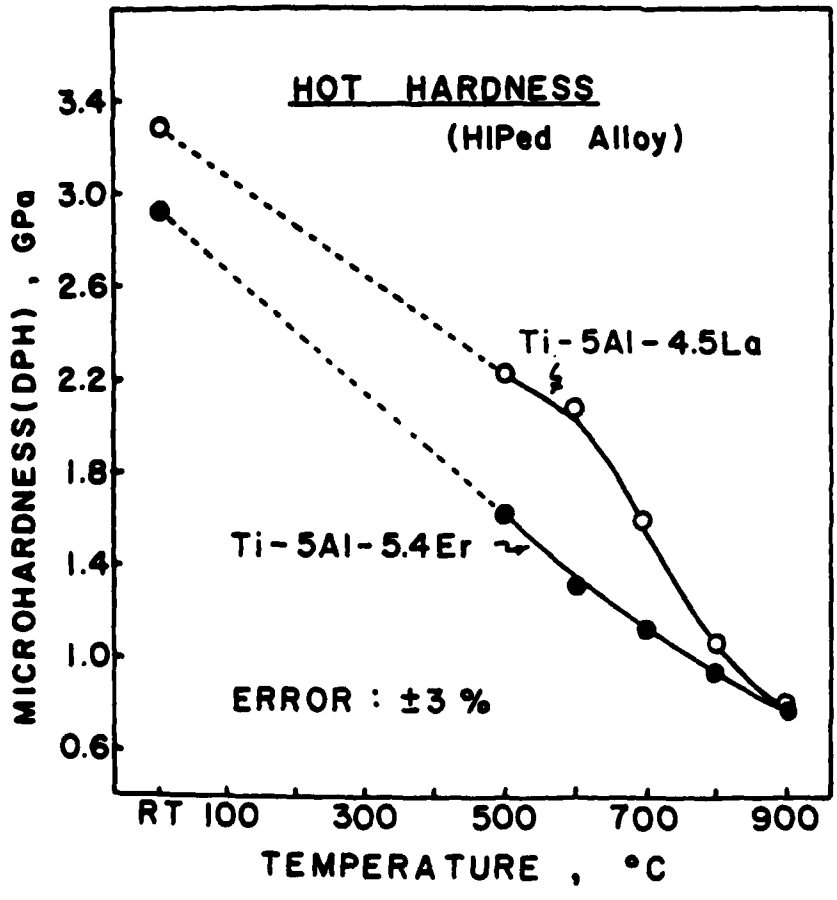

Figure 10 - Change in hot hardness with temperatures in HIPed Ti-5Al-4.5La and -5.4Er alloys.

can't be determined since the quaternary phase diagrams including oxygen aren't available.

HIPed Ti-5Al-4.5La alloy systematically undergoes softening when annealing at 900°C for various durations. In order to understand the mechanisms associated with such strength reduction, Hall-Petch strength and Orowan-Ashby stress for the annealed alloys were calculated from the data in Table I, shown in Fig. 11.

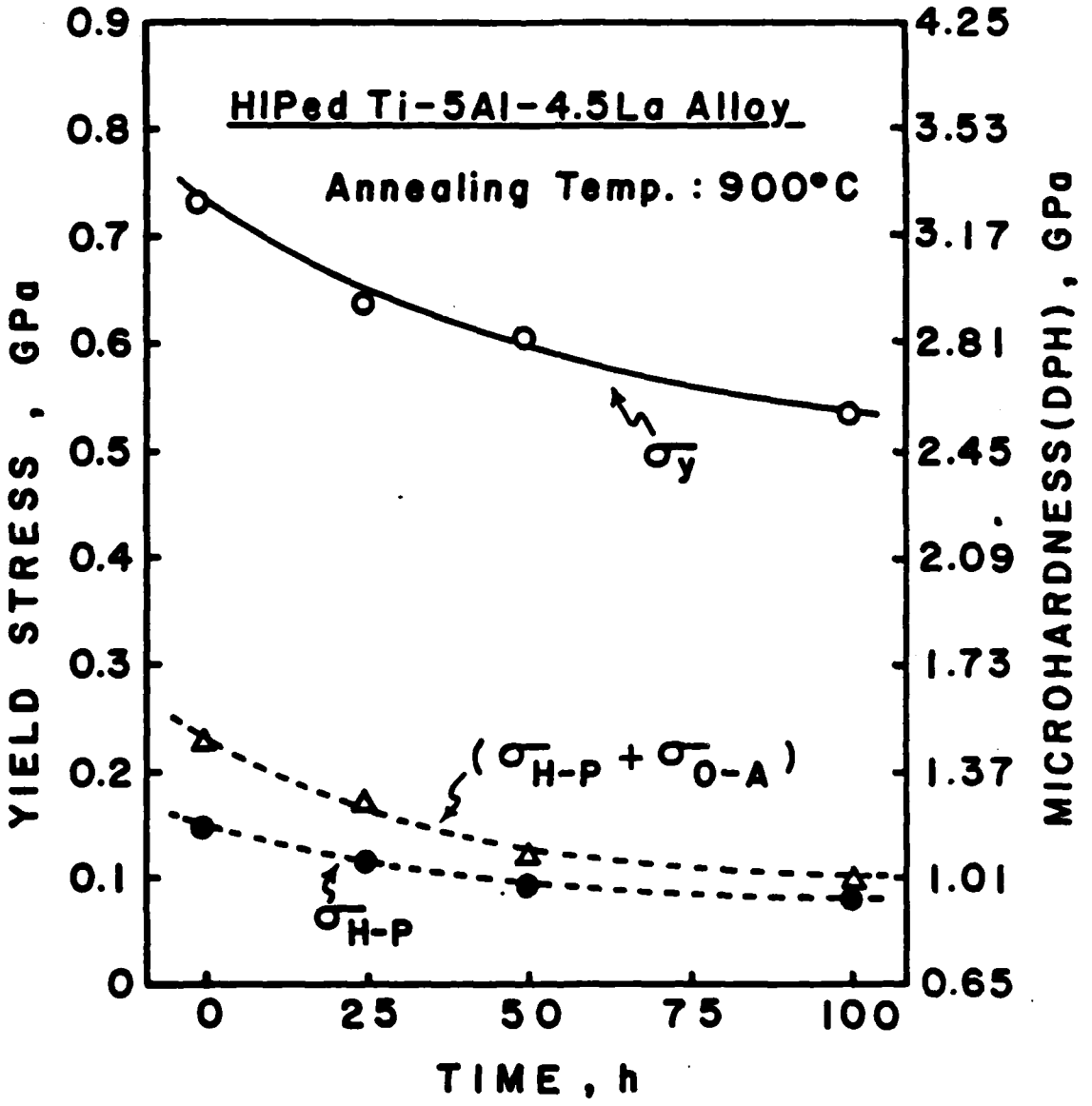

Figure 11 - Plot of room temperature hardness vs. annealing time (900°C) in HIPed Ti-5Al-4.5La alloy.

The yield stress of the alloy is written as

$$\sigma_y = \sigma_m + \sigma_s + \sigma_{H-P} + \sigma_{O-A}$$

where $\sigma_{H-P} = k \cdot D^{-1/2}$;

$$\sigma_{O-A} = \left(\frac{1}{1.18}\right) \frac{G \cdot b}{2\pi L} \left(\frac{1}{1-\nu}\right) \ln\left(\frac{d}{2b}\right)$$

σ_m, σ_s, σ_{H-P}, σ_{O-A}, k, D, G, b, L, ν and d are the yield stress of pure Ti, the yield stress increase due to the solid solution of Al and La, Hall-Petch stress, Orowan-Ashby stress, proportionality constant, grain diameter, shear modulus, Burgers vector, mean interparticle spacing, Poissons ratio and particle diameter. σ_{H-P} and σ_{O-A} were determined using appropriate values of k, G and ν taken from the previous work (20) and by converting the hardness values into yield stress using the conversion factor (20). The sum of σ_{H-P} and σ_{O-A} makes up ~30% of the yield stress at the HIPed state, but decreases to ~20% after annealing (900°C, 100 h). Nevertheless, the reduction of the yield stress after the 100h annealing is larger than the sum of the reduction in σ_{H-P} and σ_{O-A}, indicating the possibility of other mechanisms being involved. In fact, it is likely that the subgrain structure similar to those shown in Fig. 3c may be another source of the alloy strengthening. This substructure strengthening (21,22) is expected to decline rapidly upon annealing at 900°C. In addition, it is noted that the Orowan contribution entirely diminishes after 100 h annealing while the Hall-Petch strength remains relatively strong. This is because the Hall-Petch relation is less sensitive to the grain size than in the Orowan-Ashby equation in relation to the interparticle spacing.

Conclusion

1. Arc melt-spun ribbons of Ti-5Al-4.5La and Ti-5Al-5.4Er can be HIPed into full density at 850°C/2.1 GPa/3h. As a result, microstructural coarsening under HIP conditions is minimal.

2. Rare earth dispersoids in these alloys were identified as a mixture of two different types of compounds: rare earth oxide forms and binary intermetallic compounds without Ti.

3. The occurrence of alloy softening after high temperature annealing (900°C) is primarily the result of particle coarsening and grain growth.

4. Superior mechanical properties (hardness) of the La-containing alloy over the Er-containing alloy at room and high temperatures have been demonstrated; this appears to be attributable to better microstructural stability in the La-containing alloy than in the Er-containing alloy.

In practice, it is envisioned that this type of alloy may be in use at 900°C in the future when new rare earth dispersoids of better coarsening resistance can be found and the matrix is reinforced by alloying elements. Another benefit of having such stable particles is that grain growth may be significantly retarded by the particles. Also, it is necessary to reinforce the matrix, since the hot hardness measurements show the existence of serious matrix softening at 900°C.

Acknowledgement

We gratefully acknowledge the support of the Office of Naval Research in the Rapidly Solidified Titanium Program at Northeastern University. We thank Drs. S. Hsu and R. Raman for their help in hot hardness measurements at GTE Laboratories. The authors also appreciate the Barnett Institute's continuing support of Ti alloy research. Contribution # 242 from the Barnett Institute.

References

1. E.W. Collings, R.E. Maringer, and C.E. Mobley, "Amorphous Glassy Metals and Microcrystalline Alloys for Aerospace Application," Technical Report AFML, TR-78-70 (June 1978).

2. E.W. Collings, C.E. Mobley, R.E. Maringer, and H.L. Gegel, Proc. Third Int. Conf. Rapid Quenched Metals, 1 (1978) pp. 188-191.

3. E.J. Chapin and R. Liss, Report of NRL Program (December 1955).

4. B. Love, WADC Tech. Report, No. TR57-666, Part II (March 1959).

5. N.J. Grant, U.S. Patent No. 3,070,468 (1962).

6. M.B. Vordahl, U.S. Patent No. 3,622,406 (1971).

7. S.M.L. Sastry, P.J. Meschter and J.E. O'Neal, "Structure and Properties of Rapidly Solidified Dispersion-Strengthened Titanium Alloys: Part 1. Characterization of Dispersoids Distribution, Structure and Chemistry" Met. Trans. A., 15 (1984) pp. 1451-1463.

8. S.H. Whang, "Rapidly Solidified Ti Alloys Containing Novel Additives," J. Metals, 36 (1984) pp. 36-40.

9. S.H. Whang, "Precipitate Hardened Titanium Alloy Composition and Method of Manufacture," U.S. Patent No. 4,512,826 (1985).

10. S.M.L. Sastry, T.C. Peng, and L.P. Beckerman, "Structure and Properties of Rapidly Solidified Dispersion-Strengthened Ti Alloys: Part II, Tensile and Creep Properties," Met. Trans. A., 15A (1984) pp. 1465-1474.

11. C.S. Chi and S.H. Whang, "Effects of Novel Additions (Ce,B) on the Microstructure and Mechanical Properties in RS Ti Alloys," TMS-AIME Paper Selection F83-14 (1983).

12. C.S. Chi and S.H. Whang, "Rapidly Solidified Ti Alloys Containing Metalloids and Rare Earth Metals - Their Microstructures and Mechanical Properties," Proc. MRS Symposium, 28 (1984) pp. 353-360.

13. C.S. Chi and S.H. Whang, "Microstructural Characteristics of Rapidly Solidified Ti Alloys Containing La," unpublished work.

14. S.M.L. Sastry, T.C. Peng, and J.E. O'Neal, "Rapid Solidification and Powder Metallurgical Processing of Titanium Alloys," Proc. 1984 Int. Powder Met. Conf. Totonto, Canada June (1984).

15. M.F. Ashby, Proc. Second Bolton Landing Conf. on Oxide Dispersion Strengthening, G.S. Ansell, ed., Gordon and Breach, Science Publisher (1968) p. 143.

16. C. Zener, Trans. Met. Soc. AIME. 175 (1949) p. 15.

17. T. Gladman, Proc. Roy. Soc. A294 (1966) p. 298.

18. Y.Z. Lu and S.H. Whang, "Ostwald Ripening of Rare Earth Dispersoids in Rapidly Solidified α-Ti Alloys," Paper presented at TMS-AIME Annual Meeting, New York, NY (1985).

19. D.G. Konitzer, B.C. Muddle, and H.L. Fraser, "A Comparison of the Microstructure of As-Cast and Laser Surface Melted Ti-8Al-4Y," Met. Trans. A., 14A (1983) pp. 1979-1988.

20. H. Conrad, "Effect of Interstitial Solutes on the Strength and Ductility of Titanium" pp. 123-403 in Progress in Materials Science, 26, Pergamon Press, Ltd (1981).

21. D.H. Warrington, JISI, 201 (1963) p. 610.

22. J.Rezek and G. B. Craig, TMS-AIME, 221 (1961) p. 715.

RAPIDLY SOLIDIFIED Ti ALLOYS FOR HIGH TEMPERATURE APPLICATIONS

S. H. WHANG

Submitted to J. Materials Science, Accepted and to be published in early 1986.

RAPIDLY SOLIDIFIED TI ALLOYS

FOR HIGH TEMPERATURE APPLICATIONS

Sung H. Whang*

Barnett Institute of Chemical Analysis and Materials Science
Northeastern University
Boston, Massachusetts 02115

The application of rapid solidification technologies (RST) to titanium alloy systems is relatively new and became the subject of active research since it was demonstrated that novel Ti alloys of higher temperature capability can be synthesized through new alloy design based on rapid solidification processing. Effects of rapid solidification on the occurrence of metastable phases, microstructures and mechanical properties in binary and ternary Ti alloys are reviewed.

In particular, earlier results from RS α-Ti alloy research have shown that many different novel dispersoids, some of which are coarsening-resistant at elevated temperatures (600-800°C), can be created in the matrix through RST. The alloys containing novel dispersions also exhibit good creep resistance at elevated temperatures. Further study on α/β- and β-Ti alloys through RST, in conjunction with development of various processing technologies for bulk alloy manufacturing is clearly desirable.

---

*present address: Department of Metallurgy and Materials Science
Polytechnic Institute of New York
333 Jay Street
Brooklyn, New York 11201

I. INTRODUCTION

Historically, the development of high temperature Ti alloys dates back to the 1960's when Ti alloys were largely strengthened by precipitating silicide in order to provide adequate creep strength at elevated temperatures [1-4]. Furthermore, Zr and Mo were added to strengthen the matrix and stabilize silicide dispersion. These Zr- and Si-containing alloys have been optimized with respect to creep strength and other structure-sensitive properties for use in a temperature range of 500-600^{o}C [5], slightly larger than the 0.4 homologous temperature. In fact, this homologous temperature of Ti alloys for practical application is much lower than that of superalloy, where maximum temperatures can reach as high as 0.9 homologous temperature. The fact that conventional Ti alloys do not have high temperature capability has motivated the development of high temperature Ti alloys.

Nevertheless, there are a number of stumbling blocks to developing higher temperature (>600^{o}C) Ti alloys. The identified obstacles are: 1) no coherent and stable precipitate at high temperatures, similar to γ' in superalloy, was found in Ti alloy systems; 2) at temperatures above α transus temperature, the silicide coarsening rate is very high, due to high diffusivity of the solute (Si) [6]; 3) a rapid oxidation reaction occurs above 600^{o}C, seriously challenging high temperature applications [7,8]. As a result, some efforts have been directed toward: a) increasing the allotropic temperature via alloying with strong alpha stabilizing elements; (b) introducing precipitates or dispersoids other than silicides into the matrix through rapid solidification processing [9-11]; (c) applying oxidation resistant coatings to the alloy surface.

Alternatively, there have been a number of attempts to replace α-Ti alloy with Ti intermetallic compounds for high temperature applications [12-18], i.e., titanium aluminides: TiAl and Ti_3Al. These aluminides have good oxidation resistance and high moduli, but they have poor ductility as well as poor formability, thus limiting the practical use of these aluminides at high temperatures [12]. Nevertheless, efforts have been made to improve the ductility of these aluminides at high temperature by introducing various alloying elements into the aluminides [16].

A recent approach to high temperature Ti alloy development is mainly to create fine and stable dispersoids in the Ti matrix through rapid solidification processing. Additive elements include metalloids (B,C,Si), rare earth metals (Y, La, Ce, Nd, Er, etc.) and an actinide element (Th). By and large, all these elements have negligible solubility in Ti at room temperature, but dissolve in Ti in a limited amount at high temperatures. Further, these elements form stable dispersoids in the Ti matrix, providing dispersion strengthening at elevated temperatures. Previously, a significant amount of rare earth metals (~1 at.%) was dissolved into Ti through the ingot metallurgy process [19-22], but the resulting alloy phase contained coarse rare earth particles ranging from one to several microns in diameter in the as-casted ingot [22]. Further development of high temperature Ti alloy by the addition of rare earth metals through the ingot metallurgy technique appeared to be at an impasse in the presence of such coarse particles. The recent advent of rapid solidification technology has restored research interest in Ti alloys with rare earth-addition, since the formation of such coarse particles is prevented and fine and uniform particles are created. Although the possibility of developing high temperature alloys applicable at the temperature range of 600-800°C has been

demonstrated, measures must be taken in order to prevent severe surface oxidation at these temperatures. In this regard, research on rapidly solidified Ti alloys for high temperature applications is still in the experimental stage, and further property evaluation for practical applications is needed.

This paper reviews the research in rapidly solidified Ti alloys in the last ten years.

2. RAPID SOLIDIFICATION PROCESSING (RSP) OF TI ALLOYS.

Despite rapid progress in RSP technology over more than a decade, the full-scale development of Ti alloys through RSP has been hindered by the reaction of Ti with crucible materials and with the environment. Although many alloy powder processes for near-net shape Ti metallurgy in the 1970's have emerged, the methods neither intend to nor do they produce a high quench rate (> 10^3K/sec) during the powder production. For example, the rotating electrode process (REP) [23] produces Ti alloy powder of mean diameter 175μm in Ar atmosphere. The estimated cooling rate from the microstructure doesn't exceed 10^3K/sec [24]. Hence, it is considered a conventional processing technique.

In parallel, during the last decade, melt extraction techniques have been developed for quenching Ti alloys into fibers [25,26]. Added recently were arc melt-spinning [10,27], laser spin atomization [28], electron-beam melting/splat quenching [9,29], and ultrasonic gas atomization [9]. The pendant drop melt extraction techniques produce so-called L/D powder, or C-, D- and L-shaped fiber of Ti-6Al-4V, and other heavily alloyed Ti, such as Ti-5.4Al-3.6V-8Fe-3Cu [30]. The melt-extraction techniques provide

contamination-free fiber when processed in a vacuum chamber. Lab-scale as well as pilot-scale arc melt-spinning technique has been used in producing Ti alloy ribbon of amorphous and microcrystalline forms [10, 27]. This technique adopts the combination of a water-cooled cold copper crucible with an arc heating scheme that uses non-consumable tungsten electrodes under argon atmosphere. As a result, Ti alloy ribbons or flakes processed by this technique are also contamination-free, since they are melted in the cold copper crucible and spun in an inert gas atmosphere. The ribbon produced has a uniform thickness of 20 to 50μm.

2.1 MELT EXTRACTION PROCESS

The first attempt to produce fine fiber or filament of metals and alloys in a clean environment was made by this technique. There are two methods of melt extraction procedure: crucible melt extraction and pendant drop melt extraction (PDME) (Fig. 1a) [26]. In the former, a rotating copper disk with a sharp peripheral angle, immersed in the melt, drags out metal filaments from the melt. The fiber shape depends upon the immersion depth and the speed of the disk. The shapes include D, C, and L, as shown in Fig 1b. Although the surface of the melt is covered with slag, this technique was used primarily for non-reactive metals such as iron, steel, aluminum, etc. The second technique, pendant drop melt extraction, may be regarded as a non-crucible melt spinning technique. Ti alloy rod hanging above the spinning disk is heated to melt by an electron beam, or a laser beam or other clean heat sources. The thickness (d) of the fiber produced in this technique is expressed with an empirical relation [30]:

$$d = C \cdot V^{-1/2}$$

where C and V are proportionally constant (and the surface velocity of the disk.) It should be noted that the exponent, 0.5, is half of the figure in ordinary melt-spinning, ~1.0 [31,32]. Under the well controlled processing conditions, Ti alloy fiber of ~58μm has been produced at the estimated cooling rate of ~10^5K/sec. Also, the melt extraction techniques are able to produce short fibers of a length-to-diameter ratio of 20:1 using a notched disk. These flakes, so called L/D powder, are amenable to direct compaction and consolidation without further reduction in size, i.e., cutting or chopping. In electron beam melting/splat quenching [29], similar to PDME, the molten droplet from Ti alloy stock by electron beam heating falls onto the face of the spinning disk and produces a shallow U-shaped flake, i.e. a boomerang-shaped flake.

2.2 ARC MELT-SPINNING

In contrast to the ordinary melt-spinning technique [10,27,33], in which various crucibles (quartz tubing, clay, ceramic) are used to melt metals and alloys by induction or resistant heating, the arc melt-spinning technique (AMS) uses a cold copper crucible with an orifice and arc electrode to melt-spin alloys. The molten alloy is injected through the orifice of the copper crucible by the gas pressure differential between the melting and spinning compartments (Fig. 2a). The ribbon and the chopped flake produced by the rotary-blade ribbon cutter are shown in Fig. 2b. This melt-spin technique has advantages over other techniques in that a) uniform and thin ribbon of reactive alloys as well as refractory alloys (Nb, Ta, Mo, W) can be produced without contamination; and b) the molten jet can be shaped into a desired geometry and spun into a relatively thin sheet (20 - 50μm thick), providing a high cooling rate ($5 \times 10^5 - 10^7$ deg/sec). Many α-Ti alloys containing rare-earth metals have been processed into ribbon materials by this technique.

2.3 ATOMIZATION

In centrifugal atomization [28,29], the surface tension of the molten alloy becomes an important intrinsic parameter for the effectiveness of the atomization, since the surface tension opposes the centrifugal force which breaks the molten alloy into fine droplets: i.e., the higher the surface tension, the stronger the centrifugal force required. The surface tension of a molten alloy decreases linearly with the melt temperature, whereas it changes radically with a small amount of a particular additive element [34]. Based on the balance between the surface tension versus the centrifugal force, the following relation was derived [23].

$$r = \frac{\sqrt{1.5}}{\omega} \cdot \left(\frac{\sigma}{R \cdot \rho}\right)^{1/2}$$

where r, ω, R, σ and ρ are the radius of droplet, angular speed and radius of spinning rod, surface tension, and density, respectively. In the centrifugal atomization, the rotational speed to overcome the surface tension of the melt, N (rpm), is proportional to $\sigma^{1/2}$, where σ is the surface tension of the droplet. Figure 3 shows a schematic diagram of a laser melt-spin atomization unit. In this technique, an extruded Ti alloy rod, melted by laser beam at the one end, rotates at a speed up to 35,000 rpm, generating various mean sizes of spherical powder depending upon the rotational speed. The powder produced, Ti-6Al-4V, reportedly has an average particle distribution ranging from 0.01 to 0.65mm diameter, with a corresponding rotating speed from 303 to 838 rad/sec or 8,000 to 29,000 rpm (rod diameter 3cm) (Figs. 4a & b). It is apparent from this report that the rotational speed of the rod should increase far beyond 60,000 rpm in order to produce an average powder size of ~75μm diameter, provided the relation given above is correct.

Rapidly solidified alloy powder was also produced by an ultrasonic gas atomizer using a zirconia crucible coated with rare earth oxide [29]. The gas stream of supersonic velocity (Mach 2 ~ 2.5), a pulse frequency of 100KHz, and a pressure 8.3 MPa, strikes the molten jet at a shallow angle (~22.5^{o}). The resulting powder is a spherical shape from 10 to 100μm diameter. This technique requires special care of coating materials, which are easily damaged during operation. The stability of the coating at high temperature, and its chemical reaction with Ti will be the main concern in this technique. Typical processing techniques and corresponding cooling rates are summarized in Table 1.

A large difference in cooling rate is observed between the various techniques. For example, the cooling rate of atomized powder was determined by measuring dendritic arm spacing in Ti-15V-3Al-3Sn-3Cr [29]. A plot of the particle diameter (D) of laser melt-spin atomized powder vs. cooling rate, estimated from the dendritic arm spacing, yields a linear correlation in a log normal scale. The slope in the plot is roughly ~ $\dot{T} \propto D^{-2}$ [29], which is in agreement with ideal cooling, but in disagreement with Newtonian cooling [28,31], where $\dot{T} \propto D^{-1}$. Such deviation cannot be accounted for, since sufficient information in not available.

For another example, a ternary alloy containing a rare earth metal (Ti-5Al-4.5La) when quenched by the H-A technique (Fig. 5a) reveals fine martensitic structure combined with precipitates of 5nm diameter; the same alloy composition by AMS techniques shows a particle size of 50-200nm diameter (Fig. 5b) [36]. Similarly, binary Ti-(5.9-7.9)Ni alloys processed by PDME and electron beam melting/splat quenching (EBSQ) show beta eutectoid decomposition while splat alloy by the H-A technique does not indicate such decomposition. This fact suggests that at the break-off point from the copper disk, the temperature of the alloy ribbon is high, possibly above 750^{o} (Fig. 6) [37].

On the other hand, Ti_{60} Ni_{30} Si_{10} ribbon has been routinely melt spun into glassy alloy by AMS techniques, indicating that the alloy temperature at the break-off is below the first crystallization temperature of this alloy, i.e., 470^{o}C [38]. These conflicting results demonstrate a large variation in cooling rates, depending on composition, additive elements, processing techniques and other processing parameters. A systematic investigation is due, in order to further understand the relationship between the cooling rate and processing variables.

Table 1

Processing Techniques and Their Cooling Rates

Technique	Shape and Size (μm)	Estimated Cooling Rate	Environment
Hammer and Anvil (H-A)	Foil 10 - 50	10^6 - 10^7	Inert Gas (I.G.)
Pendant Drop Melt Extraction (PDME)	Fiber: 0.025-0.125 (mm)	10^3 - 10^5	I.G.
Arc Melt Spinning (AMS)	Ribbon 15 - 50	10^5 - 10^6	I.G.
Laser Spin Atomization	Spherical Powder 100 - 650	10^2 - 10^4	I.G.

3. CONSOLIDATION

Since powder products from rapidly solidified materials take various shapes, size distribution, and surface conditions, depending upon the processing techniques, the consolidation and thermomechanical processing of the powders requires different consolidation conditions. It is often found that improvement in powder bonding and coarsening of powder microstructure occur simultaneously with annealing. Preliminary studies on optimization of these conditions with respect to mechanical properties have been carried out.

An earlier work, rapidly quenched Ti-6Al-4V flakes produced by pendant drop melt extraction technique were vacuum hot pressed at 955°C for one hour under the pressure of 5.5 MPa [26]. Alternatively, the same flakes were cold pressed under the pressure of 345MPa and canned in a seamless steel tubing followed by outgassing at 870°C for 15h. HIPing of the canned powder was performed at 955°C under 167MPa. Consolidated alloys by both methods

yield essentially 100% density, but result in grain growth during high temperature consolidation.

Since microstructural coarsening during consolidation becomes a critical factor for high temperature strengthening in dispersion strengthened RS Ti alloy, current consolidation schemes for RS Ti alloys are focused primarily on preventing microstructure coarsening while achieving full densification. In order to achieve both objectives, consolidation techniques that allow low working temperatures are employed. For example, Ti flakes processed by electron beam melting and splat quenching were vacuum hot pressed at 800-950^{o}C under 50-100MPa. Subsequently, the flakes were forged at 800^{o}C into 4.0μm thick plates and hot rolled at 800^{o}C into 1.5mm thin sheets [29]. The flakes (1~2 mm long x 1~2 mm wide) produced by the arc melt-spinning process were HIPed at 850^{o}C/3h/2.1GPa using mild steel can [36]. The consolidated alloy shows full density and good bond character. (Fig. 8 shows typical ribbon, chopped flake, and HIPed alloy.) All these temperatures used for the dispersion strengthened alloys are roughly 100^{o}C lower than conventional consolidation temperatures. One of the attractive aspects of Ti alloy consolidation is that the surface oxide of precursor alloys dissipate from the surface of the powder by diffusion during hot consolidation.

4. MICROSTRUCTURAL OBSERVATIONS

Microstructural characteristics of rapidly quenched Ti alloys have been examined in two states: as-quenched and heat-treated, as in hot consolidation and thermomechanical processing. The microstructure of the as-quenched state is characterized by supersaturation of solute atoms, and refined microstructures consisting of β-grain, acicular α-grain, martensitic

structure, precipitate, etc. Heat-treated alloys undergo further changes in microstructure toward the next metastable state or equilibrium state. Despite consolidation and thermomechanical processing, a significant portion of microstructural refinement can be retained in the final product, depending upon the thermal history of consolidation and thermomechanical processing. As a result, microstructures of bulk alloy consolidated from rapidly solidified materials are an order of magnitude finer than those seen in conventional ingot Ti alloys. In particular, coarsening of rare earth dispersoid Ti alloys is minimal upon reduced temperature consolidation and deformation.

4.1 *SOLID SOLUBILITY OF SOLUTE*

One of the benefits of RS Ti alloy is the increase in solid solubility upon rapid quenching; this permits almost every additive element to dissolve into solid solution or cluster form at a desired level for precipitation hardening later. At the same time, serious segregation of additive elements leading to formation of coarse particles is prevented. The increase in solid solubility of solute in an individual system is a function of cooling rate [39], but for a given cooling range, the relative solubility of various alloying elements is associated with atomic size [40], electronegativity [41], and electronic structure [42] of alloying elements.

Table 2 shows α phase extension in binary Ti alloy systems due to rapid quenching. A large solubility extension is seen in the types of alloy systems where eutectoid or peritectoid transformation occurs, while almost no extension is realized in the system of monotectic-peritectic transformation system. It appears that in such a monotectic-peritectic system, the undercooling of the liquid below a solidus temperature is

difficult to attain, due to a large temperature range of the mush zone in the phase diagram. One exception in the solubility extension is that metalloid atoms (C, B) having unfavorable atomic size as a substitutional solute in Ti undergo extensive dissolution through a different mechanism, i.e., interstitial solid solution. In Ti-B alloys, the lattice parameter increases with increasing B concentration. The appearance of boride particles cannot be seen up to 10 at % B. This evidence suggests that boron atoms may dissolve in the Ti matrix as an interstitial solute [43].

By and large, the experimental results from rapidly quenching Ti binary alloy show that α-phase extension can be accomplished at the expense of intermetallic compounds, not at the expense of the ω-phase (or β-phase), since the occurrence of the ω phase is almost independent of cooling rate and strongly depends upon electron concentration per atom (e/a) [44]. For example, Fig. 8 shows the alloy phases from the equilibrium and rapid quench phase diagrams [45,46]. The occurrence of both α-phase extension and a metastable β-phase replaces the TiFe compound phase, but the boundary between metastable α-phase and a metastable β-phase (or ω-phase) may be associated with electron concentration of the alloy composition.

Table 2

Comparison of Equilibrium and Non-Equilibrium Maximum Solid Solubility in Binary Ti Alloys determined from TEM Micrograph

Alloy System	Solute Concentration in α phase at %	Ref.	Phase Diagram Type	Solution Type	Maximum Primary Solid Solubility
Ti-V	~6	[46]	β-isophormous	Sub.	~3.0 (650°C, α)
Ti-Mo	<2.0	[46]	β-isomorphous	Sub.	0.4 (6.75, β)
Ti-Fe	~2.5	[46]	Eutectic	Sub.	~21 (1085, β)
			Eutectoid		~0.2 (590, α)
Ti-Co	~2.5	[46]	Eutectic	Sub.	~14.5 (1020, β)
			Eutectoid		~ 0.8 (685, α)
Ti-C	~10	[42]	Eutectic		0.55 (1645, β)
			Peritectoid	Int.	<0.55 (920, α)
Ti-B	~6	[43]	Eutectic	Int.	<~1 (1540, β)
			Peritectoid		0.43 (886, α)
Ti-Si	~6	[47]	Eutectic		~5 (1330, β)
			Eutectoid	Sub.	0.67 (850, α)
Ti-Y	~1.0	[48]	Monotectic		0.5 (1355, β
			Peritectoid	Sub.	~0.2 (875, α)
Ti-Ce	~0.6	[49]	Monotectic		~2 (1390, β)
			Peritectoid	Sub.	~1 (900, α)
Ti-La	0.3	[48]	Monotectic		~1 (1550, β)
			Peritectoid	Sub.	~1 (900, α)

Sub: Substitutional Solid Solution
Int: Interstitial Solid Solution

4.2 MICROSTRUCTURAL REFINEMENT

Microstructural refinement in rapidly-quenched Ti alloy can be achieved indirectly and directly. The former involves quenching the melt into glassy phases from which crystalline phases are generated by devitrification and microstructure controlled by means of heat treatment conditions [50]. Hence, the final microstructures are directly related to the devitrification conditions. Easy glass formation of an alloy is dependent upon phase diagram features (alloy chemical factors) [51,52], undercooling (nucleation and growth mode factor) [53,54], and cooling rate (processing factor) [55,56]. Hence, any comparison of glass forming properties between two arbitrary compositions requires evaluation of these factors. Typical Ti alloy systems yielding glassy phases include Ti-Ni, Ti-Si, Ti-Cu, Ti-Ni-Si, Ti-Zr-Si(or B) [38,57,58]. These glassy phases turn into extremely fine microstructures upon devitrication through appropriate heat treatment [10,50]. Although devitrified Ti alloys generate extremely fine microstructures and mechanical strength, they contain a large volume fraction of intermetallic compounds or metalloid compounds. To date, bulk alloy processing and applications have not been explored.

Direct refinement has been well recognized in the study of other alloy systems. The dendritic arm spacing [59,60], eutectic interphase spacing [61] and grain size [62] of as-quenched alloys are of an exponential function of cooling rate, i.e., $\xi = A \cdot \dot{T}^{-n}$ where ξ, A, $\dot{T}$ and n are microstructural scale, proportionality constant, cooling rate and characteristic exponent, respectively. From the relationship, conversely, the cooling rate can be estimated by measuring microstructural refinement. Figure 9 shows typical β-grain in $Ti\text{-}Mn_{10}$ after rapid quenching by H-A technique. Measured diameters of the β-grains produced by many different

techniques are plotted against the estimated cooling rate (Fig. 10). The correlation line is linear in a log normal scale, and has a slope n = ~ 0.4 [24]. Hence, the curve in the plot may be expressed as

$$d = A \cdot \dot{T}^{-0.4}$$

where d is grain diameter.

In a similar manner, α-phase also undergoes microstructural refinement upon rapid quenching. α-grain of high aspect ratio is seen in as-quenched $TiSn_{2.5}$ alloy foil (Fig. 11a). In contrast, in $TiZr_{10}Si_6$ alloy foil, refined cellular grains containing very fine martensitic structure are observed in Fig. 11b and c. Another example of refined martensitic structure is shown in Fig. 11d. These refined microstructures are typical examples occurring near Ti rich terminal compositions.

4.3 PRECIPITATES AND DISPERSOIDS

In the past, silicide dispersion has been the prime strengthener for high temperature Ti alloys at elevated temperatures, but below 600°C. The silicides provide good creep strength up to 600°C, but they coarsen rapidly above 600°C, resulting in reduction in creep strength as well as in post creep ductility. The dispersion in the Si-containing Ti alloys is titanium silicide, i.e., the Ti-containing compound. They are Ti_3Si (Hex., $D8_8$) in Ti-Si alloy systems [63,64] and $(Ti,Zr)_5Si_3$, a pseudo binary type compound in the Ti-Zr-(Al)-Si alloy system [1,2].

In contrast, Ti alloys containing rare-earth metals, which have been processed through rapid solidification, evidence rare earth dispersion (without Ti) in the as-quenched as well as annealed state. These

dispersoids may be classified into two different types: 1) rare earth oxide and 2) intermetallic compounds between rare earth (R.E.) and alloying elements (Al, Sn, etc.). Those dispersoids in binary Ti-R.E. systems were identified as sesquioxide ($R.E._2O_3$) [65], since a significant amount of oxygen already is dissolved in pure titanium. Ternary Ti alloys containing Al (or Sn) and R.E. were found to contain both oxide and R.E.-Al (or -Sn) intermetallic compounds [35,38]. Extraction replicas, prepared from Ti-5Al-3La foil annealed at 900°C/1h, yield diffraction ring patterns of Al_3La (Hex. Do_{19}) and Al_4La (Orth., DI_3) identified by TEM [48,66]. Similarly, diffraction ring patterns of Ti-9.5Sn-5.3La alloy after heat treatment at 800°C/h were identified as α-Ti (matrix) and La_2Sn (Hex., $B8_2$) (dispersoids) [48]. Also extraction replicas (Fig. 12) from Ti-10Al-9Er foil were studied by electron microprobe. The microprobe spectra from different particles of the replica show different patterns (as shown in Fig. 12b and 12c, in which Fig. 12b exhibits spectra of Al and Er, while Fig. 12c shows only Er [36]), but no oxygen peak was found in the spectra since the sensitivity of the probe to the small amount of oxygen is limited. The dispersoid in $Ti_{89}Al_8Y_3$ alloy treated by laser surface melting was identified as Y_2O_3 by diffraction spot patterns [67]. All these observations lead to the conclusion that both oxide and rare earth intermetallic compounds coexist in the matrix unless Ti is purified free from oxygen. The oxygen concentration in Ti alloy varies depending upon starting materials, alloying process, and atmosphere during heat treatment. The fraction of oxide and intermetallic compound phase is determined by phase equilibria in the quaternary phase diagram including oxygen. These quaternary diagrams, however, have not been characterized so far. Table 3 includes recent findings in the identity of rare earth dispersoids in Ti alloys. It should be noted that silicides in rapidly

solidified Ti alloys take spherical shape, as opposed to the rod- or needle-shaped silicide precipitates in slowly cooled Ti alloys. The growth of silicide in the highly disturbed matrix containing a high concentration of defects is apparently different from the undisturbed matrix.

Table 3

Structure of Dispersion in Rapidly-Solidified Ti Alloy

Alloy wt %	Age Temperature °C	Identified Structure	Analytical Technique	Particle Shape	Ref.
Ti-Zr-Si	500-550	$(Ti,Zr)_5Si_3$ $D8_8$		Equiaxed Rapid Sol.	1,2
Ti-Y(Ce,Dy,Er Gd,La,Nd)		RE_2O_3 Sesquioxide	TEM & Auger	Circular or Rectangular	65
Ti-8Al-4Y (at .%)	Laser Melting	Y_2O_3	TEM	Circular or Disk	67
Ti-5Sn-3Y	700	Y_5Sn_3 & Y_2O_3	CER-EDXS-EDRP	Circular or Rectangular	68
Ti-5Al-4.5La	700	Al_3La & Al_4La	CER-EDRP	Circular	48,66
Ti-5Sn-4.5La	700	La_2Sn	EDRP-EELS	Circular	48

CER: Carbon Extraction Replica; EDXS: Energy Dispersive X-ray Spectroscopy; EDRP: Electron Diffraction Ring Pattern; EELS: Electron Energy Loss Spectroscopy

4.4 MICROSTRUCTURAL COARSENING

Recently, Ostwald ripening of silicide in rapidly-quenched Ti-5Al-2Si alloy has been studied at 700°C and 800°C, respectively. Figures 13a and b show bright field micrographs of as-quenched Ti-5Al-2Si splat foil and the

coarsened silicide particles after 800°C/4h in Ti-5Al-2Si alloys. The measured particle radius is plotted against annealing time (shown in Fig. 14a), and the cube of the radius against annealing time yields a linear correlation (Fig. 14b), indicating that volume-diffusion is the dominant mechanism at these temperatures. From the slope in Fig. 14b, the coarsening rate (m^3/sec) was determined as listed in Table 4. The diffusivity of solute (Si) was calculated (Table 4) based on the assumption that the coarsening process is controlled solely by solute, and the volume fraction factor is assumed according to one of the existing models [69]. The results show that a high coarsening rate is caused by high diffusivity of solute (Si). A time invariant distribution function $\rho^2 h(\rho)$ [70] was plotted against ρ, defined as $r/\bar{r}$ where $\bar{r}$ is average particle radius, shown in Fig. 15. A significant deviation in size distribution from the LSW model [71,72] at high ρ values was observed, i.e., the size range in Ti-5Al-2Si was wider than that predicted in the LSW model. Also, coarsening behavior of rare-earth particles (La_2Sn) in Ti-5Sn-4.5La was studied by TEM [73]. Figs. 16a and 16b show micrographs of as-quenched and annealed (800°C/60h) Ti-5Sn-4.5La foils. No particle larger than 50Å dia. can be found in the as-quenched alloy (Fig. 16a).

The radii of the coarsened particles (identified as La_2Sn) are plotted against annealing time at 800°C (Fig. 17). At this temperature, coarsening is again governed by the volume diffusion mechanism. All these measured values and estimated diffusivity of solutes are tabulated in Table 4. The much slower coarsening rate of La dispersoids when compared with silicide in Ti, is very impressive. The estimated diffusivity of La is three orders of magnitude lower than that of Si at 800°C. Superior coarsening resistance of La dispersoids provides high temperature strength (>600°C), which will be

discussed in the next section.

The effect of rare earth addition to Ti on microstructural kinetics was studied [74]. The addition of Y increases the incubation time of recrystallization and decreases recrystallization rate. In contrast, grain growth kinetics in Ti-Er, Ti-Y and Ti-Al-La [36] show that the time exponent n remains less than 0.5. ($D=kt^n$, where D, K, and t are grain diameter, proportionality constant, and annealing time, respectively.) Nonetheless, no apparent effect of rare earth addition (Ti-Er, Ti-Y) on n value was observed.

Table 4

Determined Particle Coarsening Parameters in RS Ternary Ti Alloys

Alloy Composition	Dispersoid	Total Volume Fraction of Precipitate (%)	Coarsening Rate (m^3/sec)	Estimated Diffusivity of Solute (cm^2/sec)	Ref.
Ti-5Al-2Si	Ti_5Si_3	~8	2.1×10^{-27} (700°)	$\sim 7.5 \times 10^{-13}$	6
			3.45×10^{-26} (800°C)	$\sim 1.2 \times 10^{-11}$	
Ti-5Sn-4.5La	La_2Sn	1.4	9.4×10^{-29} (800°C)	$\sim 4 \times 10^{-14}$	73

5. MECHANICAL PROPERTIES

Preliminary investigation has shown the achievement of significant improvement in the mechanical properties of binary and ternary Ti alloy systems processed by RSP. The properties investigated comprise a) ambient temperature strength: yield strength, ultimate tensile strength, hardness and elongation and b) high temperature strength: yield strength, ultimate tensile strength, hardness, elongation, and creep. Nevertheless, microstructure sensitive properties such as fatigue and fracture toughness have not been reported on in depth.

5.1 AGE HARDENING

One of the distinctive phenomena in rapidly solidified Ti alloys containing metalloids and rare earth metals is age hardening arising from heat treatment after rapid quenching by either solution treatment (Si additive) or liquid quenching (all other additives). Details of age hardening were reported in liquid quenched $TiZr_{10}Si_x$, where x=2-8 [47]. The results show that strength increase is attributed to precipitation of silicide particles. The silicide particles maintain equiaxed shape after coarsening at high temperature. The precipitates take two types of intermetallic compounds: 1) Ti containing compounds; 2) non-Ti containing compounds, i.e., rare earth - oxides and rare earth - simple metal compounds. The degree of supersaturation, cooling rate or additive concentration, therefore, determines the intensity of aging. Figures 18 and 19 show typical aging behavior of rare earth containing alloys upon isothermal annealing and isochronal annealing, respectively. The aging temperature (~700°C) is much higher than that in silicon containing alloys (~500°C). The isochronal annealing experiment confirms the aging behavior and overaging at high temperatures (800-900°C) [32].

5.2 AMBIENT TEMPERATURE STRENGTH

When Ti alloys are rapidly quenched and consolidated into bulk form, room temperature strength can increase by as much as 15-40% from that of conventional alloys of similar composition processed by ingot metallurgy. Typical examples are given in Table 5; these examples demonstrate significant improvement in both strength and elongation as a result of changing the processing technique from ingot metallurgy to rapid solidification processing. Furthermore, rapid

solidification permits the least soluble solute in Ti to dissolve into the Ti matrix, which is not possible through conventional ingot metallurgy. As a result, in rapidly quenched Ti alloys, the volume fraction of dispersoids can be controlled at an optimum level. In particular, room temperature deformation is significantly affected by grain size, the size and volume fraction of dispersoids and oxygen concentration [75]. The former two parameters are controlled by cooling rate and heat treatment conditions, while the latter can be minimized by a non-reactive environment during hot temperature processing. Although strength measurements have been carried out on binary and ternary Ti alloy systems, experimentation on fracture toughness and fatigue has to be carried out in order to evaluate the overall impact of rapid solidification processing on mechanical properties.

5.3 HIGH TEMPERATURE PROPERTIES

For high temperature applications, the temperature dependence of mechanical properties in rapidly solidified Ti alloys has been studied in temperature ranges up to 900°C. The properties investigated are tensile strength, hot hardness, and creep strength. Tensile strength decreases in RS-Ti alloys containing rare earth metals below 600°C as a result of lattice softening and weakening of work hardening (dislocation dissipation). It is shown that, at 700°C, ultimate tensile strength decreases nearly to the yield stress (Fig. 20); i.e., there is an absence of work hardening, while grain growth (α-phase) and coarsening of rare earth dispersoids are minimal below 600°C. Figure 21 shows sharp decreases in microhardness of Ti-5Al-4.5La alloys above 600°C.

On the other hand, under isothermal conditions at elevated temperatures (above 600°C), softening progresses as a function of time, resulting from grain growth and particle coarsening. Such an event with Ti-5Ai-4.5La alloy

undergoing softening at an annealing time at 900°C is demonstrated in Fig. 22. The calculated Hall-Petch stress (σ_{H-p}) and Orowan-Ashby stress (σ_{O-A}) [76] support the above explanation [36].

Preliminary creep experiments on binary Ti-1.5Nd and Ti-1.0Er reveal that a significant creep rate reduction is seen at intermediate temperatures (~700°C), while mild improvement is shown in creep resistance at low temperatures (~482°C). Such a discrepancy comes from the fact that the dispersoid does not interact with diffusion creep at low temperatures, but becomes an effective barrier to dislocation creep by pinning dislocation [75].

For further understanding of the relationships between processing, microstructures and properties in RS Ti alloys, standardized processing methods and subsequent characterization of mechanical properties are desired in the future.

Table 5

Comparison of Mechanical Properties of Rapid Solidification Processed (RSP) and Ingot-Metallurgical (I/M) Ti-Al-Er Alloys [77]

Alloy	Heat Treatment	Yield Stress (MPa)		Ultimate Tensile Stress (MPa)		Total Elongation (%)	
		RSP	I/M	RSP	I/M	RSP	I/M
Ti-5Al-2Er	ST	670	469	735	536	27.0	—
Ti-7.5Al-2Er	ST	850	680	920	756	—	7.0
Ti-9Al-2Er	ST	880	750	928	790	11.0	0.1
Ti-5Al-2Er	STA (625°C)	700	510	763	564	13.8	10.0
Ti-7.5Al-2Er	STA (625°C)	952	815	973	843	7.7	6.0
Ti-9Al-2Er	STA (625°C)	931	802	952	824	1.6	0.2
Ti-5Al-2Er	STA (550°C)	714	515	780	590	54.0	18.0
Ti-7.5Al-2Er	STA (550°C)	973	830	990	865	12.0	9.0
Ti-9Al-2Er	STA (550°C)	—	810	—	835	—	0.3

ST = Solution treat at 860°C for 3 h and water quench
STA = ST plus aging at 625°C for 25 h or 550°C for 500 h

6. CONCLUSION

Currently, the development of rapidly solidified Ti alloy is confined to laboratory scale, though it has demonstrated a strong potential for developing into industrialized products. There is no doubt that refinement of rapid solidification processing techniques will likely stimulate more detailed research and eventually lead to industrialized applications. It has been shown that general scientific principles involved in rapid solidification technology are also applicable to Ti alloy systems. As a result, similar benefits deriving from RST are anticipated from RS Ti alloy application. Although only RS processed high temperature α-Ti alloys were discussed in this review, α/β Ti alloys or β-Ti alloys also can be processed by RST in an effort to improve desired properties. Research in this area will undoubtedly be opened up in the near future when RS Powder processing techniques gain their maturity parallel to titanium alumide research.

ACKNOWLEDGEMENTS

The author greatfully acknowledges the support of the Office of Naval Research for rapidly solidified Ti research. I would like to thank Drs. F.H. Froes, S. Krishnamurthy, R.E. Maringer, and S.M.L. Sastry for permitting me to cite unpublished materials and providing me valuable photos for this review. For continuing support of rapidly solidified materials programs I also thank Prof. B.C. Giessen and the Barnett Institute of Northeastern University. [Contribution #241 is from the Barnett Institute.] Finally, thanks as well are due to Mrs. Jean Chatoff for help in the preparation of the manuscripts.

REFERENCES

1. K. C. Antone, Trans AIME, 242 (1968) 1454.
2. H.M. Flower, P.R. Swann, and D.R.F. West, Met. Trans., 2A (1971) 3289.
3. N.E. Paton and M.W. Mahoney, Met. Trans., 7A (1976) 1685.
4. C.G. Rhodes, N.E. Paton, and M.W. Mahoney, J. Metals, 30 (1978) 54.
5. D. Eylon, S. Fujishiro, P.S. Postans, and F.H. Froes, J. Metals, 36 (1984) 55-62.
6. S.H. Whang, Y.Z. Lu, and B.C. Giessen, Proc. MRS Symposium, 28 (1984) 367-373.
7. J. Stringer, Acta Met., 8 (1969) 758.
8. P. Kofstad, J. Less-Common Metals, 12 (1967) 449.
9. S.M.L. Sastry, T.C. Peng, P.J. Meschter, and J.E. O'Neal, J. Metals, 35, No. 9 (1983) 21-28.
10. S.H. Whang, J. Metals, 36 (1984) 36-40.
11. S.H. Whang, U.S. Patent No. 4,512,826 (1985).
12. D. Shechtman, M.J. Blackburn, and H.A. Lipsitt, Met. Trans., 5A (1974) 1373-1381.
13. C.G. Rhodes, C.H. Hamilton, and N.E. Paton, in Report AFML-TR-78-130 (1978).
14. H.A. Lipsitt, D. Shechtman, and R.E. Schafrik, Met. Trans., 11A (1980) 1369-1375.
15. S.M.L. Sastry and H.A. Lipsitt, in Proceedings of the 4th Int. Conf. on Titanium, H. Kimura and O. Isumi, eds., The Metallurgical Society of AIME, (1980) 1231-1243.
16. M.J. Blackburn and M.P. Smith, U.S. Patent No. 4,294,615 (Oct. 1981).
17. P.L. Martin, M.G. Mendiratta, and H.A. Lipsitt, Met. Trans., 14A (1983) 2170.
18. R.J. Kerans, Met. Trans., 15A (1984) 1721.
19. E.J. Chapin and R. Liss, Report of NRL Program (December 1955).
20. B. Love, WADE Tech. Report, No. TR57-666, Part II (March 1959).
21. N.J. Grant, U.S. Patent No. 3,070,468 (1962).

22. M.B. Vordahl, U.S. Patent No. 3,622,406 (1971).

23. P.R. Roberts and P. Loewenstein, in Powder Metallurgy of Titanium Alloys, F.H. Froes and J.E. Smugeresky, eds., TMS-AIME (1980) 21-36.

24. T.F. Broderick, A.G. Jackson, and F.H. Froes, unpublished work.

25. R.E. Maringer and C.E. Mobley, J. Vac. Sci. Technol., 11, No. 6 (Nov/Dec. 1974) 1067-1071.

26. R.E. Maringer, C.E. Mobley, and E.W. Collings, The American Institute of Chemical Engineers, Vol. 74, No. 180 (1978) 111-116.

27. S.H. Whang, C.S. Chi, and Y.Z. Lu, submitted to Proc. Fifth Int. Conf. Rapidly Quenched Metals, S. Steeb and H. Warlimont, eds., Elsevier Science Publishers B.V., (1985) 115-118.

28. D.G. Konitzer, K.W. Walters, E.L. Heiser, and H.L. Fraser, Met. Trans. 15B (March 1984) 149-153.

29. S.M.L. Sastry, T.C. Peng, and J.E. O'Neal, Proc. Int. Powder Met. Conf. and Exh., Toronto, Canada (June 1984)..

30. E.W. Collings, R.E. Maringer, and C.E. Mobley, Technical Report AFML-TR-78-70 (1978).

31. H.H. Liebermann and C.D. Graham, IEEE Trans. Magn. MAG-12 (1976) 921.

32. S. Kavesh, in Metallic Glasses, J.J. Gilman and H.J. Leamy, ASM, Metals Park, Ohio (1976) 36-73.

33. S.H. Whang and B.C. Giessen, NBS Report on Rapid Solidification Processing, NBS Washington, D.C. (1982) 439-442.

34. H.H. Liebermann, J. Non-cryst. Sol., 61 & 62 (1984) 719-724.

35. P.R. Roberts and P. Loewenstein, in Powder Metallurgy of Titanium Alloys, F.H. Froes and J.E. Smugeresky, eds., TMS-AIME (1980) 21-36.

36. C.S. Chi and S.H. Whang, 1985 TMS-AIME Symp. on Rapidly Solified Materials, S.M.L. Sastry and B. McDonald, eds., in press.

37. S. Krishnamurthy, A.G. Jackson, H. Jones, and F.H. Froes, unpublished work.

38. D.E. Polk, A. Calka, and B.C. Giessen, Acta Met., Vol. 26 (1978) 1097-1103.

39. A.K. Sinha, B.C. Giessen, and D.E. Polk, in Treatise Solid State Chemistry, 3 (1976) 1-88.

40. W. Hume-Rothery, G.W. Mabbott, and K.M. Channel-Evan, Phil. Trans., R. Soc. London, Ser. A, 233 (1934) 1-97.

41. L. Darken and R. Gurry, in Physical Chemistry of Metals, McGraw-Hill, New York (1952) 86-90.

42. W. Hume-Rothery, in The Structure of Alloys of Iron, Pergamon Press, Oxford (1966).

43. Y.Z. Lu and S.H. Whang, TMS-AIME meeting, St. Louis, MO (October 1982), to be published.

44. E.W. Collings, in The Physical Metallurgy of Titanium Alloys, Chapter 4, American Society for Metals, Metals Park, Ohio (1984).

45. R. Ray, B.C. Giessen, and N.J. Grant, Met. Trans., 3A (1972) 627-629.

46. S.H. Whang and C.S. Chi, TMS-AIME Conference, New York, NY (February 1985), to be published.

47. S.H. Whang, Y.Z. Lu, and Y.W. Kim, J. Mat. Sci. Lett., 4 (1985).

48. C.S. Chi and S.H. Whang, unpublished work, to be published.

49. C.S. Chi and S.H. Whang, TMS-AIME paper selection F83-14 (1983).

50. S.H. Whang and Y.Z. Lu, Proc. Rapid Solidification Processing III, National Bureau of Standards (1982) 286-290.

51. D. Turnbull, J. Phys. (Paris), Colloque C4, 35 (1974) 1.

52. B.C. Giessen and S.H. Whang, J. Phys., Colloque C8, 41 (1980) 95-102.

53. J.H. Perepezko and J.S. Paik, in Rapidly Solidified Amorphous and Crystalline Alloys, B.H. Kear, B.C. Giessen, M. Cohen, eds., Elsevier, NY (1982) 42.

54. W.J. Boettinger, ibid., 99.

55. D.E. Polk and B.C. Giessen, in Metallic Glasses, J.J. Gilman and J.H. Leamy, eds., ASM, Metals Park (1978).

56. H.A. Davies, Rapidly Quenched Metals III, Vol. 1, B. Cantor, ed., The Metals Society, London (1978) 1.

57. S.H. Whang, Mat. Sci. and Eng., 57 (1983) 87.

58. S.H. Whang, Scripta Met., 18 (1984) 309-312.

59. W.E. Brower, R. Strachan, and M.C. Flemings, Cast Met. Res. J. 6 (1970) 176.

60. V.K. Sarin and N.J. Grant, Met. Trans., 8A (1972) 875.

61. W. Kurz and D.J. Fisher, Acta Met., 28 (1980) 777.

62. P.G. Boswell and G.A. Chadwick, Scripta Met., 11 (1977) 459.

63. H. Nowotny, H. Auer-Welsbach, J. Bruss, and A. Kohl, Monatsh. Chem., 90 (1959) 15-23.

64. L.V. Luzhnikor, V.M. Novikova, and A.P. Mareev, Metalloved i Term. Obrabotka Metal. 2 (1963) 13-16.

65. S.M.L. Sastry, P.J. Meschter, and J.E. O'Neal, Met. Trans., 15A (1984) 1451-1463.

66. C.S. Chi and S.H. Whang, Proc. MRS Sym., Elsevier Publishing Co., 28 (1984) 356-360.

67. D.G. Konitzer, B.C. Muddle, and H.L. Fraser, Met. Trans., 14A (1983) 1979-1988.

68. Y.Z. Lu and S.H. Whang, TMS-AIME Conf., New York (February 1985).

69. A.J. Ardell, Acta. Met., 20 (1972) 61.

70. A.J. Ardell and R.B. Nicholson, J. Phys. Chem. Solids, Vol. 27 (1966) 1793-1804.

71. I.M. Lifshitz and V.V. Slyozav, J. Phys. Chem. Solids, 19 (1961) 35.

72. C. Wagner, Z. Elecktrochem., 65 (1961) 581.

73. Y.Z. Lu, C.S. Chi and S.H. Whang, as [27], 949-952.

74. B.B. Rath et al., in Titanium '80, H. Kimura and O. Isumi, eds., AIME, Vol. 2 (1980) 1185-1196.

75. S.M.L. Sastry, T.C. Peng, and L.P. Beckerman, Met. Trans., 15A (1984) 1465-1474.

76. M.F. Ashby, Proc. Second Bolton Landing Conf. on Oxide Dispersion Strengthening, G.S. Ansell, ed., Gordon and Breach Science Publisher (1968) 143.

77. S. M. L. Sastry, T. C. Peng, and J. E. O'Neal, Proc. on Int. Powder Metall. Conf., Toronto, Canada (June 1984).

Figure Captions

Fig. 1 — Pendant Drop Melt Extraction Process [26]

a) Schematic Drawing
b) D-Shape Fiber Product. Photo courtesy of Dr. R.E. Maringer, Battelle Columbus Labs.

Fig. 2 — Arc Melt Spin Process

a) Schematic Drawing of Arc Melt Spinning Unit
b) Produced Ribbon and Chopped Ribbon Powder

Fig. 3 — Schematic Drawing of Laser Melt-Spin Atomizer [9]

Fig. 4 — Particle Size Distribution of Ti-6Al-4V Alloy [29]

a) Powder Diameter vs. Accumulative Weight Percent
b) Powder Diameter vs. Rod Rotation Speed

Fig. 5 — TEM Micrograph of Ti-5Al-4.5La Alloy

a) As-splat Foil by the Hammer-Anvil Technique
b) As-Quenched Ribbon by Arc Melt-Spinning Technique

Fig. 6 — TEM Micrograph of Ti-7.9Ni Fiber by Pendant Drop Melt Extraction [37]. Photo courtesy of Drs. S.S. Krishnamurthy and F.H. Froes, Air Force Wright Aeronautical Labs.

Fig. 7 — HIPed Ti-5Al-4.5La Alloy from Arc Melt Spin Ribbon

Fig. 8 — Ti-Fe Phase Diagram and Room Temperature Phases by Slow Cooling and Rapid Quenching

Fig. 9 — As-Splat Foil of $TiMn_{10}$ Alloy by H-A Technique

Fig. 10 — Plot of Beta Grain Size vs. Estimated Cooling Rate in Various Ti Alloys [24]. Courtesy of Dr. F.H. Froes, Air Force Aeronautical Labs.

Fig. 11 α-Phase Morphology in As-Quenched Binary Ti Alloys by H-A Technique

a) $TiSn_{2.5}$ Splat Foil
b) $TiZr_{10}Si_6$ Splat Foil
c) Dark Field Micrograph of b)
d) $TiNi_{2.5}$ Splat Foil

Fig. 12 Carbon Extraction Replica from Annealed Ti-5Al-5.4Er Alloy at 760°C/2h.

Fig. 12b Electron Microprobe Spectra of Carbon Extraction Replica from Ti-10Al-9Er Alloy annealed at 930°C/36h

Fig. 12c Electron Microprobe Spectra of Different Particles in the same replica

Fig. 13 TEM Micrographs of Ti-5Al-2Si Alloy

a) As-Splat Foil by H-A Technique
b) The Same Foil after Annealed at 800°C, 4h.

Fig. 14a Plot of Average Silicide Particle Size as a Function of Annealing Time in Ti-5Al-2Si

Fig. 14b Plots of Cube of Average Particle Radius vs. Annealing Time in Ti-5Al-2Si

Fig. 15 Relative Particle Size Distribution in Ti-5Al-2Si

Fig. 16 TEM Micrographs of Ti-5Sn-4.5La Alloy

a) As-Quenched Foil by H-A Technique
b) The Same Foil after Annealed at 800°C, 60h

Fig. 17 Plot of Cube of Average Particle Radius vs. Annealing Time in Ti-5Sn-4.5La

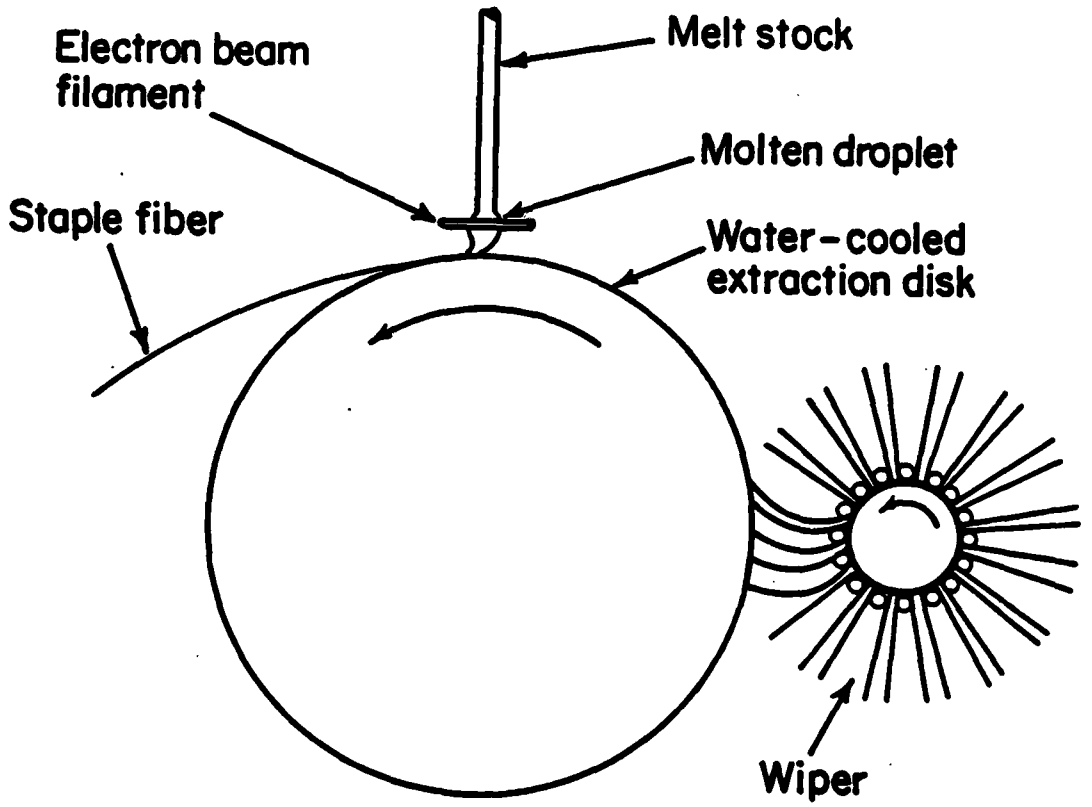

Fig. 1 Pendant Drop Melt Extraction Process

a) Schematic Drawing

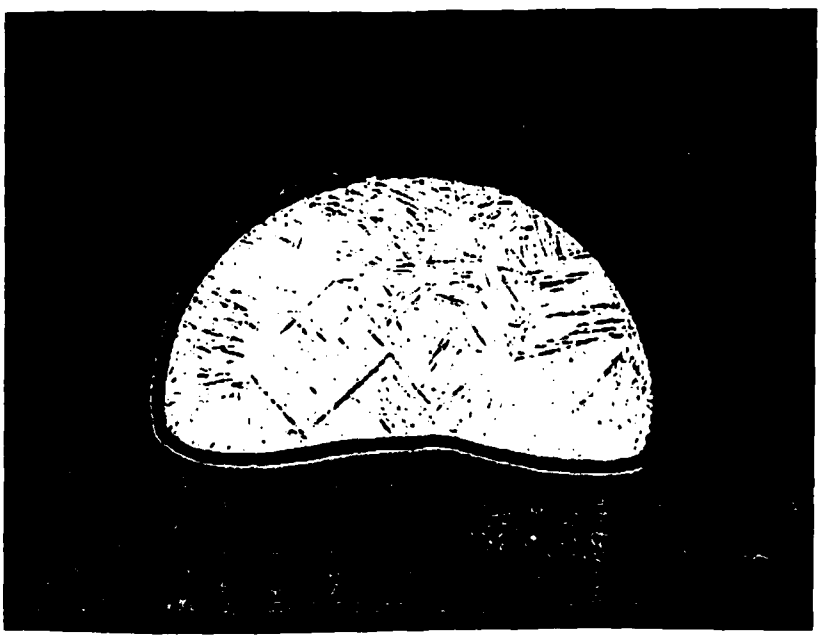

Fig. 1 Pendant Drop Melt Extraction Process

b) Shape Fiber Product

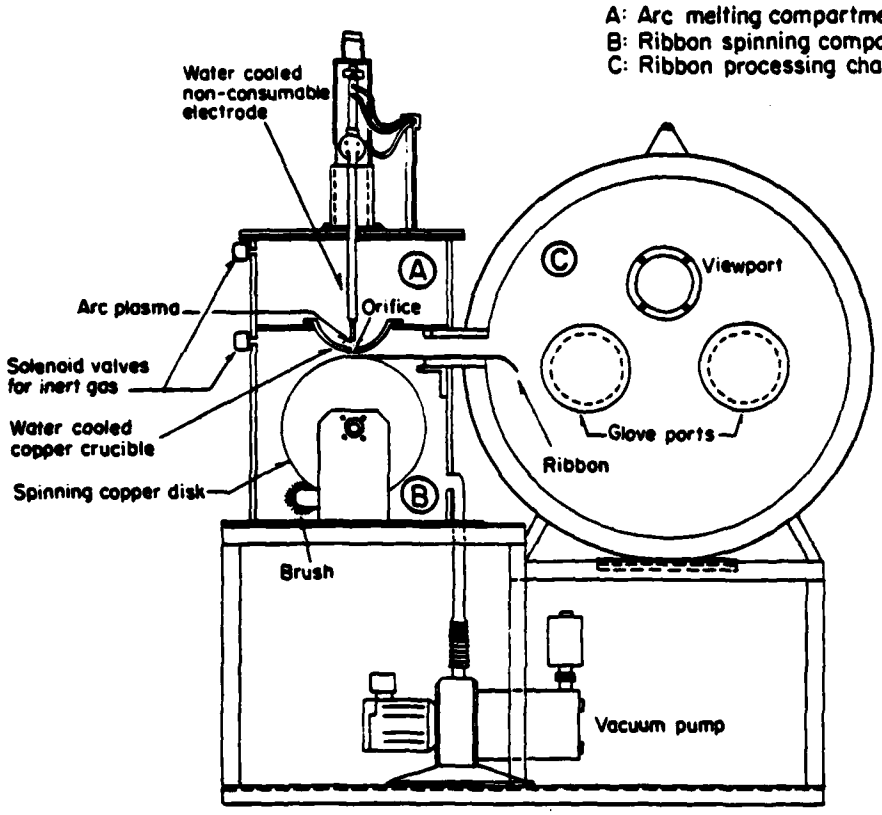

a) Schematic Drawing of Arc Melt Spinning Unit

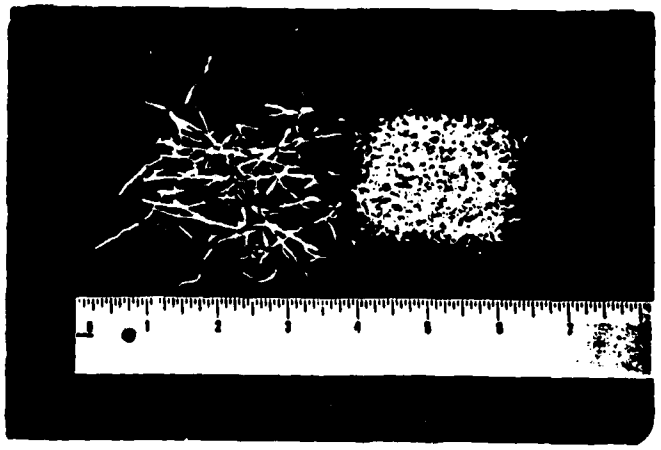

b) Produced Ribbon and Chopped Ribbon Powder

Fig. 2 Arc Melt Spin Process

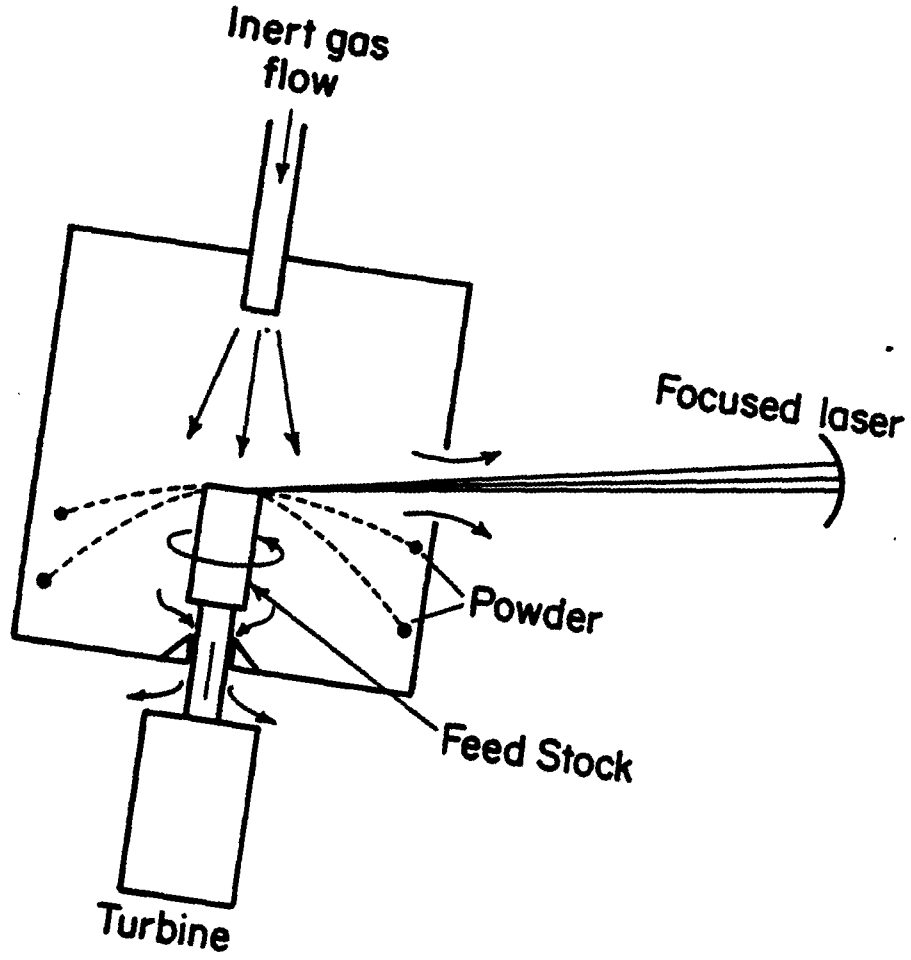

Fig. 3

Schematic Drawing of Laser Melt-Spin Atomizer

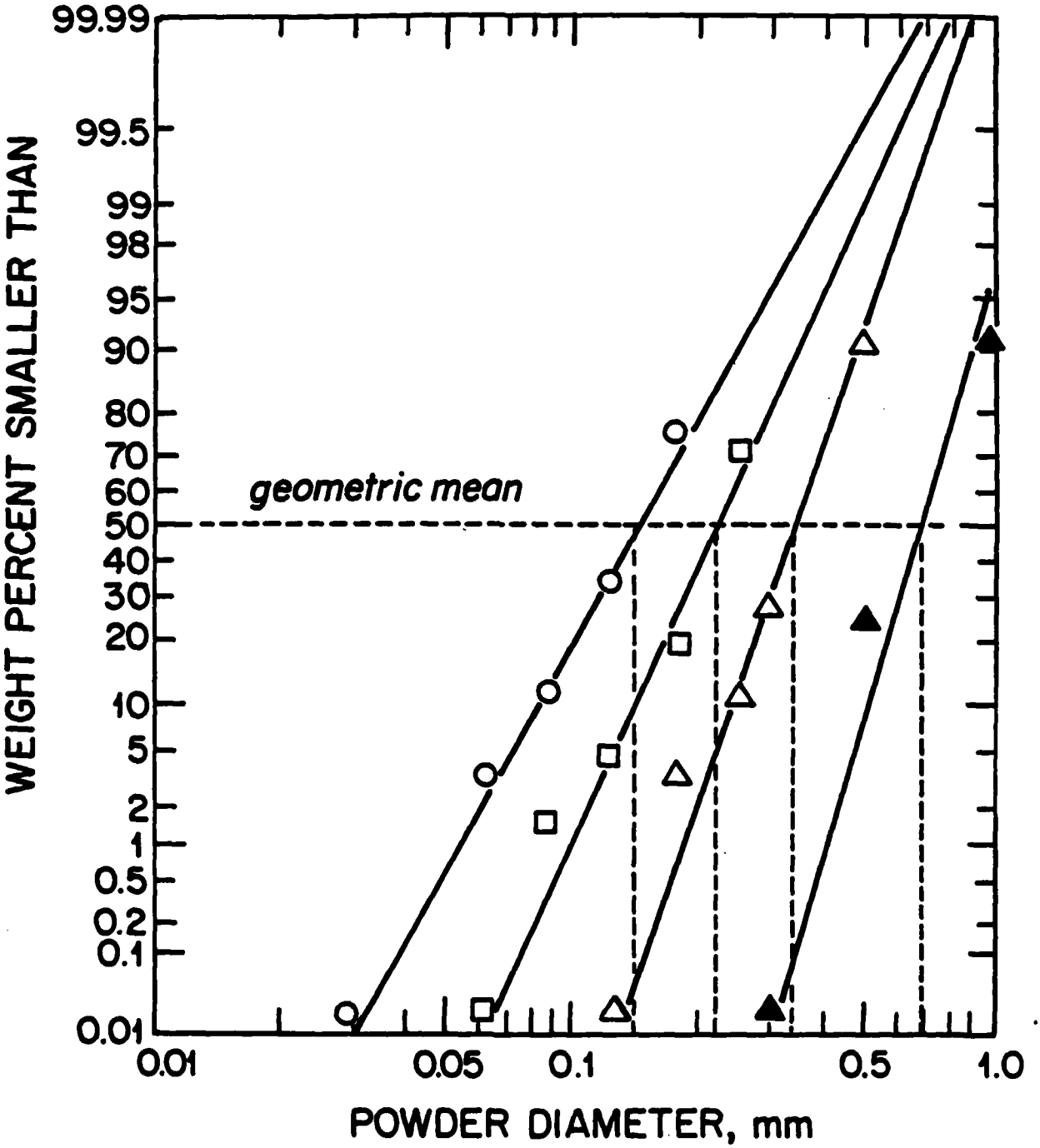

Fig. 4 Particle Size Distribution of Ti-6Al-4V Alloy

a) Powder Diameter vs. Accumulkative Weight Percent

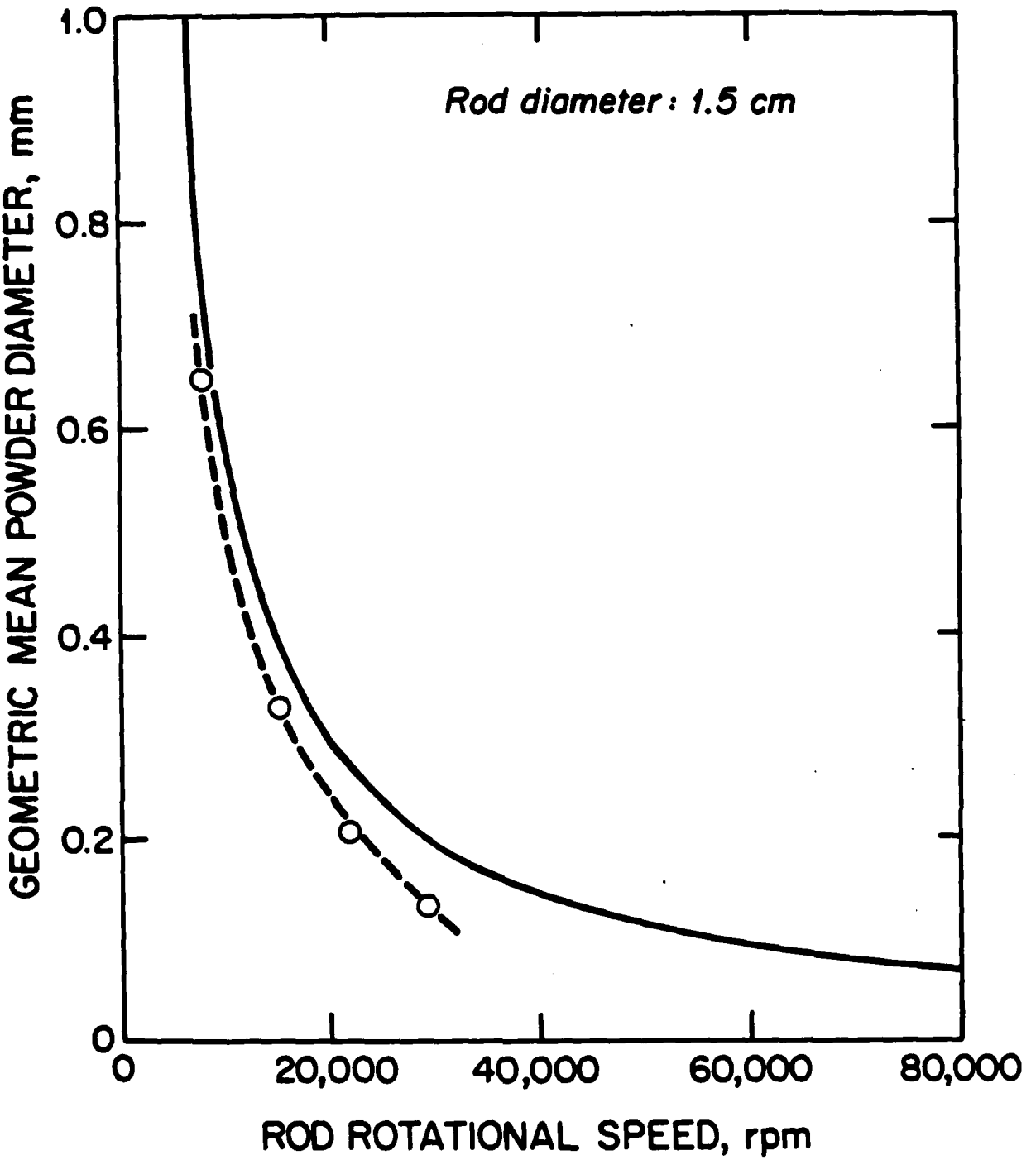

Fig. 4 Particle Size Distribution of Ti-6Al-4V Alloy

b) Powder Diameter vs. Rod Rotation Speed

Fig. 5 TEM Micrograph of Ti-5Al-4.5La Alloy
a) As-splat Foil by the Hammer-Anvil Technique

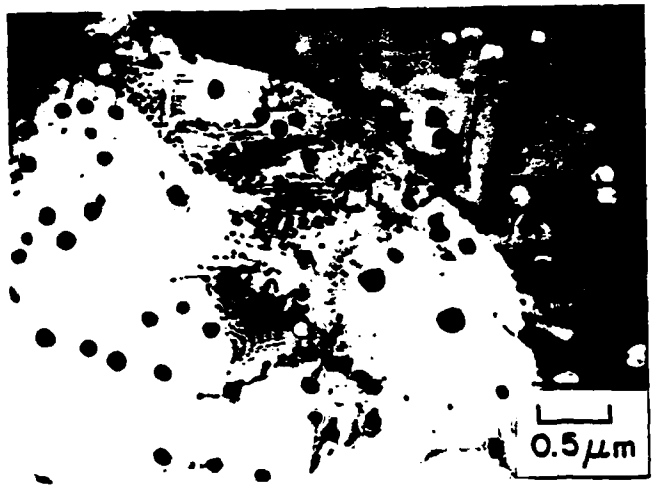

Fig. 5 TEM Micrograph of Ti-5Al-4.5La Alloy
b) As-Quenched Ribbon by Arc Melt-Spinning Technique

Fig. 6 TEM Micrograph of Ti-7.9Ni Fiber by Pendant Drop Melt Extraction

Fig. 8 Ti-Fe Phase Diagram and Room Temperature Phases by Slow Cooling and Rapid Quenching

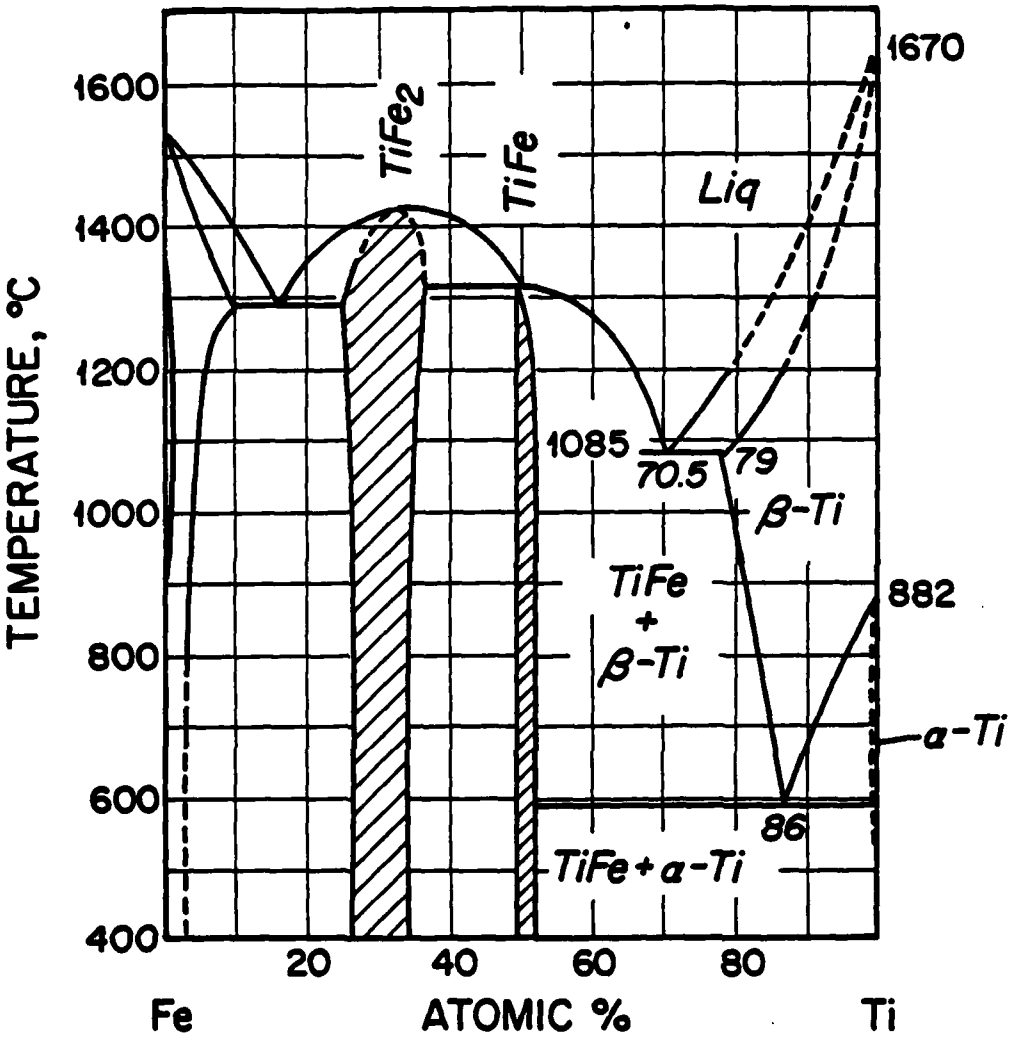

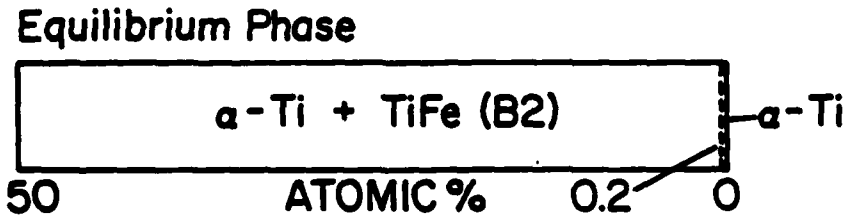

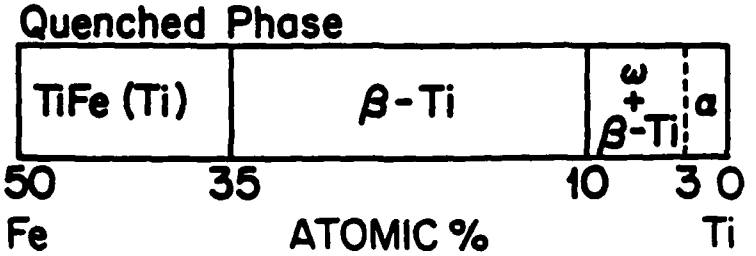

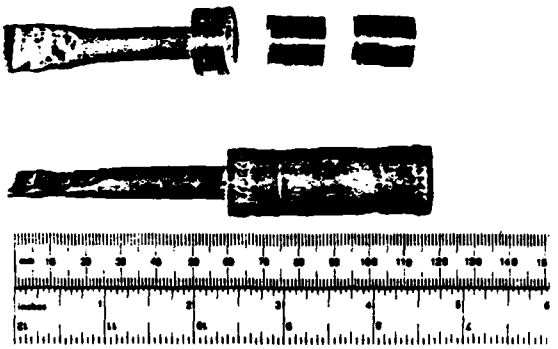

Fig. 7 HIPed Ti-5Al-4.5La Alloy from Arc Melt Spin Ribbon

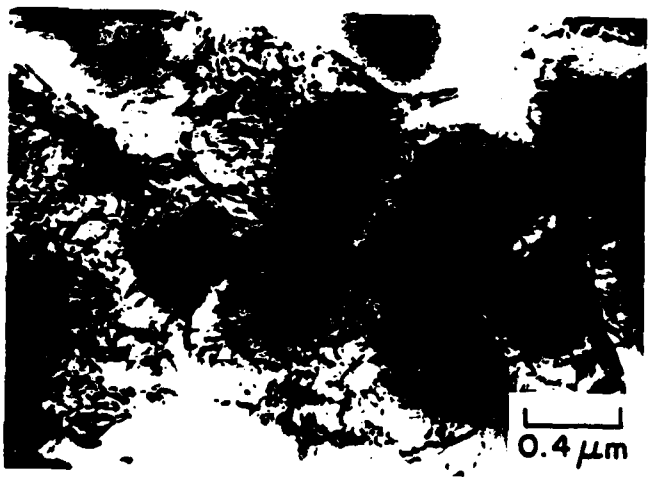

Fig. 9 As-Splat Foil of $TiMn_{10}$ Alloy by H-A Technique

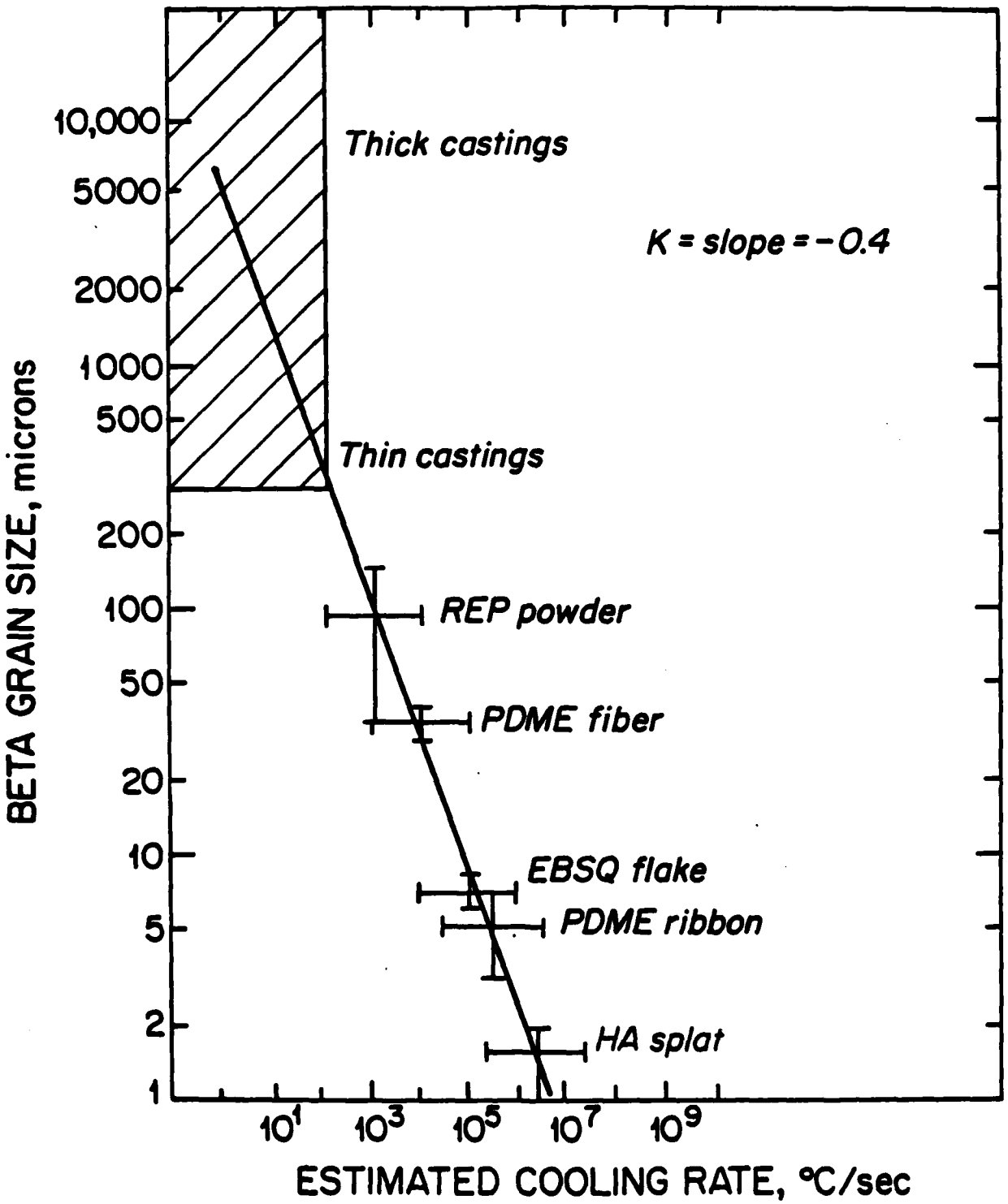

Fig. 10 Plot of Beta Grain Size vs. Estimated Cooling Rate in Various Ti Alloys

a) $TiSn_{2.5}$ Splat Foil

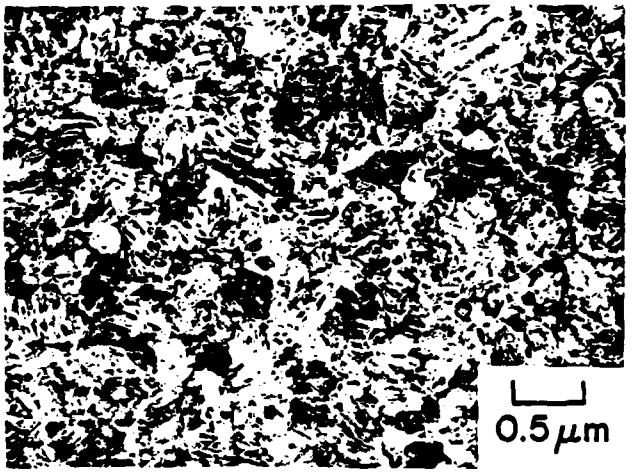

b) $TiZr_{10}Si_6$ Splat Foil

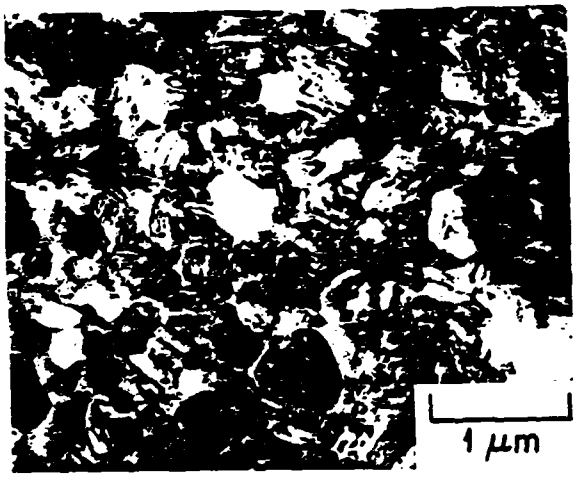

c) Dark Field Micrograph of b)

d) $TiNi_{2.5}$ Splat Foil

Fig. 11 α-Phase Morphology in As-Quenched Binary Ti Alloys by H-A Technique

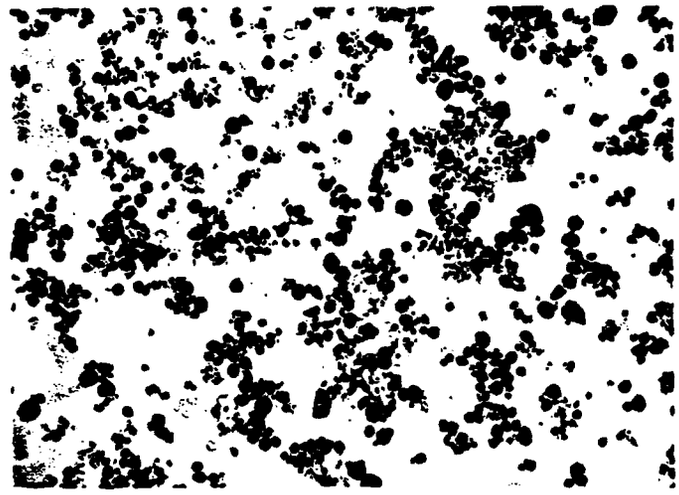

Fig. 12a Carbon Extraction Replica from Annealed Ti-5Al-5.4Er Alloy at 760°C/2h.

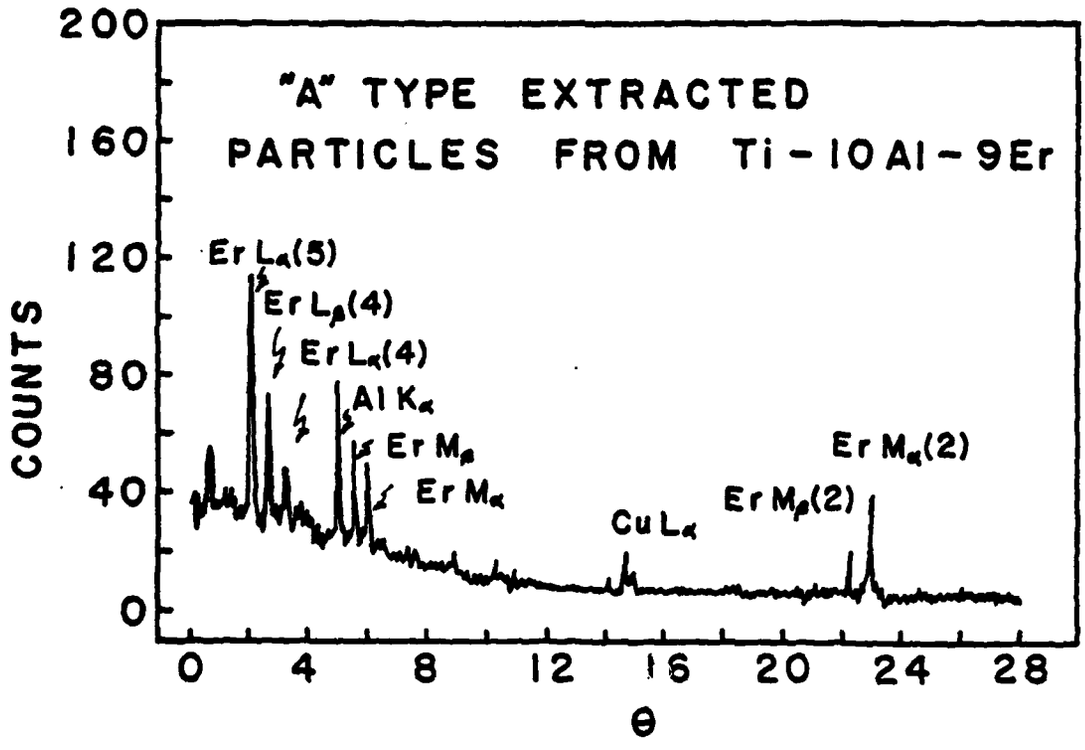

Fig. 12b Electron Microprobe Spectra of Carbon Extraction Replica from Ti-10Al-9Er Alloy Annealed at 930°C/36 h

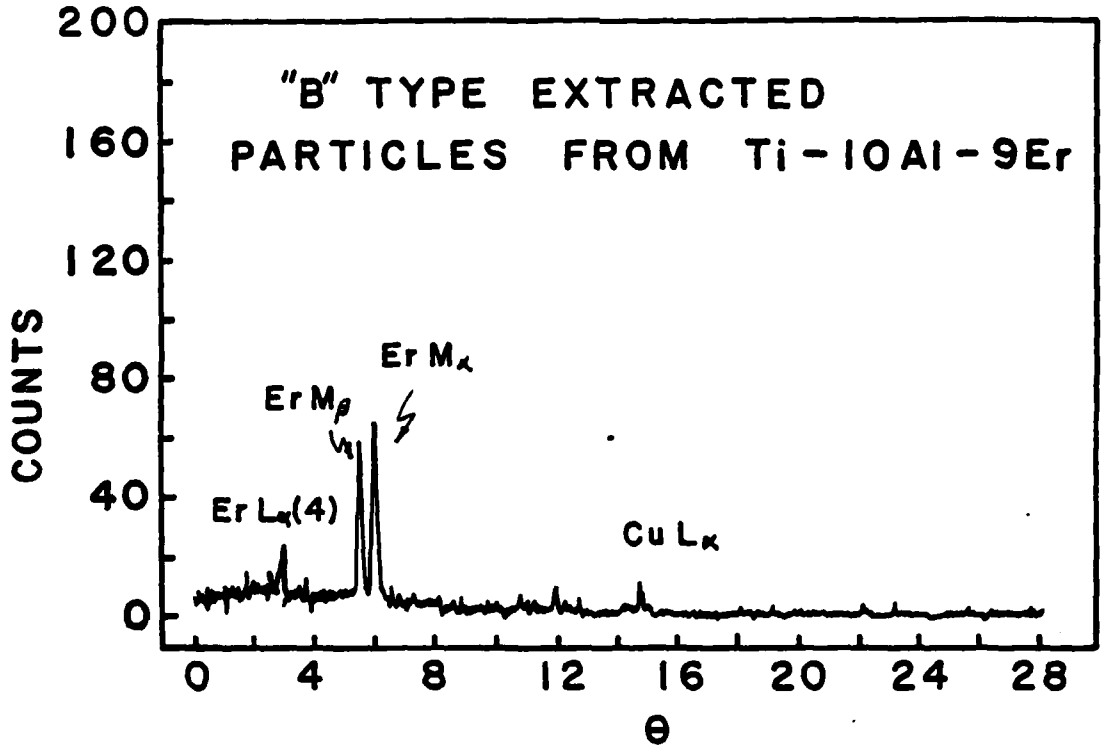

Fig. 12c Electron Microprobe Spectra of Different Particles in The Same Replica.

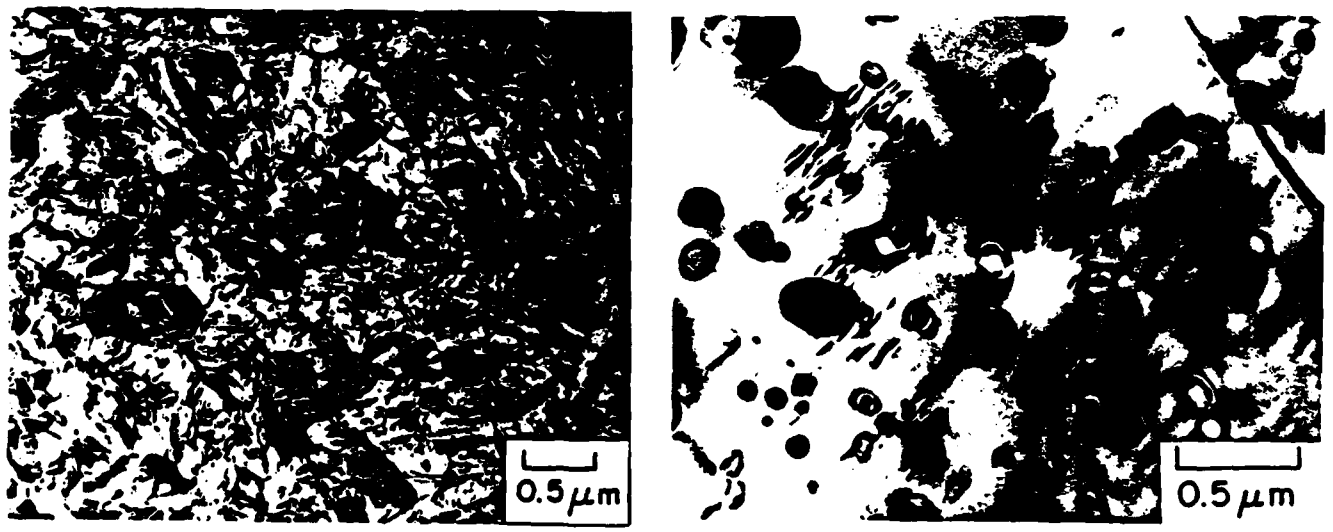

a) As-Splat Foil by R-A Technique

b) The same Foil after Annealed at 800°C, 4h.

Fig. 13 TEM Micrographs of Ti-5Al-2Si Alloy

Fig. 14b Plots of Cube of Average Particle Radius vs. Annealing Time in Ti-5Al-2Si.

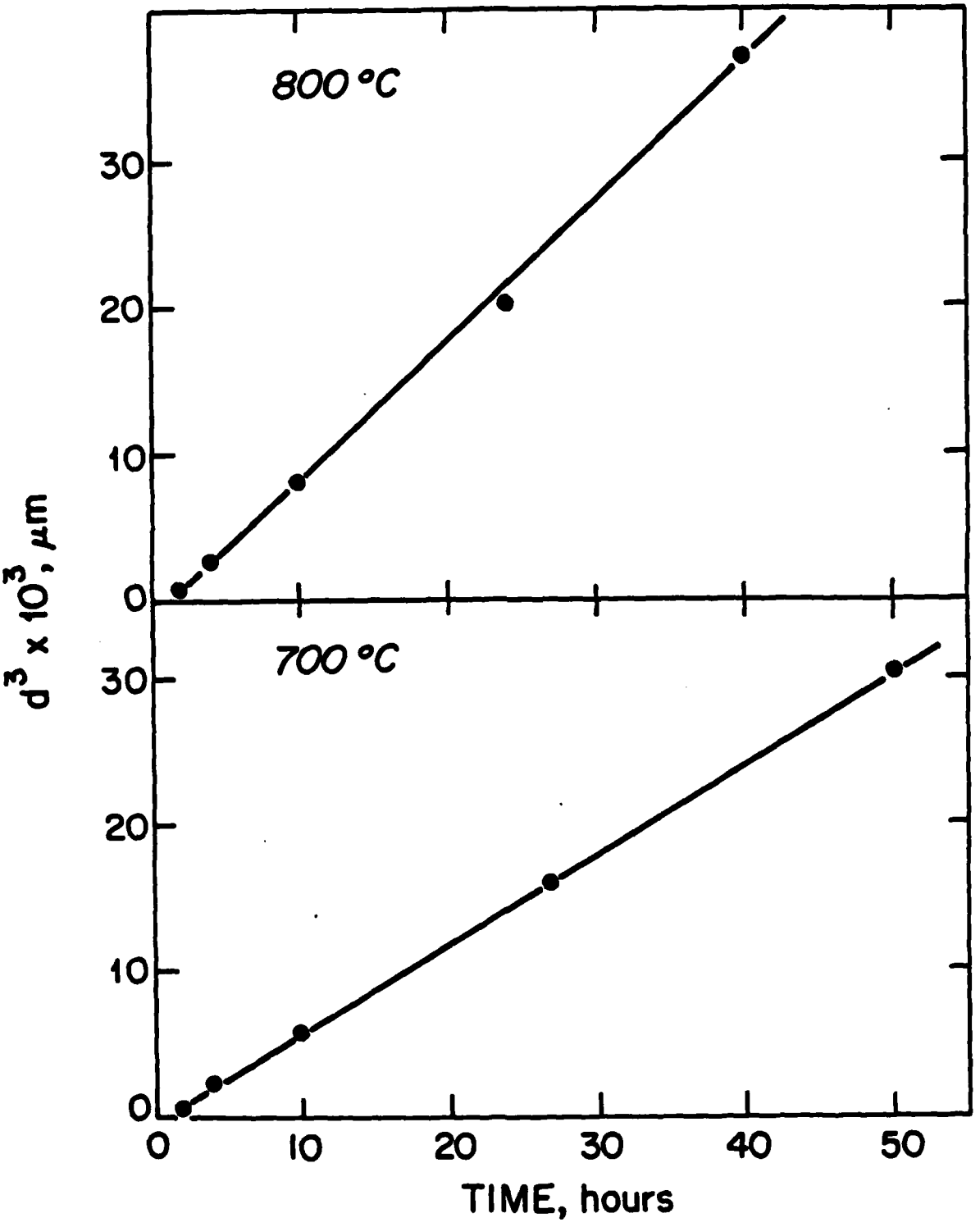

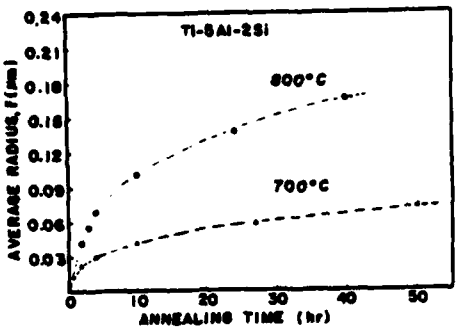

Fig. 14a Plot of Average Silicide Particle Size as a Function of Annealing Time in Ti-5Al-2Si.

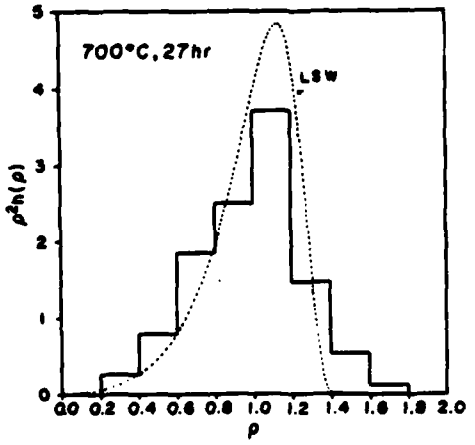

Fig. 15 Relative Particle Size Distribution in Ti-5Al-2Si

Fig. 16 TEM Micrographs of Ti-5Sn-4.5La Alloy

a) As-Quenched Foil by H-A Technique

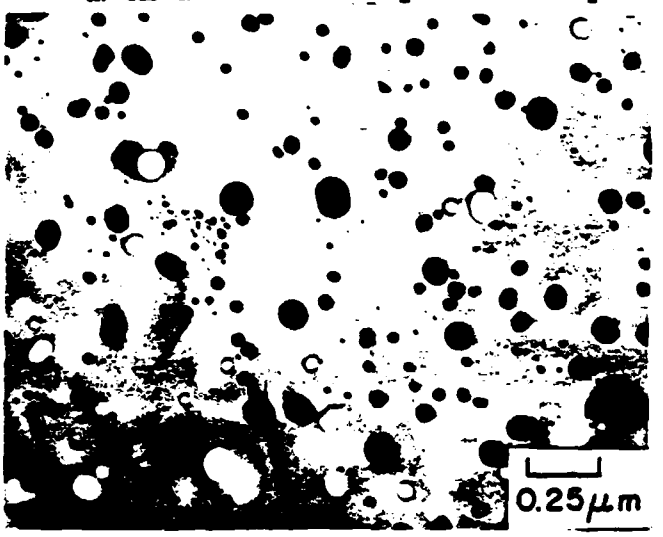

b) The Same Foil after Annealed at 800°C, 60h

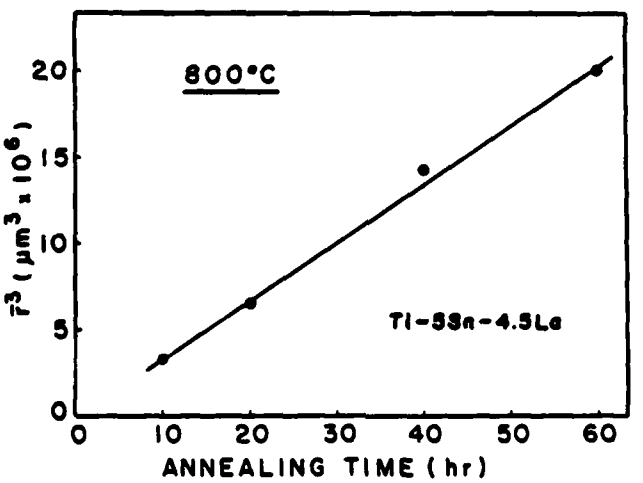

Fig. 17 Plot of Cube of Average Particle Radius vs. Annealing Time in Ti-5Sn-4.5La.

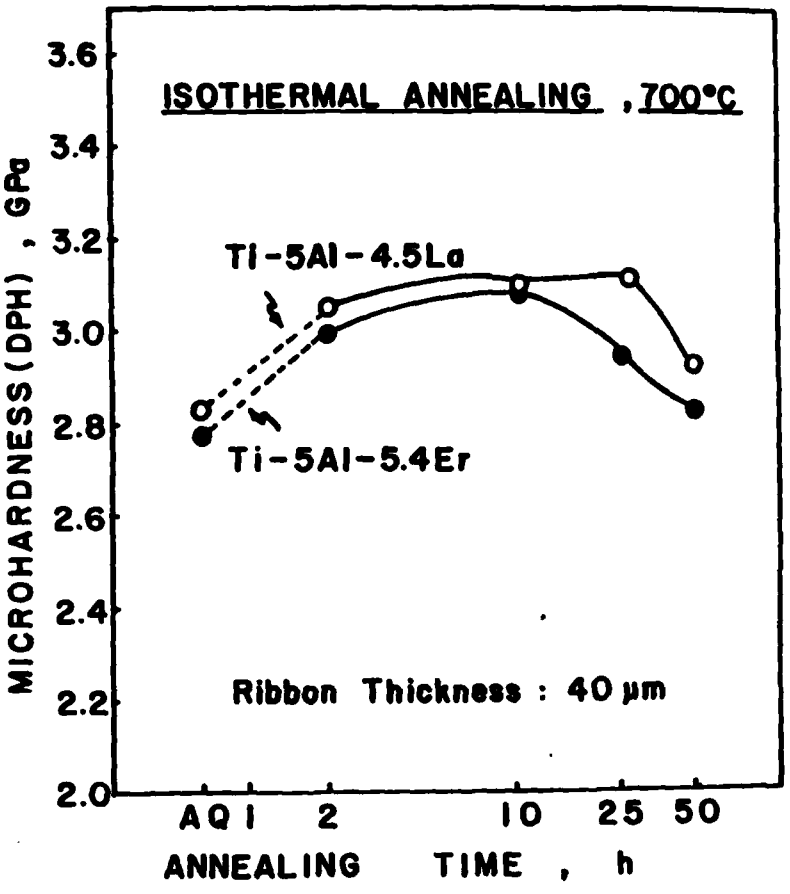

Fig. 18 Plot of Microhardness vs.Isothermal Annealing Time in Ti-5Al-4.5La and 5.4Er Ribbons

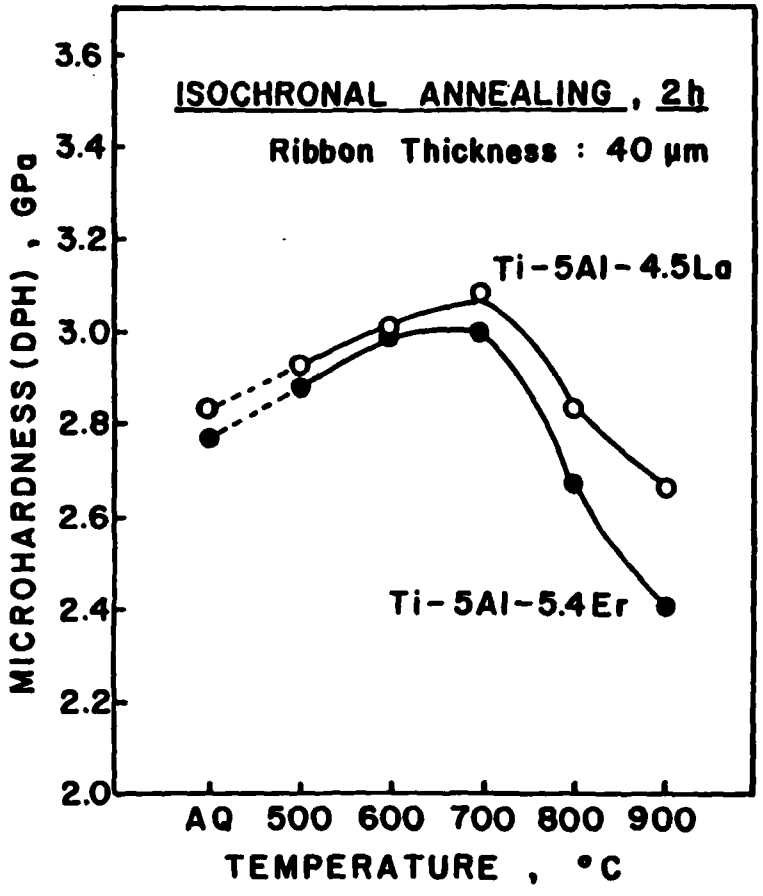

Fig. 19 Plot of Microhardness vs. Isochronal Annealing Time in Ti-5Al-4.5La and-5.4Er Alloy

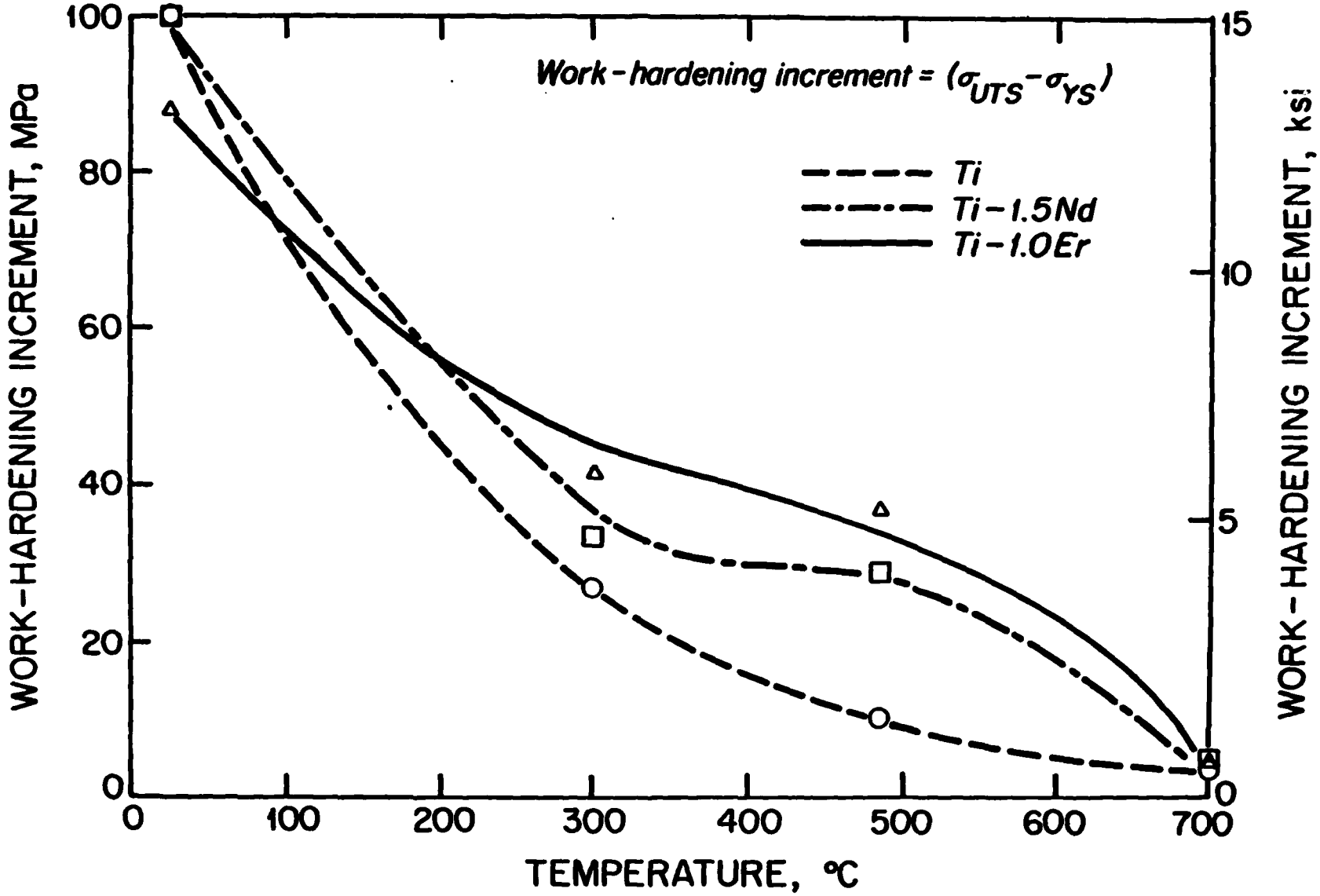

Fig. 20 Temperature Dependence of Work Hardening in Ti and Ti

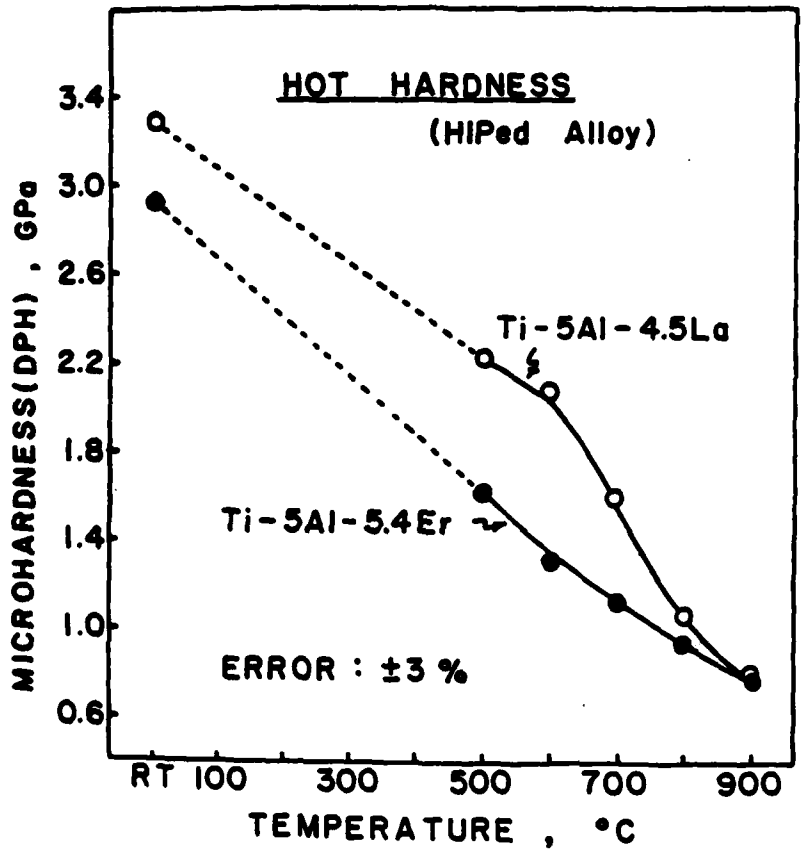

Fig. 21 Hot Hardness of HIPed Ti-5Al-4.5La and 5.4Er Alloys

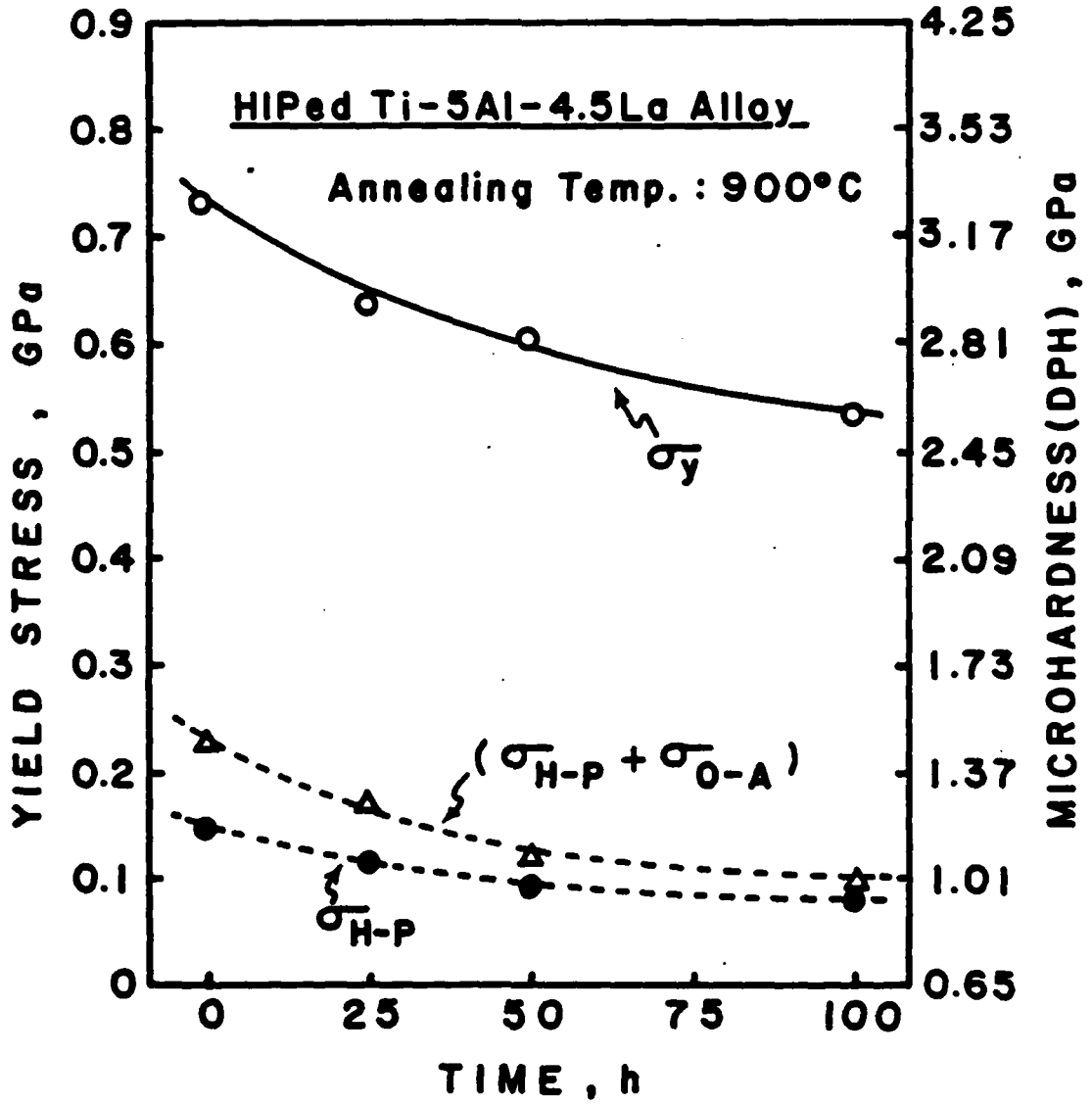

Fig. 22 Plot of Microhardness (or Yield Stress) vs. Annealing Time at 900°C in HIPed Ti-5Al-4.5La and -5.4Er.

ARC MELT SPIN PROCESS FOR REACTIVE AND REFRACTORY ALLOYS

S. H. WHANG

Submitted to ASM Sym. on Rapidly Solidified Materials, San Diego, Feb. 1986, P. Lee and R. C. Carbonara eds., ASM, Metals Park, OH, Proceedings in press.

Submitted to ASM Conference on Rapidly Solidified Materials
San Diego, February 3-5, 1986

"Arc Melt Spin Process For Reactive & Refractory Alloys"

Barnett Institute
Northeastern University
Boston, MA 02115

Abstract

Melt spinning of reactive and refractory alloys has been performed by arc melt spin process in a pilot-scale quantity. The preparation of a melt in the cold copper crucible is significantly different from that in the ordinary melt spinning. The temperature profile of the melt at the steady state condition as well as the melt-spinning parameters were investigated. The microstructure of melt-spun ribbons of Ti and Mo were studied by SEM, optical and electron microscopes.

RAPID SOLIDIFICATION PROCESSING AS AN ALTERNATIVE choice has become a center of attention in the field of materials processing since many conventional problems appear to be resolved and new alloy phases can be synthesized through this process [1]. In fact, many novel microstructures and alloy phases can be synthesized through imposing some contraints on thermodynamic hierarchy and kinetic process during rapid solidification [2,3].

Mass production of rapidly solidified metals and alloys has been primarily relied upon melt spin and atomization techniques. Both techniques use crucibles of a variety of materials such as quartz, ceramics, clay, graphite, etc. for the preparation of molten alloys. Nevertheless, processing of reactive or refractory alloys using these crucibles is not adequate since crucible materials react with the melt of reactive alloys or undergo softening at the molten temperatures of refractory alloys.

In order to overcome such problems, an arc furnace combined with a spinning disk was used [4,5]. The arc furnace consists of a cold copper crucible with an orifice and an electrode. This cold copper crucible was introduced into the melt spin process in order to prepare molten reactive alloys (Ti, Zr) or refractory alloys (W, Mo, Nb, Ta).

Presently, the arc melt spinning technique is available only in a bench scale as well as pilot scale. The melt spinning by the cold copper crucible is significantly different from ordinary melt spinning in that the melt prepared in the cold copper crucible developes a large temperature gradient between the bottom and the top surface of the melt. As a result, melting and spinning are performed rather under restrictive processing conditions.

This paper deals with such unique aspects of melt spinning conditions and presents resulting microstructures in Ti and Mo alloys.

ARC MELT SPIN PROCESSING

The pilot melt spinning unit is shown in Fig. 1 [2,3]. The cylindrical chamber on the left hand side consists of two compartments: the melting compartment at the top and the spinning compartment at the bottom. The chamber on the right hand side provides room for retrieving spun ribbons and for subsequent ribbon treatments including chopping and pulverizing in Ar atmosphere. The melting compartment contains a copper crucible with a water cooled jacket and a non-consumable tungsten electrode. The copper crucible has an orifice at the bottom, which allows the melt to flow onto a spinning disk beneath the orifice in the spin compartment. The configuration between the crucible and the disk is the same as that in the ordinary melt spinner. The gas pressure differential exerted on the melt tends to be higher in the arc melt spin process than that in the ordinary melt spin process.

present address:
Department of Metallurgy & Materials Science
Polytechnic Institute of New York
333 Jay Street, Brooklyn, NY 11201

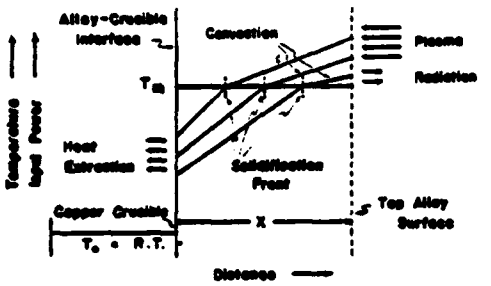

Fig. 5. A schematic diagram showing a possible temperature profile in the transient stage of alloy melting

gradient may exist in the molten zone due to the melt convention.

TEMPERATURE PROFILE - In the arc melt spin process, continuous casting can be performed, in principle, by continuous feeding of the fresh alloy into the crucible. In this case, preferably the feed alloy shoulb be preheated close to the melting temperature of the alloy in order to facilitate melting and superheating by the arc electrode. The heat conduction at steady state condition before casting is considered in the following.

$$k \frac{\partial^2 T}{\partial x^2} + \frac{q}{t} = 0 \qquad (1)$$

$$q = q_b + q_t + q_r \qquad (1\text{-}1)$$

$$q_b = h_i (T_b - T_o) \qquad (1\text{-}2)$$

$$q_t = h_c (T_s - T_a) \qquad (1\text{-}3)$$

$$q_r = \sigma \cdot \varepsilon \cdot (T_s^4 - T_o^4) \qquad (1\text{-}4)$$

where k,q and t are thermal conductivity of Ti, heat flux along x axis and thickness of the melt along x direction. Since k value is nearly constant as a function of temperature [6], Eq. 1 is roughly correct. In Eq. (1-2), q_b, h_i, T_b, T_o are heat flux at the bottom of the melt, heat transfer coefficient at the interface, temperature at the bottom of the melt, and room temperature. q_t, h_c, T_s, T_a in Eq. (1-3) are heat flux leaving at the top surface of the melt, heat transfer coefficient between the melt and argon gas, surface temperature of the melt, and the temperature of argon gas near the surface. In Eq. (1-4), q_r, ε, σ are heat loss rate due to radiation, total emissivity, and Stefan-Boltzman constant.

In equation (1-1), q_b is the dominant figure; q_t is very much dependent upon Ar gas temperature T_a; and q_r will increase with the depth of the melt since the surface temperature should increase with the melt depth to keep the bottom part molten. When the surface temperature increases above 2500°C in Ti alloy and 3000°C in Mo alloy, the heat loss due to radiation becomes a significant portion of the total heat loss.

On the other hand, when the melt starts to flow through the nozzle, and at the same time the fresh alloy is introduced into the melt from autofeeder. Additional heat loss occurs due to the temperature difference between the melt leaving the crucible and the fresh alloy. Additional heat requirement for the continuous casting, therefore, is

$$q_c = M * [C_p * (T_b - T_c) + H_f] \qquad (2)$$

where M, T_c, C_p, H_f are spun alloy mass per unit time, the temperature of fresh charge, average heat capacity, and heat of fusion at the temperature. Hence, this quantity is largely dependent on the pre-heating temperature T_c and the spinning rate M.

A complete description of the temperature profile in this case becomes extremely complex under the multi-electrode mode since the melt convection by arc heating is coupled with the melt flow toward the orifice. A comprehensive study of heat conduction in such a melt may be carried out by a numerical method.

MELT-SPIN PARAMETER - The spinning conditions for Ti and Mo alloys are listed in table 1.

By and large, ribbon thickness can be controlled by the disk speed and the orifice size as is the case in the ordinary melt spinning [7,8]. Nevertheless, the control of the orifice size is limited to a minimum ~1 mm diameter. Below this size, the melt flow meets resistance due to freezing or high viscosity of the melt. The ribbon thickness produced in both alloy systems ranges from 20μm to 50μm.

The spun Ti alloy ribbons are shown in Fig. 6 and the Mo alloy ribbon in Fig. 7. The difference between the two alloy ribbons is that Mo alloy ribbon has much more narrow

Table 1

Alloy	Orifice Size	Disk Speed	Gas Injection Pressure	Protective Atmosphere
Ti and Mo alloys	1 mm dia	20-40 m/sec	0.07-0.1 MPa	Ar

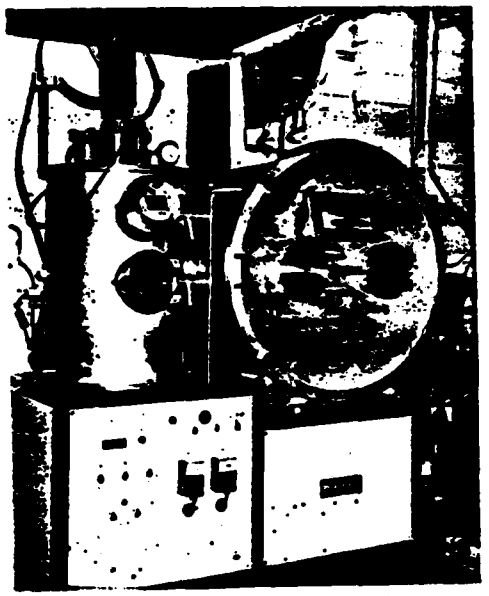

Fig. 1. Pilot arc melt spin unit/Front view

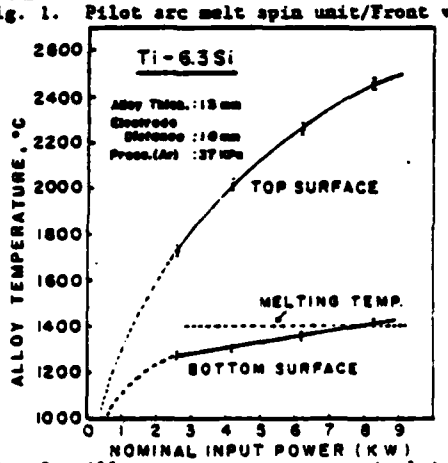

Fig. 2. Alloy temperature vs. nominal input power

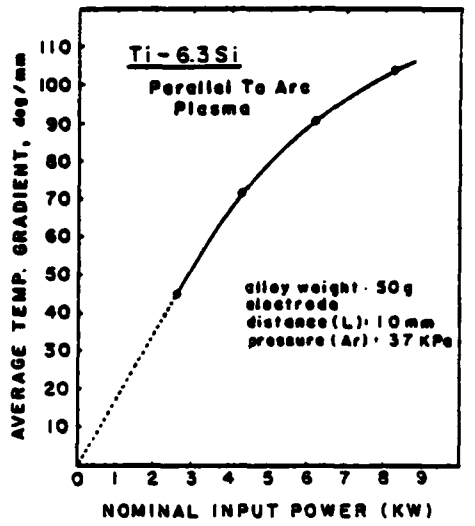

Fig. 3. Average temperature gradient vs. nominal input power

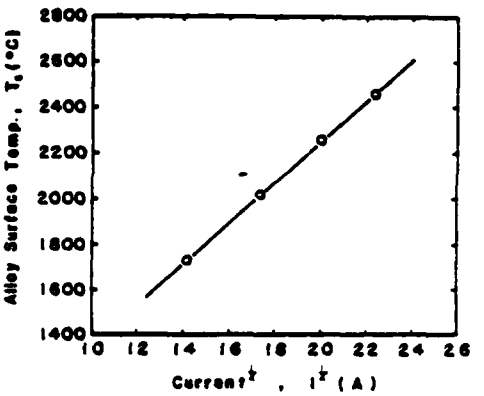

Fig. 4. Melt surface temperature vs. nominal current

MELTING - A coin shaped alloy button was melted in the cold copper crucible by a non-consumable, tangsten electrode. The temperatures of the top surface and the bottom surface of the button were monitored by optical pyrometer and thermocouple, respectively. Fig. 2 shows that the temperature increases with increasing nominal input power, i.e., more rapidly at the top and slowly at the bottom. This difference eventually leads to a large temperature gradient in the melt as shown in Fig. 3. The temperature of the top surface, where arc plasma impinge into the melt, increases proportionally to the square root of current (Fig. 4). Such temperature profile of the melt is significantly different from that of the melt in non-conductive crucible such as ceramic crucibles. As a result, the melt tends to develop a skull at the bottom. In order to avoid the skull, the depth of the melt should be limited to a few centimeter in Ti alloys. Therefore the shape of the melt is thin slab-like and the heat conduction problem may be treated as one dimensional problem in the first approximation. Furthermore, the fact that the melt of a large diameter and shallow depth heated by multi-electrodes makes the heat conduction more close to one dimensional problem. Fig. 5 shows a hypothetical situation of the temperature profile of the melt in the arc furnace. In fact, it is anticipated that a freezed layer or mush zone (in alloy case) can develop near the bottom of the melt under the low input power. Simplistic temperature gradient in the melt, is shown in Fig. 5, i.e., a large temperature gradient is expected in solid layer while a small temperature

Chang

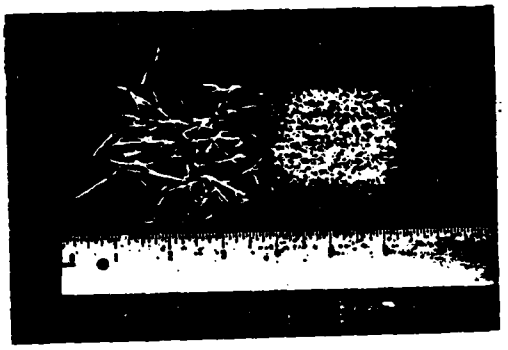

Fig. 6. Melt-spun ribbon of Ti-5Al-5.4Er and its chopped flake

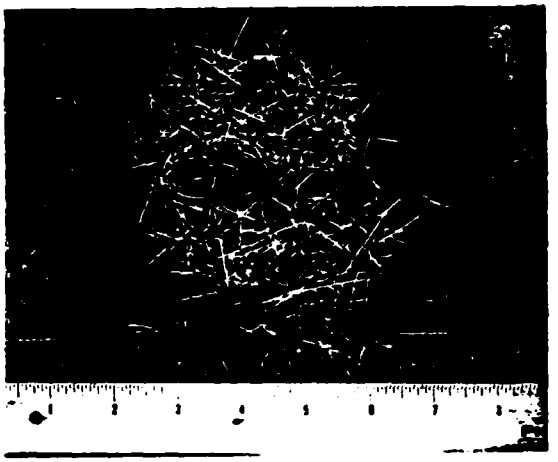

Fig. 7. Melt-spun Mo alloy ribbon

Fig. 8a. Melt-spun Ti-$Zr_{10}Si_6$ ribbon (50x)
Free surface side

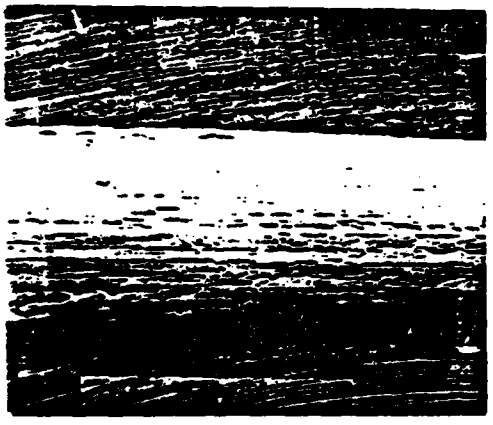

Fig. 8b. Substrate side

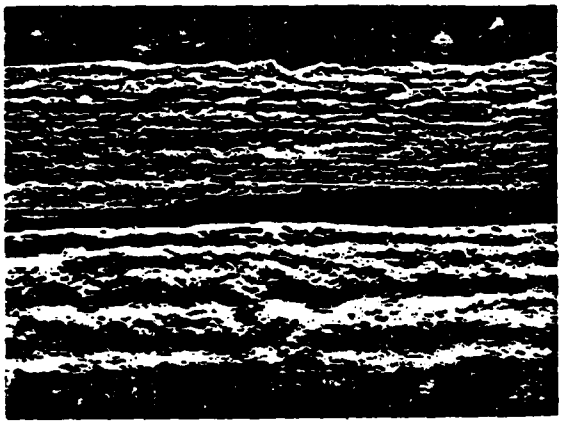

Fig. 9a. Surface topography of Mo alloy ribbon
Top: Substrate side (50x)
Bottom: Free surface side (50x)

Fig. 9b. Substrate side (200x)

Likang

width than that of Ti alloy ribbon. This narrowness of Mo alloy ribbon may be rationalized by the fact that higher surface tension of Mo alloy [9] keeps the melt spreading on the disk.

The surface topography of Ti alloy is shown in Fig. 8a and 8b while that for Mo alloy is in Fig. 9a and b. The substrate side surface of Ti ribbon looks smooth in contrast with that of Mo alloy ribbon where the surface is rough. It appears that a poor wetting exists between the molten Mo and the copper.

Since the ribbon thickness is relatively thin, the estimated average cooling rate reaches larger than 10^8K/sec [10]. As a result, fine microstructure is generated as shown in Fig. 10, in which average dispersoid size is less than 1,000A and the average grain diameter is ~ 10 microns.

CONSOLIDATION - Many hot consolidation techniques are available for Ti ribbon powder. The principles behind the consolidation of RS materials may be said: 1) preservation of refined microstructures from rapid quenching; 2) formation of sound intra particle bond. Consequently, consolidation temperature for RS Ti alloys is approximately 100°C lower than that for conventional consolidation, where a significant microstructure coarsening occurs during the processing. Therefore, for the consolidation of RS Ti and Mo alloy powder, consolidation techniques that allow low temperature compaction and consolidation should be used. Typical examples are HIPing, and possibly Rapid Omnidirectional Compaction (ROC). When the consolidated alloy does not yield satisfactory bond character, low temperature forging or low temperature extrusion may be supplemented. Alternatively, low temperature vacuum hot press may be followed by forging, rolling, or extrusion [11]. By and large, such alloyed powder that has high strength than those of elemental powder requires high pressure for compaction as well as consolidation. Figure 11 shows HIPed Ti alloy exhibiting a full density, which is processed at 850°c, 2.1 GPa, and 3 h.

The microstructues after consolidation were studied by optical as well as TEM. Basically, the average dispersoid size after HIPing remains nearly the same as that in as-quenched ribbon (Fig. 12a) whereas the average grain size increases from 8 to 13 μm in diameter (Fig. 12c) [12]. Also, at this temperature, dislocation network associated with low temperature HIPing is apparent as shown in Fig. 12b.

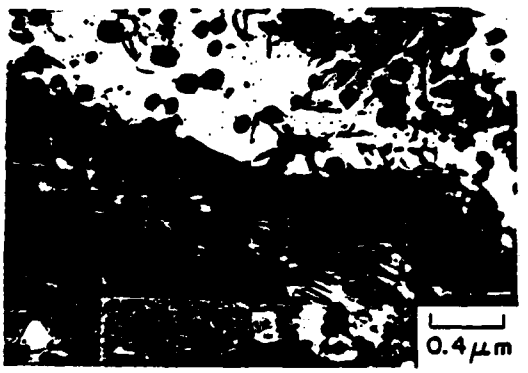

Fig. 10. Microstructures of as-spun Ti-5Al-5.4 Er ribbon

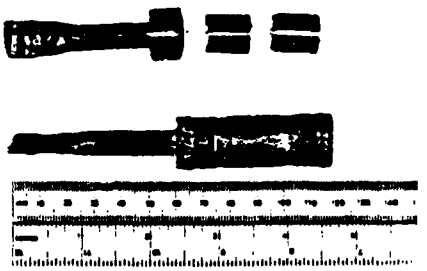

Fig. 11. HIPed Ti alloy from Ti-5Al-4.5La flakes

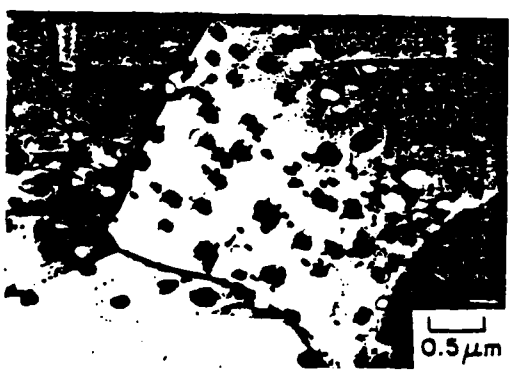

Fig. 12a. Microstructure of HIPed Ti-5Al-4.5La at 850°C/2.1GPa/3h. Uniform dispersoids

Wana

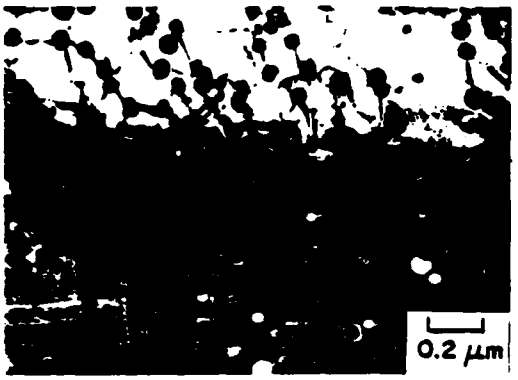

Fig. 12b. Dipersoids coupled with dislocations

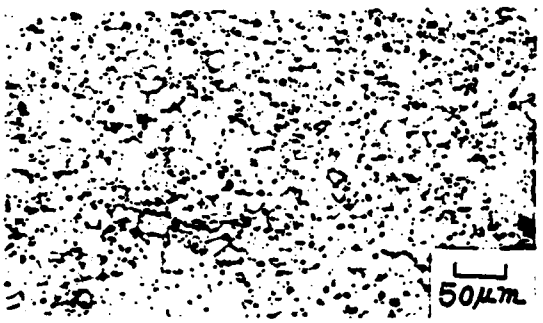

Fig. 12c. Uniform grain size

SUMMARY

1. Melt spinning of Ti and Mo alloys has been successfully performed by arc melt spin process.

2. Restrictive processing parameters for arc melting and casting in the cold copper crucible were studied.

3. These processing parameters include large temperature gradient in the melt, rapid heat extraction through the cold copper crucible and unusually large radiation loss from the melt surface.

4. Very complex temperture profile and fluid flow pattern developes in the continuous arc melting and spinning of Ti and Mo alloys.

5. Microstructure of RS Ti and Mo ribbon processed by this technique undergo extensive refinement, indicating very high cooling rate (10^{5-6} K/sec) involved during solidification.

6. Full consolidation of RS Ti and Mo alloys can be carried out at relatively low temperatures with the aid of high pressure HIPing.

ACKNOWLEDGEMENT

The author gratefully acknowledges the support of the Office of Naval Research for rapidly solidified Ti alloy research. Many thanks are due to Dr. C.S. Chi and Mr. Y.Z. Lu for their assistance in carrying out these experiments.

Contribution #214 from the Barnett Institute.

REFERENCES

1. Proc. 1st and 2nd Int. Conf. on Rapid Solidification Processing, R. Mehrabian, B.H. Kear and M. Cohen, eds., Baton Rouge, Claitor's Publishing Div., 1977 & 1980.

2. M. Cohen, B.H. Kear and R. Mehrabian, Rapid Solidification Processing II, pp. 1-23, Mehrabian, et al. eds., Claitor's Baton Rouge, LA (1980).

3. W.J. Boettinger, Proc. MRS Sym. Vol. 8, pp. 15-31, B.H. Kear, B.C. Giessen, M. Cohen, eds. (1982).

4. S.H. Whang and B.C. Giessen, Proc. Third Conf. Rapid Solidification Processing, pp. 439, R. Mehrabian ed., NBS (1982).

5. S.H. Whang, J. Metals, 36, 34 (1984).

6. C.Y. Ho, P.W. Powell, and P.W. Liley, J. Phy. and Chem. Ref. Data, Vol. 3, 1974 supplement No. 1, Am. Chem. Soc. and Am. Inst. Phy. for Nat. Bur. Stand.

7. H.H. Lieberman and C.D. Graham, IEEE Trans. Magn., Mag-12, 921 (1976).

8. S. Kavesh, in Metallic Glasses, pp. 36-73, J.J. Gilman and H.J. Leamy, ASM, Metals Park, Ohio (1976).

9. Germot Lang, in Handbook of Chem. & Phys., F-32, CRC Press (1980).

10. T.F. Broderick, A.G. Jackson, and F.H. Froes, unpublished research, Materials Laborstories, Wright-Patterson Air Force Base, OH 45433.

11. S.M.L. Sastry, T.C. Peng, and J.E. O'Neal, Proc. Int. Powder Met. Conf. and Exh., Toronto, Canada (June 1984).

12. C.S. Chi and S.H. Whang, Proc. Sym. Rapidly Solidified Materials, S.M.L. Sastry, and Bruce MacDonald, eds., TMS-AIME (Feb. 1985).

FORMATION OF METASTABLE PHASES IN RAPIDLY QUENCHED BINARY Ti ALLOYS

S.H. WHANG and C.S. CHI

Submitted to 1985 Materials Society Meeting on Rapidly Solidified Alloys and Their Mechanical and Magnetic Properties, B.C. Giessen, D.E. Polk and A.I. Taub, to be published.

FORMATION OF METASTABLE PHASES IN RAPIDLY QUENCHED BINARY Ti ALLOYS

S.H. WHANG AND C.S. CHI
Department of Metallurgy & Materials Science
Polytechnic University
333 Jay Street
Brooklyn, New York 11201

ABSTRACT

Rapid quenching of binary Ti alloys from the melt results in various metastable phases. A systematic study has been conducted in order to elucidate principles associated with the formation of metastable phases in binary Ti alloys resulting from rapid quenching. These metastable phases that include α', α'' phases, metastable β phase, and ω phase are discussed with regard to their occurrence and the extension of α phase as a function of cooling rate. Effect of cooling rate and mechanical stress applied during cooling on metastable phase formation was investigated.

INTRODUCTION

When metals and alloys are subjected to rapid quenching from the molten state, various metastable states are introduced in alloy phases and microstructures as well. These metastabilities in rapidly quenched alloys and materials have been well documented in recent years [1].

Metastable phases in binary Ti alloys known as α', α'', metastable β phase and ω phase have been studied in the past [2,3]. All these phases are competing each other in a sense and overlapped compositionally in a narrow range [4,5]. In particular, martensite transformation and occurrence of ω phase can't be separable compositionally while ω phase formation appears to be associated with electronic concentration per atom [6,7].

In recent years, Ti alloys have been routinely processed by rapid solidification techniques at the cooling range of 10^5-10^7 K/sec. The resulting alloy phases increase their meta-stability with increasing cooling rate. It is of interest to understand how further increased cooling rate affects solid solubility of solute, martensite transformation temperature and ω phase formation.

EXPERIMENTS

Splat foils (20um thick uniform) of binary Ti alloys were produced by the hammer-and-anvil technique. Solubility extension, occurrence of ω phase and martensite transformation were studied by varying solute concentration.

In addition, foils of different cooling rates and mechanical stress levels were prepared by varying 1) the hammer pressure; 2) the size of splat alloy piece while alloy composition was kept constant: $Ti_{97.2}Fe_{2.8}$.

These foils were electropolished into thin films for TEM examinations. Alloy phase identification was carried out by bright field micrograph as well as by selected area electron diffraction patterns.

RESULTS AND DISCUSSION

a) Solubility Extension of Solute

Titanium rich terminal compositions of binary Ti alloy systems that can be classified into four different types of phase diagram were investigated as to solid solubility extension in the α phase. The four types of phase diagrams are 1) β-isomorphous; 2) eutectoid type (at β→α transformation); 3) peritectoid type (at β→α transformation); 4) monotectic - peritectic type.

Figure 1 shows TEM micrograph of splat quenched Ti-Mo alloys. These three micrographs reveal three different stages of transformations as a function of concentration. Martensite structure (α', α") are present in both Ti-$Mo_{2.5}$ (Fig. 1a) and Ti-Mo_5 (Fig. 1b). In addition, diffraction patterns of Ti-Mo_5 alloy (Fig. 1b) show the existence of ω and β phases. In contrast, Ti-Mo_{10} alloy reveals both ω and β phases without α', α". These results demonstrate that occurrence of ω phase and martensite transformation compositionally overlap each other.

Solubility extension of α phase in a number of binary Ti alloys at the cooling rate 10^6 K/sec is tabulated in Table 1. Moderate increase in

Table 1**

Type	Alloy System	Max. Eq. Solu. of α	Ext. Sol. of α	Invariant Reaction Pt.
β-Isomorphous	Ti-V	3.5	6	
	-Nb	2.5	5	
	-Ta	2.2	7.5	
	-Mo	0.4	2.0	
Eutectoid	Ti-Cr	0.5	< 5	13.5
	-Mn	0.35	2.5	14.5
	-Fe	0.44	2.5	15
	-Co	0.8	2.5	6
	-Ni		5	
	-Cu	1.2	7.5	5.5
	-Si	0.8	6	1.1
Peritectoid	Ti-C	~ 0.55	10	
	-B	0.43	10	
	-Al	1.5		
	-Ge	2.7	2.5	
	-Sn	9	10	
Monotectic-peritectic	Ti-Y	0.1	~ 1	0.2
	-La	< 1	~ 0.3	~ 1
	-Ce	< 1	~ 0.6	~ 1

** All atomic percent

the solubility is observed in β-isomorphous type system, significant increase in eutectoid type systems and no appreciable increase situation in monotectic-peritectic type systems. There are two different trends in peritectoid type systems, i.e., very large increase in Ti-metalloid solutes (C,B); no

increase in Ti-Ge and -Sn systems. Furthermore, lattice parameter increases with increasing boron concentration in Ti-B systems [8], which indicates interstitial solid solution of boron in Ti lattace. Therefore, it seems obvious that such unusual solubility extension can't be explained by resorting to equilibrium phase diagrams: Ti-B and Ti-C where substitutional solid solution is dominant. In β-isomorphous system, rapid quenching tends to stabilize β phase while supressing α+β decomposition. Hence, the solubility extension appears to occur at the expense of α+β field i.e., α+β field is reduced to a narrow compositional range. Solid solubility extension in monotectic-peritectic systems is not significant, probably due to the large atomic size of rare earth metals and the positive heat of formation.

b) Martensite Transformation and ω Phase Formation

Previous report indicates that martensite transformation temperature in binary Ti alloys does not change with the cooling rate exceeding the critical cooling rate: 32°C/s[9]. In order to elucidate the discontinuity effect of cooling rate on martensite transformation, specimen foils of different cooling rates were prepared and studied by TEM, which are shown in Fig. 2a, b, and c. The alloy produced by the highest cooling rate: 10^6K/sec does not show any martensite transformation(Fig. 2a), but the alloy produced at a half of the highest cooling rate by increasing the alloy thickness to 40 um shows fine martensite structure(Fig. 2b). Furthermore, when the cooling rate is reduced to one third of the highest cooling rate, the martensite structure has fully grown into long rod shape(Fig. 2c). It is interesting to point out that again martensite and ω phase co-exist in Fig. 2b and c. Also, it should be noted that ω phase shown in Fig. 2b is much finer than that in Fig. 2c. In the similar manner, ω phase in Fig. 2a is difficult to identify in contrast to those in Fig. 2b and c. From these observations, it becomes clear that both martensite and ω phase are not truly athermal in Ti-Fe alloy system. Also, the M_s line and lower boundary of ω phase formation can not be separated compositionally as shown in these micrographs.

This circumstance can be visualized in a schematic diagram shown in Fig. 3, in which M_s line may be suppressed by increasing cooling rate from $\sim 10^3$ to $\sim 10^6$. The resulting e/a value for ω phase as well as M_s is shifted to a low value as indicated by a hatched box. This is consistent with non-athermal behavior in Ti-Nb[10]. In fact, various decompositions: $\alpha' \rightarrow \alpha + \beta$; $\alpha'' \rightarrow \alpha''_{lean} + \alpha''_{rich} \rightarrow \alpha+\beta$; metastable $\beta \rightarrow \omega+\beta$ have been observed in Ti-Nb alloy [10,11].

It was reported that ω formation in Ti-10V-2Fe-3Al is triggered by mechanical stress during solidification [12]. It is interesting to see whether ω phase formation is affected by increasing applied pressure during cooling in Ti-Fe alloy, i.e., by increasing the splat hammer pressure. The alloys in Fig. 4a and 4b were produced under different mechanical pressures: 62.5 psi and 200 psi, respectively. Nevertheless, no difference in density and size of ω phase can be found between them. Based on this evidence, ω phase formation in this alloy is not affected by the applied stress of this range.

SUMMARY

1. For a given cooling rate, the solid solubility increase in binary Ti alloys is closely related to the equilibrium phase diagram features. An exception, however, is found in the peritectoid type systems, where the increasing tendency between metal and metalloid solutes is clearly different.

evidenced by lattice parameter increase in Ti-B alloy system.

2. Both martensite transformation and ω phase growth can be suppressed by rapid quenching. This indicates that martensite transformation may not be athermal in a rigorous sense. Also, it is logical to assume that ω phase formation in binary Ti alloys may be suppressed under cluster size by a sufficient cooling rate.

3. No identifiable effect on martensite transformation and ω phase formation is found in the increase in mechanical stress during solidification and cooling.

ACKNOWLEDGEMENT

We gratefully acknowledge the support of Ti alloy program by the Office of Naval Research, Arlington, VA (Contract No. N00014-85-K-0787).

The authors thank Professor Bill Giessen and Barnett Institute, Northeastern University for their support given to titanium research while the authors were members of the Institute. Thanks are due to Mr. Young-Woon Kim for his TEM study on this work.

REFERENCES

1. Proc. 2nd Int. Conf. on Rapidly Quenched Metals, N.J. Grant and Giessen, Eds., MIT Press 1976; Proc. 3rd Int. Conf. on ROM, B. Cantor Ed., The Inst. of Metals, London 1978; Proc. 4th Int. Conf. on ROM, T. Masumoto and K. Suzuki, The Japan Institute of Metals, Sendai, Japan 1981; Proc. 5th Int. Conf. on ROM, S. Steeb and H. Warlimont, Wurzbur, Germany, 1984.

2. J.C. Williams, Titanium Science and Technology, R.I. Jaffee and H.M. Burte, Eds., Pellus Press, New York, 1973, p. 1494.

3. E.W. Collings, The Physical Metallurgy of Titanium Alloys, American Society of Metals, Metals Park, OH 44073, 1984, p. 75.

4. B.S. Hickman, Trans. TMS-AIME, 345, p. 1329-35, 1969.

5. S.L. Sass, J. Less-Common Metals, 28, p. 157-173, 1972.

6. Yu.A. Bagariatskii, G.I. Nosova, and T.V. Tagunova, Transl. Dok. Akad. Nauk., SSSR, 122, p. 593-96, 1958.

7. B.S. Hickman, Met. Trans, 245, p. 1329-1336, 1962.

8. Y.Z. Lu and S.H. Whang, unpublished work.

9. K.S. Jepson, A.R.G. Brown, and J.A. Gray, The Science , Technology and Application of Titanium, R.I. Jaffee and N.E. Promisel, Eds., Pergamon Press, 1970, p. 677-690.

10. H.M. Flower, R. Davis, and D.R.F. West, Titanium and Ti Alloys, Scientific and Technological Aspects, Eds., J.C. Williams and A.F. Belov, Plenum Press, 1982, p. 1703-15.

11. R. Davis, H.M. Flower, and D.R.F. West, Acta Metall, 27, p. 1041-52, 1979.

12. T.W. Duerig, R.M. Middleton, G.T. Terlinde and J.C. Williams, Titanium '80 Science and Technology, H. Kimura and O. Izumi, Eds., The Met. Society of AIME, 1980, p. 1503-12.

Fig. 1a As-quenched Ti-$Mo_{2.5}$ foil: 20μm thick

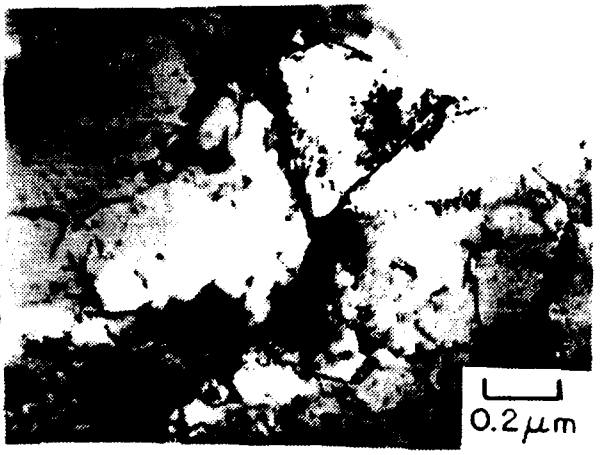

Fig. 2a As-quenched Ti-$Fe_{2.8}$ foil: 20μm thick

Fig. 1b As-quenched Ti-Mo_5 foil: 20μm thick

Fig. 2b As-quenched Ti-$Fe_{2.8}$ foil: 40μm thick

Fig. 1c As-quenched Ti-Mo_{10} foil: 20μm thick

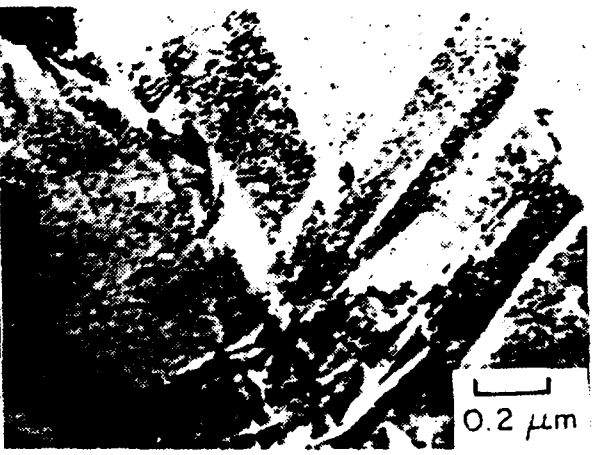

Fig. 2c As-quenched Ti-$Fe_{...8}$ foil: 60μm thick

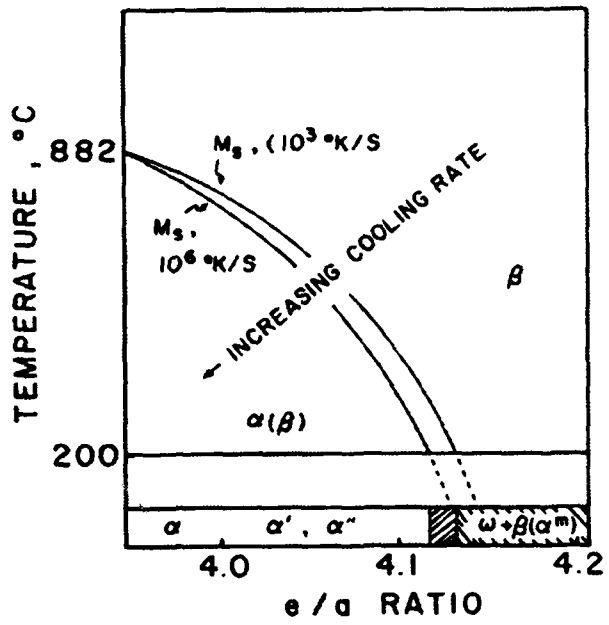

Fig. 3 Schematic Diagram of M_s Temperature as a Function of e/a Ratio.

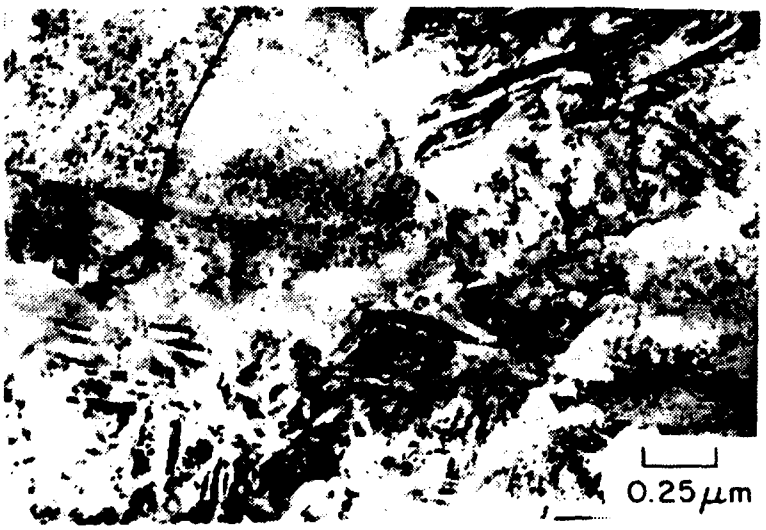

Fig. 4a As-quenched Ti-$Fe_{2.8}$ foil: 30μm thick and 62.5psi Ar pressure for the hammer.

Fig. 4b As-quenched Ti-$Fe_{2.8}$ foil: 32μm thick and 200psi Ar pressure for the hammer.

PARTICLE COARSENING OF RARE EARTH DISPERSOIDS IN Ti-5Sn-R.E.

(R.E. IS 3Y, 4.5La AND 7.5Th)

Y. Z. LU AND B. C. GIESSEN

NORTHEASTERN UNIVERSITY, BOSTON, MA 02115

S. H. WHANG

POLYTECHNIC UNIVERSITY, BROOKLYN, NY 11201

Submitted to 1985 MRS sym on Rapidly Solidified Alloys, B.C. Giessen, D.E. Polk and A.I. Taub eds., Proceedings to be published.

PARTICLE COARSENING OF RARE EARTH DISPERSOIDS IN Ti-5Sn-R.E. SYSTEMS (WHERE R.E. IS 3Y, 4.5La AND 5.4Er.)

Y. Z. Lu, and B. C. Giessen
Barnett Institute
Northeastern University, Boston, MA 02115
S. H. Whang
Department of Metallurgy and Materials Science
Polytechnic University, Brooklyn, New York 11201

INTRODUCTION

The development of Ti alloys has long been relied upon alloying effect and basic microstructural manipulation in the past. The discovery of Ti-6Al-4V was possible in the spirit of such design principle[1].

Nevertheless, in recent years, new approaches that deviate significantly from the conventional design practice have been undertaken to meet requirements for even higher temperature capability of Ti alloys (700-1000°C). One of the approaches is to introduce new coarsening resistant dispersions into Ti matrix through rapid solidification processing[2-5]. By trial and error, it was found that some rare earth metal dispersoids such as La and Er in Ti alloy have excellent coarsening resistance at elevated temperatures (700-900°C) [6,7] whereas rapid coarsening of silicide particles was observed[8]. Although preliminary study on Ostwald ripening behavior of La dispersoids was conducted in the past[6], similar studies on other rare earth dispersoids in Ti have not been performed. As a result, the fundamental understanding of particle coarsening mechanism for rare earth dispersoids in Ti is still lacking.

In this paper, particle coarsening of yttrium dispersoids in Ti-5Sn-3Y system will be discussed.

EXPERIMENTS

For the present experiments, Ti alloy buttons were prepared from pure Ti(99.99%), Sn(99.99%), and rare earth metals(99,9%) by melting repeatedly in an arc furnace under argon gas atmosphere. The oxygen level of Pure Ti used is less than 150 ppm. Small alloy pieces from the alloy button were splat quenched into thin foils by the hammer and anvil technique. Disk shaped specimens of 20 um thick were obtained from the middle section of the foil. For heat treatment, the disks were wrapped with Ta foil and sealed in a quartz tubing with additional Ti folis as getter materials under the vacuum of 10^{-5} torr. The tubings were annealed isothermally at the desired temperatures and durations. In order to identify crystal structures of the dispersoids in the heat treated alloys, carbon extraction replicas were prepared from the annealed foils. These replicas were studied by STEM and electron microprobe to determine the chemical constituents of the particle. The particle size and distribution of the TEM micrographs were studied using image analyzer.

RESULTS AND DISCUSSION

a) Microstructures

As shown in Fig. 1, the microstructure of as-quenched Ti-5Sn-3Y alloy shows 1) a strong grain refinement due to high cooling rate $\sim 10^6$ deg/sec 2) uniform clusters (~50A dia.) in the matrix, which appear to be attributed to the concentration of the rare earth solute exceeding the equilibrium solubility

limit, since no solid solubility extension by rapid solidification is observed in Ti-rare earth metal system [9]. These fine microstructures including fine subgrains disappear in the early stage of isothermal annealing and replaced by large equiaxed grains which contain a lage number of particles. For example, Figure 2 shows such particles in Ti-5Sn-3Y alloy annealed at 840 °C for 74 h.

Extraction replicas of the annealed Ti-5Sn-3Y alloy foil were studied by HB-5 STEM. The EDX spectra indicate that the particle contains Sn and Y (Fig. 3). Additional Cu peak in the spectra is attributed to a copper grid supporting the sample. The weight ratio of Sn vs. Y was calculated using Cliff-Lorimer equation [10]. The calculated ratio is 39%Sn and 61%Y with ±10% uncertainty. Furthermore, the selected diffraction ring patterns agree with those of Mn_5Si_3 ($D8_8$) structure. Hence, it is concluded that the particle is ,in fact, Y_5Sn_3 compound of $D8_8$ structure.

b) Particle Coarsening

Particle distribution in the Ti-5Sn-3Y alloys annealed at 760°C, 120h is shown in Fig. 4 where r and $\bar{r}$ are individual particle radius and average particle radius, respectively. The size distribution of these particles deviates significantly from the LSW model[11,12] in which the particle volume is assumed to be zero. However, the histogram is analogous to that predicted by the D-N-S model[13] where particle coalescence is considered as a mechnism for explaining the volume effect. When the average particle size $\bar{r}$ for Ti-5Sn-3Y system at three different temperatures is plotted against the annealing time(t), non-linear, smooth curves result in as shown in Fig. 5. Furthermore, the best linear correlation was obtained from the plots of the cube of the average particle size vs. time as shown in Fig. 6. This indicates that the coarsening is basically governed by volume diffusion mechanism. Therefore, the coarsening of rare earth particle in the Ti-5Sn-3Y alloy may be expressed by modified LSW model for volume diffusion[13-16], which is given as follows.

$$\bar{r}^3 - \bar{r}_o^3 = f(K,T) \cdot (t - t_o) \qquad (1)$$

with

$$f(K,T) = \frac{8}{9} \cdot \frac{K \cdot C_s(\infty) \cdot D \cdot \gamma \cdot V_m}{R \cdot T} \qquad (1\text{-}1)$$

where

$f(K,T)$ = measured slope of $\bar{r}^3$ in plot of $\bar{r}^3$ vs t

$\bar{r}_o$, $\bar{r}$ = average particle radii for the onset and final states

K = volume fraction factor

$C_s(\infty)$ = equilibrium solubility of solute in the matrix with particles of infinite size at a given temperature T

D = diffusion coefficient of solute, cm^2/sec

γ = interfacial free energy of particle, J/m^2

V_m = gram-molar volume of precipitate, $cm^3/g\text{-mole}$

t_o, t = onset and final annealing time, sec

R = gas constant, J/mole-K

T = absolute annealing temperature, K

the K value for the given volume fraction 1.05 % can be estimated from the various models where the K value varies from 1 to 1.5 depending upon model[13]. For present calculation, we chose K value given by D-N-S model since the histogram of particles in this particular system is very similar to that given by this model.

Also, since the interfacial free energy for rare earth dispersoid is not known, this value simply is assumed as 1 J/m^2 based on various reported values: 0.5 J/m^2 for precipitates in Fe-Cu system[17] and 1.5 J/m^2 for ThO_2[18]. Using these informations, appearent diffusion coefficient can be calculated from the modified LSW relation. The obtained diffusion coefficients and other data are summarized in table 1.

TABLE 1

alloy system	Temp. °C	f(k,T) (m^3/s)	Vol. Frc. %	k*	C_s	V_m (m^3/g-mol)	D (cm^2/s)
Ti-5Sn-3Y	760	0.9×10^{-28}	1.05	1.12	0.0042	1.67×10^{-5}	1.0×10^{-13}
	800	3.7×10^{-28}					4.4×10^{-13}
	840	1.52×10^{-27}					2.0×10^{-12}
Ti-5Sn-4.5La (La_2Sn)	760	1.23×10^{-29}	1.4	1.16	0.0046	2.33×10^{-5}	9.4×10^{-15}
	800	9.39×10^{-29}					7.5×10^{-14}
Ti-5Sn-5.4Er	800	1.8×10^{-28}	1.8				

* : determined by D-N-S model[13].

The apparent diffusion coefficients obtained are believed to be the diffusion coefficients for the rare earth metals in Ti. The reasons for this is as follows. Firstly, there are only two solute species involving particle coarsening in the Ti-5Sn-3Y system, i.e., Sn and Y. In the temperature range of 880-1600°C, diffusion coefficient of Sn is nearly identical to that of self diffusion coefficient of Ti[19]. Under the assumption that the diffusion coefficients of both Ti and Sn in Ti are the same at lower temperature range: 700-900°C and the particle coarsening is primarily controlled by the diffusion of Sn, the actually observed value is smaller than the predicted value (Sn) from above assumptions by four orders of magnitude in Ti-5Sn-4.5La system and by three orders of magnitude in Ti-5Sn-3Y system. Of course, uncertainty in the assumed value of the interfacial energy for the dispersoid is negligible compared to this discrepancy. Secondly, if the apparent diffusion coefficient is truly that of Sn, the obtained coefficients from both Ti-5Sn-4.5La and Ti-5Sn-3Y systems ought to be the same. In fact, they are different as much as an order of magnitude. Hence, it is concluded that the observed diffusion coefficient is that of yttrium in Ti alloy.

When the diffusion coefficient of the rare earth metals is plotted against the reciprocal temperature, the activation energy for the solute diffusion may be obtained from the slope, assuming that an arrhenius type relation is valid for the particular temperature range, i.e.,

$$D = D_o * \exp(-Q/RT)$$

where D, D_o, Q, R, and T are diffusion coefficient of the solute, frequency factor, activation energy, gas constant and absolute temperature, respectively. The obtained activation energy for Y from the linear slope is 343 KJ/mole (82 Kcal/mole). This value is relatively high compared to the activation energy for Ce diffusion in Zr at the temperature range of 880-1600°C :173 KJ/mole (41.4 Kcal/mole)[20]. Dissimilarity between the two cases is that Zr is BCC at these temperatures and Ti is Hex. at the current temperatures investigated. Therefore, a good comparison between the two cases may not be possible for this reason.

SUMMARY

1. The dispersoids in high purity Ti-Sn-R.E. alloy systems were identified as binary rare earth-Sn intermetallic compounds.
2. Particle coarsening of rare earth dispersoids in titanium is controlled primarily by the volume diffusion mechanism.
3. Particle coarsening rate for Y as well as La dispersoids in Ti-Sn is very low. Such a low rate appears to derive from the low diffusion coefficients of the rare earth metals in titanium.
4. Preliminary results show that activation energy for Y in Ti is relatively high at the temperature range of 700 - 900°C. Further measurements are necessary to deduce fundamental understanding of coarsening process for rare earth dispersoids in Ti.

ACKNOWLEDGEMENT

We greatfully acknowledge the support of Naval Research, VA (contract No. N00014-85-K-0787) for rapidly solidified Ti alloy research. The authors thank Barnett Institute of Northeastern University for the continuing support in this areas. One of the authors (S.H.W) owes Mr. Y.D. Hahn for his help during the preparation of this manuscript.

REFERENCES

1. A.E. Gorum and R. Colton, Titanium Science and Technology, 1972, pp. 11-20.
2. S.M.L. Sastry et al, J. Metals, 35, pp. 21-28, 1983.
3. S.H. Whang, J. Metals, 36, pp. 34-40, 1984.
4. S.H. Whang, J. Mat. Sci.(review article), accepted and to appear in early 1986.
5. F.H. Froes, see these proceedings.
6. Y.Z. Lu, C.S. Chi and S.H. Whang, Proc. Fifth Int. Conf. on Rapidly Quenched Metals, S. Steeb and H. Warlimont eds., El Servior Science Publishers B.V., 1985, pp. 949-952.
7. S.M.L. Sastry, P.J. Meschter and J.E. O'Neal, Met. Trans. A, 15, pp. 1451-63, 1984.
8. S.H. Whang, Y.Z. Lu and B.C. Giessen, Proc. MRS Sym.,28, pp. 367-373,

AD-A172 140 ALLOY DEVELOPMENT PROCESSING AND CHARACTERIZATION OF DEVITRIFIED TITANIUM..(U) NORTHEASTERN UNIV BOSTON MA BARNETT INST OF CHEMICAL ANALYSIS.. S H WHANG JAN 86 2\2

UNCLASSIFIED N00014-82-K-0597 F/G 11/6 NL

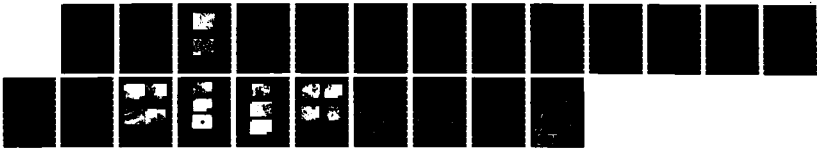

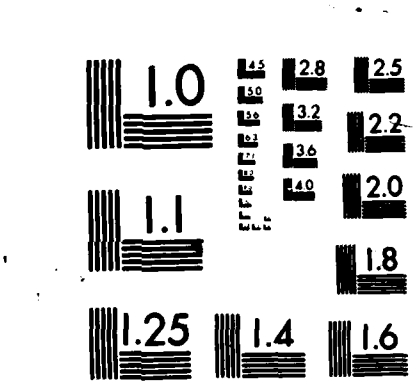
1.0
1.1
1.25
1.4
1.6
1.8
2.0
2.2
2.5
2.8
3.2
3.6
4.0
4.5
5.0
5.6

1984.
9. S.H. whang and C.S. Chi, see these proceedings.
10. G. Cliff and G.W. Lorimer, Proc 5th European Congress on Electron Microscopy, Institute of Physics, Bristol, 1972, p. 140.
11. I.M. Lifshitz and V.V. Slyozov, J. Phys. Chem. Solids, 19, 35, 1961.
12. C. Wagner, Z. Electrochem, 65, 581, 1961.
13. C.K.L. Davies, P. Nash, and R.N. Stevens, Acta Metall., 28, 179-189, 1980.
14. A.J. Ardell, Acta Met., 20, 61, 1972.
15. A.D. Brailsford and P. Wynblatt, Acta Metall., 27, 489, 1979.
16. P.W Voorhees and M.E. Glickman, Met. Trans. A, 15, pp. 1081-88, 1984.
17. C.S. Smith, Metal Interfaces, ASM, Metals Park, Ohio, 1952, p. 65.
18. P.K. Footer and C.B. Alcock, Met. Trans., 3, 2633, 1972.
19. J. Askill and G.B. Gibbs, Phys. Status Solidi., 11, 557, 1965.
20. R.P. Agarwala and A.R. Paul, Int. Conf. on Vacancies and Interstitials in Metals, Julich, 1, 105, 1968.

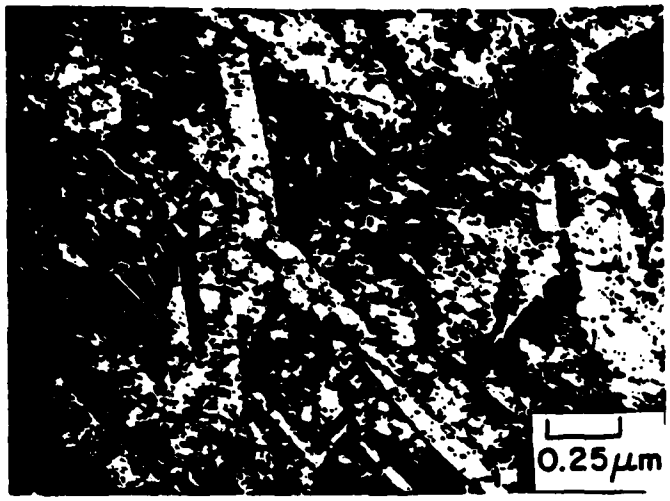

Fig. 1 As-quenched Ti-5Sn-3Y Foil (Bright Field)

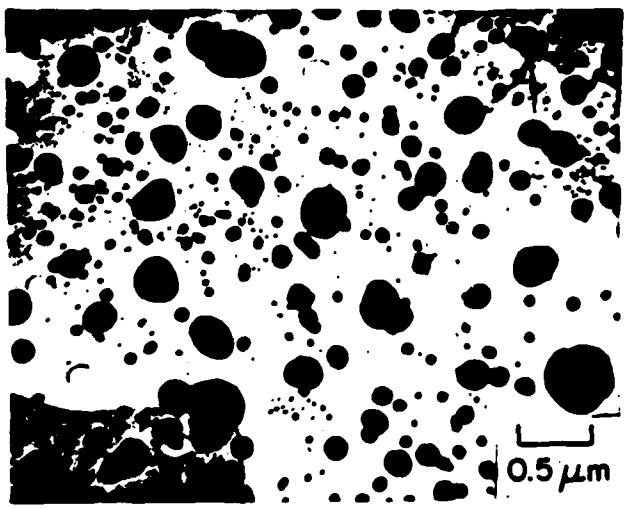

Fig. 2 Annealed Ti-5Sn-3Y Foil 840°C, 70h

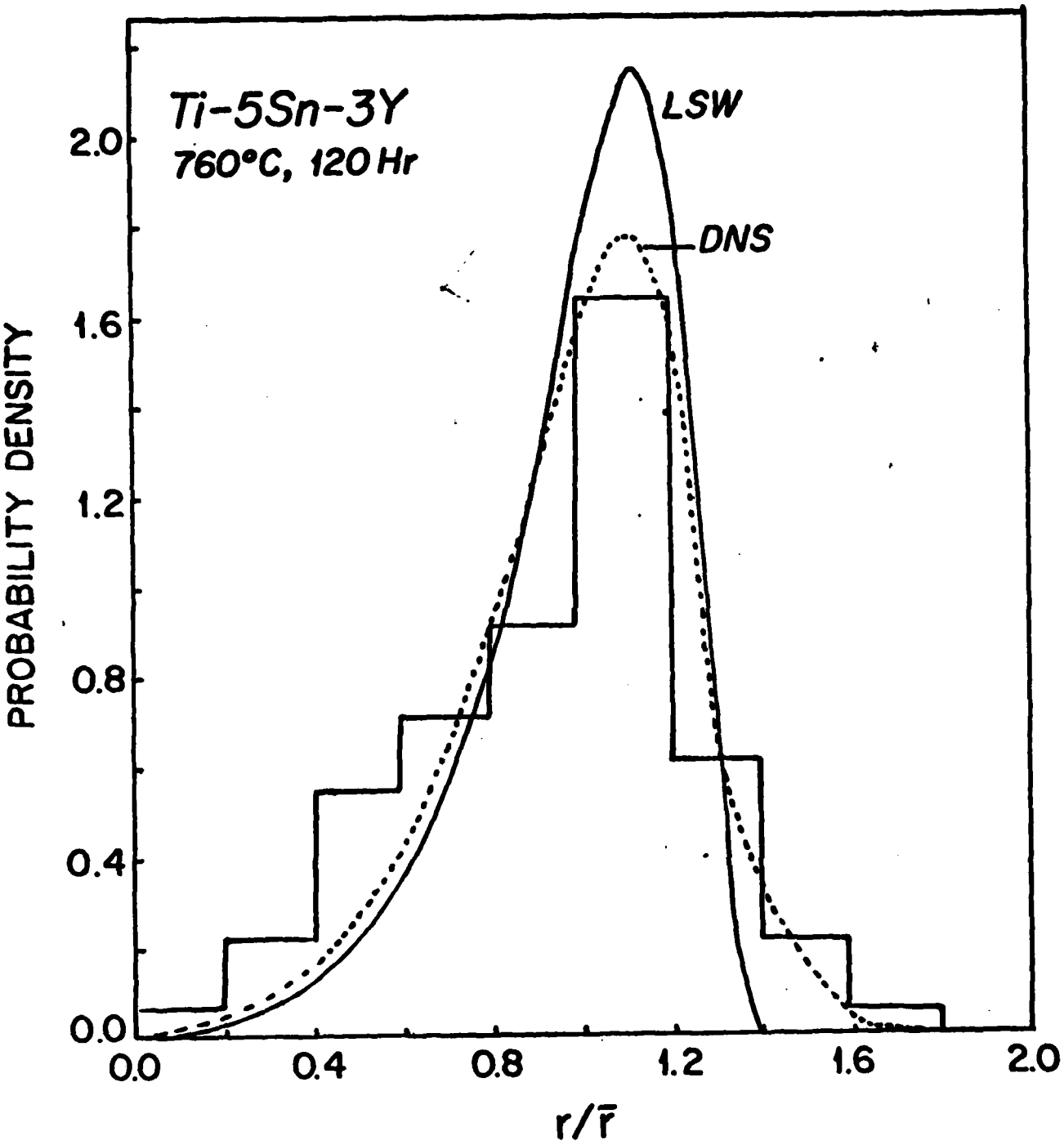
Ti-5Sn-3Y
760°C, 120 Hr
LSW
DNS
PROBABILITY DENSITY
0.0
0.4
0.8
1.2
1.6
2.0
r/r̄

Fig. 4

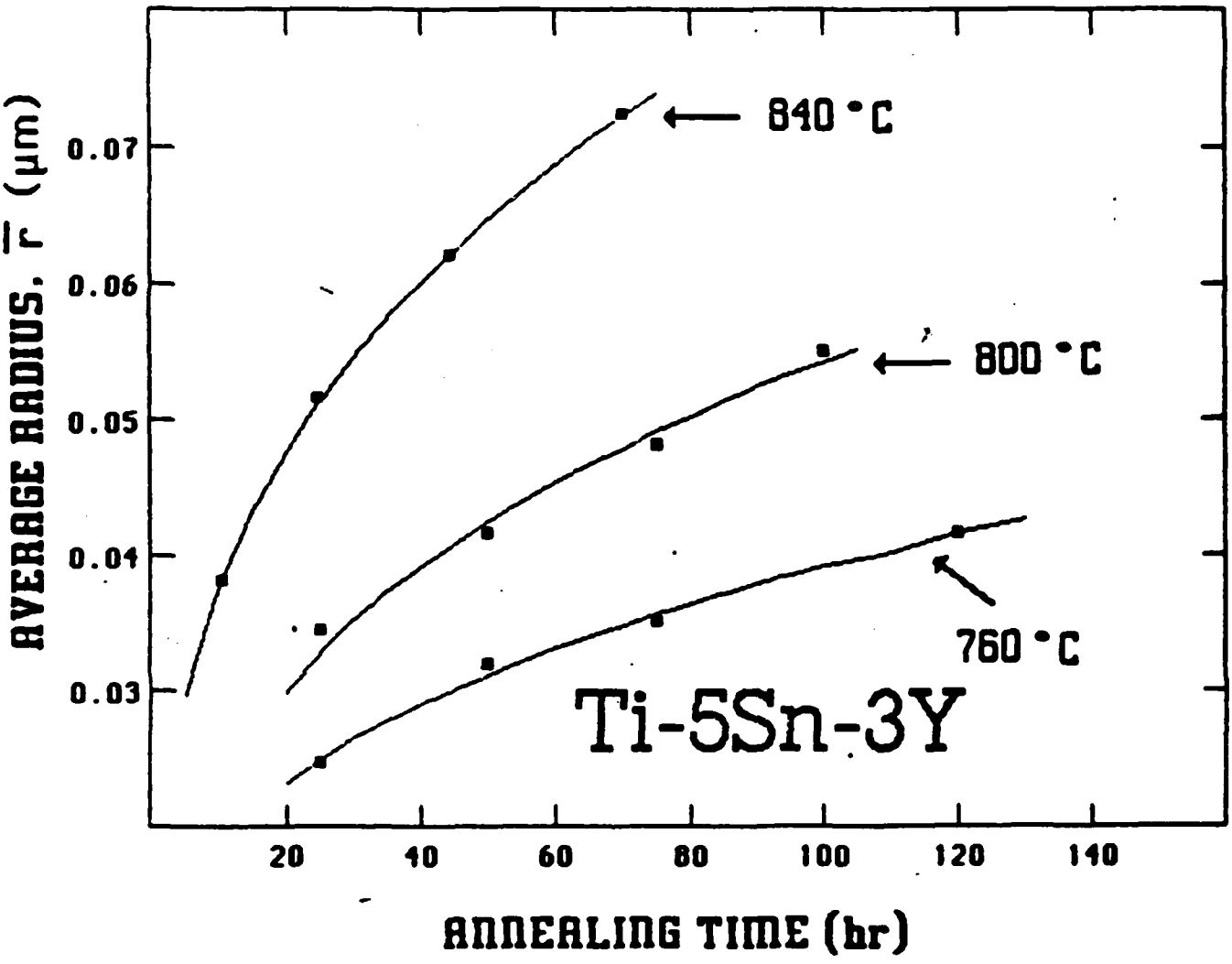
AVERAGE RADIUS, $\bar{r}$ (μm)
0.07
0.06
0.05
0.04
0.03
840 °C
800 °C
760 °C
Ti-5Sn-3Y
20
40
60
80
100
120
140
ANNEALING TIME (hr)

Fig. 5

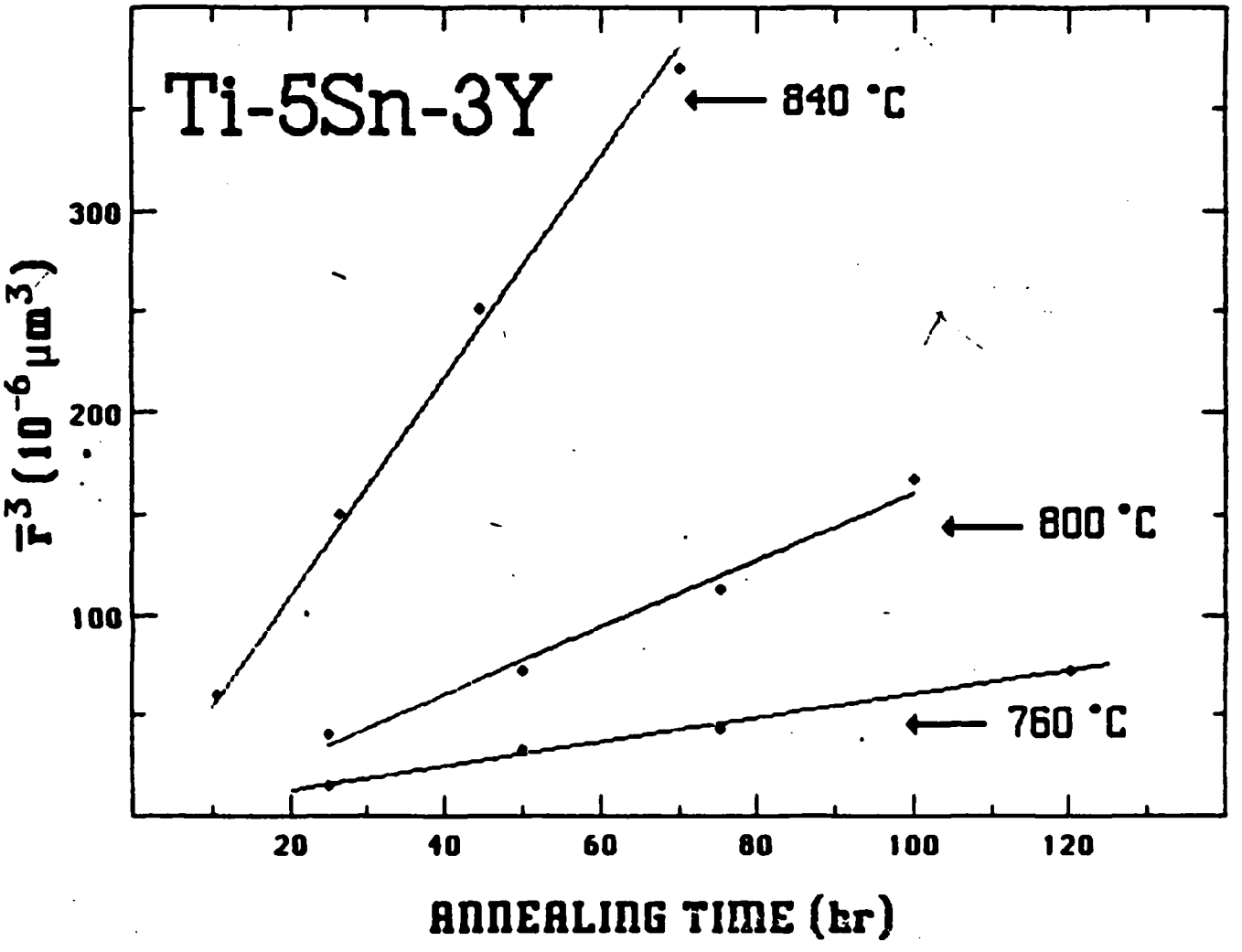
Ti-5Sn-3Y
840 °C
800 °C
760 °C
300
200
100
$\bar{r}^3$ (10^{-6} μm^3)
20
40
60
80
100
120
ANNEALING TIME (hr)

Fig. 6

PROPERTY - STRUCTURE RELATIONSHIP IN RAPIDLY SOLIDIFIED Ti-5Al-M (M IS 2.9 Y AND 7.5 Th)

S. H. WHANG

POLYTECHNIC UNIVERSITY, BROOKLYN, NY 11201

W. W. PARK, P.K. KIM AND D.H. KIM

SEOUL NATIONAL UNIVERSITY, SEOUL, KOREA

To be submitted to Materials Science and Engineering

STRUCTURE-PROPERTY RELATIONSHIP IN RAPIDLY SOLIDIFIED Ti-5Al-M SYSTEMS (WHERE M is 2.9Y AND 7.5Th)

S.H. Whang and Y-D. Hahn
Department of Metallurgy and Materials Science
Polytechnic University, 333 Jay Street, Brooklyn
New York 11201

W.W. Park, P.K. Kim and D.H. Kim
Department of Metallurgical Engineering
Seoul National University, Seoul, Korea

ABSTRACT

Ti-5Al-2.9Y and -7.5Th alloys were rapidly quenched into ribbon by arc melt spinning technique and subsequently the ribbon was consolidated into bulk alloy by HIPing. Microstructures and their stability at high temperature were studied by TEM and optical microscopy. In particular, grain growth and Ostwald Ripening of dispersoids at elevated temperatures were investigated. The results show that significant differences in microstructural coarsening and concurent mechanical responses upon heat treatment exist between the Y and Th containing alloys. In other word, the dispersoid coarsening is higher in Ti-5Al-2.9Y than in the Ti-5Al-7.5Th. Mechnical responses of the heat treated alloys are consistent with the degree of microstructural coarsening in these alloys.

INTRODUCTION

Recent Ti alloy research for high temperature applications has been directed toward two different approaches: Synthesis of high temperature Ti alloys containing stable dispersoids through rapid solidification [1-3] and modified titanium compounds for high temperature applications, in particular titanium aluminides [4,5]. In the first approach, a significant amount of rare earth metals and actinide element (Th) can be incorpo-

rated into Ti matrix through rapid solidification. Such excess amount of the additive elements eventually forms uniform dispersoids upon heat treatment.

These dispersoids are coarsening resistant at elevated temperatures (600-900°C) [6,7]. In addition, the grains of the alloys containing these dipersoids produced by rapid solidification coarsen at a slow rate (i.e., non-parabolic law) at these temperatures than those in pure titanium [8,9]. Strength(microhardness) deterioration of the alloy is found to be correlated with microstructural coarsening [10].

Following previous study on Ti-5Al-5.4La and Ti-5Al-4.5Er [10], a study of property-structure relationship in Ti-5Al-2.9Y and Ti-5Al-7.5Th alloys is discussed in this paper.

EXPERIMENTS

Alloy compositions of Ti-5Al-2.9Y and Ti-5Al-7.5Th were melt-spun by arc melt spinning technique[11,12]. The casted ribbon of ~40um thick were chopped by a rotary cutter into 1-2mm long pieces. This "powder" was consolidated by HIPing at 850°C/2.1GPa/3h.

The consolidated alloys were further heat treated isothermally and isochronally in order to investigate microstructural coarsening and concurent hardness reduction. The sliced alloys were wrapped with Ta foils and sealed in quartz tubings under vacuum before they were charged into the annealing furnace.

Microstructures of precursor as well as consolidated alloys were studied by TEM. The thin folis were prepared by the standard technique using a twin jet polisher.

RESULTS

a) Microstructures

Ribbon alloy shows fine dispersoids and comparatively large grain as shown in Figs. 1a, 1b, 2a and 2b. Yitrium dispersoid in Fig. 1 has a uniform size and distribution whereas thorium dispersoid in Fig. 2b has a bi-modal distribution. No grain boundary prone precipitate was observed in both alloys. Measured average grain size of as-spun Ti-5Al-7.5Th alloy is 5.3um dia., indicating the cooling rate 10^5 K/sec[13], which is lower than that of splat quenched alloy 10^{6-7} K/sec. As shown in Fig. 3a, as-HIPed microstructure of Ti-5Al-2.9Y alloy does not reveal further coarsening during HIPing (850°C, 3h). From the dark field (Fig. 3b) and the spot pattern (Fig. 3c), the structure of the dispersoids can't be determined, though much similarity between these patterns and those of Y_2O_3 was found. Additional spot patterns for other zone axes are needed in order to determine the structure. Bright field micrograph of as-HIPed Ti-5Al-7.5Th show no particle coarsening during HIPing (Fig. 4).

These HIPed alloys were annealed isothermallly at 900°C for 25h, 50h, 75h and 100h, respectively. The grain diameter and particle diameter of the Th containing alloy were measured for each condition and tabulated in Table 1.

TABLE 1 : Grain and dispersoid size in Ti-5Al-7.5Th annealed at 900°C

Annealing Time (h)	Grain Diameter D (um)	Dispersoid Diameter d (Å)
As-HIPed	5.3	800
25	8.4	1200
50	9.1	1600
75	9.9	2100
100	-	2500

Typical grain shape during annealing is shown in Fig. 5a and b where small and large grains are mixed together. Dispersoid size and distribution also are shown in Fig. 6a, b, c and d. No excess distribution of dispersoid at the grain boundary was observed in these micrograghs.

b) Microhardness

Microhardnesses of the two alloys were measured during isochronal annealing at high temperature and after isothermal annealing at room temprature. Both as-HIPed alloys were annealed isothermally at 900°C for 25, 50, 75, and 100h, respectively and their hardnesses were measured at room temperature (Fig. 7). The results show that a small decrease in hardness is observed in Ti-5Al-7.5Th alloy while a very large reduction in hardness occurs within 50h annealing in Ti-5Al-2.9Y alloy. The possible reasons for such a discrepancy between the two systems will be discussed in next section.

On the other hand, in the isochronal annealing, both Y and Th containing alloys show a steep decline in hardness as the temperature rises. The tendency of softening with temperature in the two alloy systems are identical as shown in Fig. 8. Also, a small difference in hardness between the two systems gradually deminishes as the temperature rises. The difference between the isothermal and isochronal annealing is that the former is a long time annealing opposed to the latter, a short time annealing. Therefore, a significant microstructural coarsening is expected in the isothermal annealing whereas no observable coarsening is anticipated in the isochronal annealing. In other word, no measurable softening due to microstructural coarsening can be detected from the isochronal annealing.

DISCUSSION

Bi-modal distribution of dispersed particles is seen in Ti-5Al-7.5Th (Fig. 2b) while no such distribution is identified in splat quenched Ti alloys containing rare earth metals[3]. In order to understand such a bi-modal distribution, the following shouled be investigated. 1. possible different nucleation modes for two different particles - fine and coarse.

For instance, if the particle nucleates in the liquid (molten state) and subsequently coarsens rapidly in the liquid, the resulting particle will have a large size. In contrast, if the particle nucleates at the solid state, where the temperature is low, the coarsening is very limited and the resulting particle size is fine. This argument may be settled when the melt-spun ribbons produced at different initial temperatures are studied.

Grain growth and dispersoid coarsening may be better understood by analyzing the data in table 1. From the plot of the grain diameter vs. time in log normal scale as shown in Fig. 9, the slope ~0.15 was obtained by assuming that the relation $D = Kt^n$ is valid in this range. This value is smaller than that predicted by the parabolic law (n=0.5). The value is compared with those for other alloy systems in table 2.

In the past, a number of theory have been developed to explain non-parabolic grain growth phenomena. One of the approaches is that the impurity in the alloy builds up at grain boundary, which imposes so called impurity-drag effect on grain boundary motion under specific conditions[14]. It has been demonstrated that the theoy can explain grain growth in many pure metals and alloys[15] Also, later, it was shown that the time exponent of the grain growth equation is functions of annealing temperature and concentration of rare earth metals[16].

On the other hand, it was shown by Gladman [17] that a correlation between the grain size and the second phase size exists, indicating a strong interation between them.

The analysis of current experiments in these alloys do not permit to adapt any of these theories since the systems contain impurity as well as second phase. The analysis on the grain growth should be done by a model accommodating the two aspects, i.e., impurity and second phase, based on more rigorous experiments.

TABLE 2. : Time exponent in various Ti alloy systems

Alloy System	Annealing Time	Time Exponent
wt. %	^oC	n

Ti-5Al-7.5Th	900	0.15
Ti-5Al-4.5La	900	0.25[10]
Ti-0.03 Er (at. %)	900	~0.38[16]*
Ti-0.3 Er (at. %)	900	~0.13[16]*
Pure Ti	900	0.33[8,9]

* : extrapolated value from data in ref. 16.

Particle coarsening rate may be determined using the data in table 1 and can be compared with previous results. The plot of d^3 vs. t provide particle coarsening rate, assuming that volume diffusion mechanism is operative. The slope obtained from this plot and the previous values for other alloy systems are listed in table 3.

TABLE 3

System	Dispersoid	Coarsening rate m^3/sec	annealing temperature
Ti-5Al-7.5Th	unknown	$\sim 10^{-27}$	900°C
Ti-5Sn-4.5La	La_2Sn(B82)	9.4×10^{-29}	800°C
Ti-5Sn-2.9Y	Y_5Sn_3(D88)	1.5×10^{-27}	840°C

The coarsening rate (m^3/sec) in Ti-5Al-7.5Th is smaller by orders of magnitude than that of the Y containing system, considering the temperature factor. From this information, it can be concluded that dispersoid coarsening is much faster in Ti-5Al-2.9Y than in Ti-5Al-7.5Th. Hence, after isothermal annealing, a large difference in hardness reduction

between the Y and Th containing systems may be self explanatory.

ACKNOWLEDGEMENT

the authors would like to acknowledge the support of this research by the office of Naval Research, VA (Contract no. N00014-82-K-0597). Also, we would like to thank Dr. C.S. Chi for providing some of TEM micrographs for this paper.

REFERENCE

1. S.M.L. Sastry, T.C. Peng, P.J. Meschter and J.E. O'neal, J. Metals, 36 (9)(1983) p. 21.
2. S.H. Whang, J. Metals, 36 (1984) p.36.
3. S.H. Whang, J. Materials Science (1986) in press.
4. H.A. Lipsitt, Sym. Proceedings of Materials Research Society Meetings, Nov. 1984, Boston, MA, vol. 39, edited by C.C. Koch, C.T. Liu and N.S. Stoloff, Publishers Choice Book Mfg. Co, PA, 1985, p.351.
5. M.J. Blackburn and M.P. Smith U.S. Patent No. 4,294,615 (Oct. 1981).
6. Y.Z. Lu, C.S. Chi and S.H. Whang, Proc. 5th Int. Conf. on Rapidly Quenched Metals, Wurzburg, Germany, Sept. 3-7, 1984, edited by S. Steeb and H. Walimont (Elservier, 1985) p.949.
7. S.M.L. Sastry, P.J. Meschter and J.E. O'Neal, Met. Trans 15A(1984) p.1451.
8. K. Okazaki, M. Momochi and H. Conrad, Titanium Science and Technology 3 (1972) p. 1649.
9. H. Hu and R.S. Cline, Trans AIME 242(1968) p. 1013.
10. C.S. Chi and S.H. Whang, Proc. 1985 TMS-AIME Sym. on Rapid Solidified Materials, edited by S.M.L. Sastry and B. MacDonald, in press.
11. S.H. Whang, C.S. Chi and Y.Z. Lu, Proc. 5th Int. Conf. on Rapid Quenched Metals edited by S. Steeb and H. Walimont (Elsevier, 1985) p.115.
12. S.H. Whang, Proc. ASM conf. on Rapidly Solidified Materials, San Diego, Calif., edited by P.W. Lee and R. Carbonara, Proceedings in press.
13. T.F. Broderick, A.G. Jackson, H. Jones, and F.H. Froes, Met. Trans A. 16A (1985) p.1951.
14. J.W. Cahn, Acta Met., vol. 10 (1962) p. 789.
15. Hsun Hu and B.B. Rath, Met. Trans (1970) p. 3181.
16. B.B. Rath, B.A. MacDonald, S.M.L. Sastry, R.J. Lederich, J.E. O'Neal, C.R. Whitsett, in Titanium '80, vol 2, edited by H. Kimura and O Izumi (AIME 1980) p.1185.
17. T. Gladman, Proc. Roy. Soc., A294 (1966)p.298.

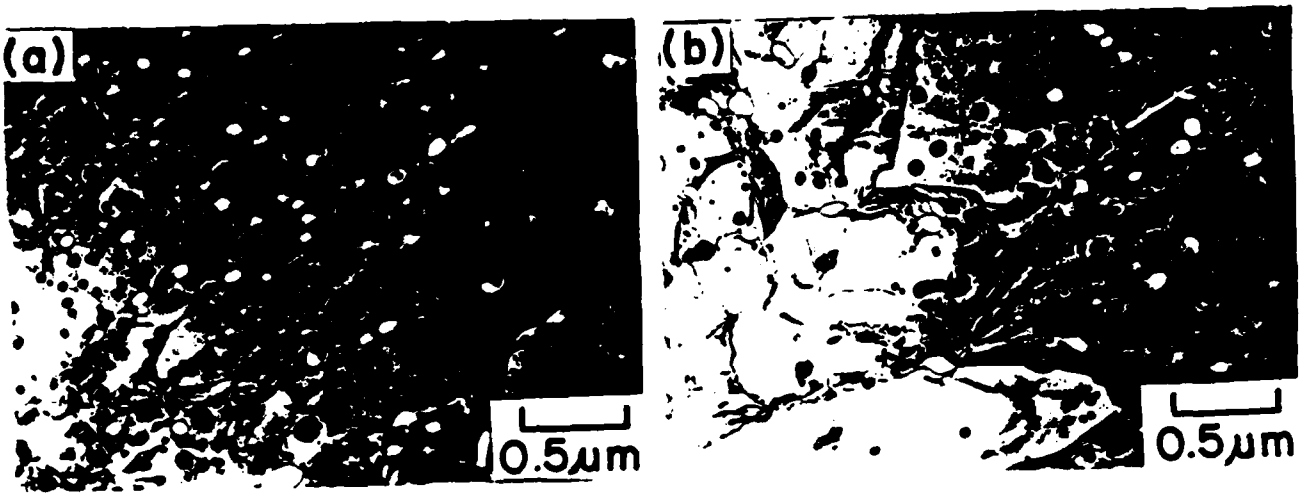

Fig. 1 TEM micrograph of as-spun Ti-5Al-2.9Y

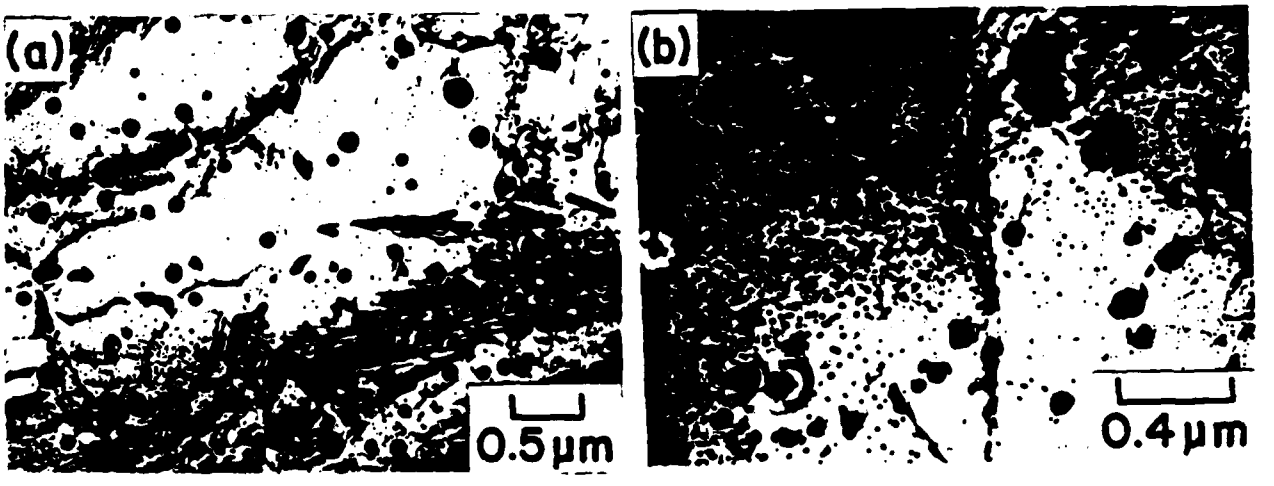

Fig. 2 TEM micrograph of as-spun ribbon of Ti-5Al-2.9Y
(a) inside grain
(b) grain boundary

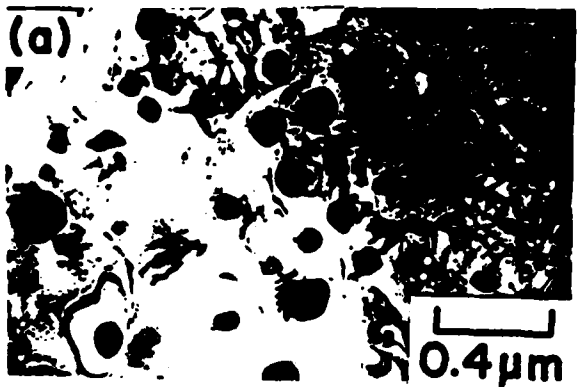

(a)

(b)

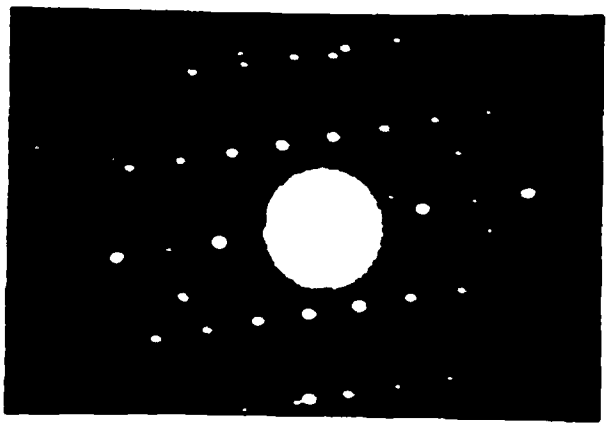

(c)

Fig. 3 As-HIPed Ti-5Al-2.9Y alloy
(a) bright field
(b) dark field
(c) diffraction pattern

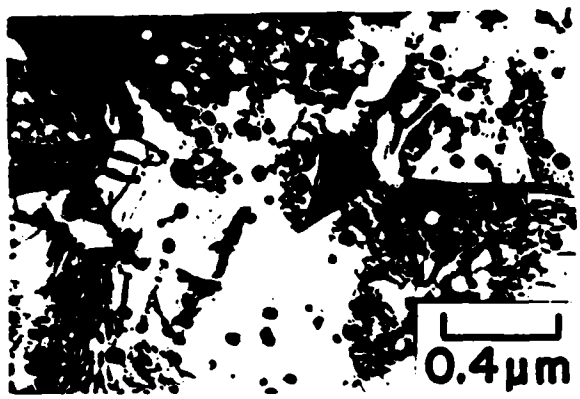

Fig. 4 As-HIPed Ti-5Al-7.5Th alloy (bright field)

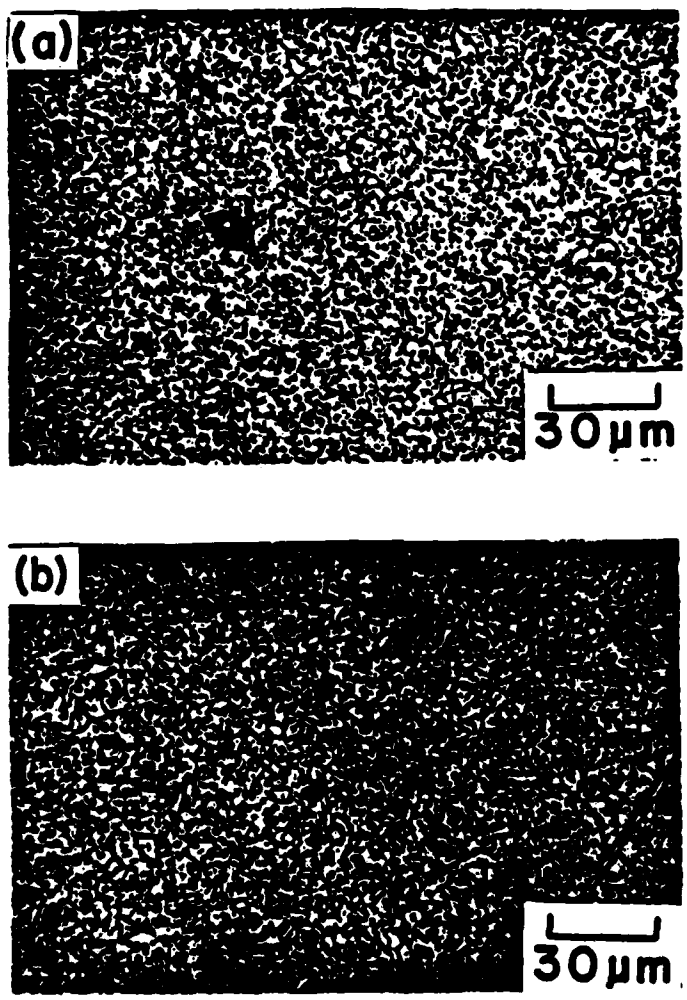

Fig. 5 Optical micrographs of HIPed and heat treated Ti-5Al-7.5Th alloy at 900°C
(a) 25h
(b) 50h

(a)

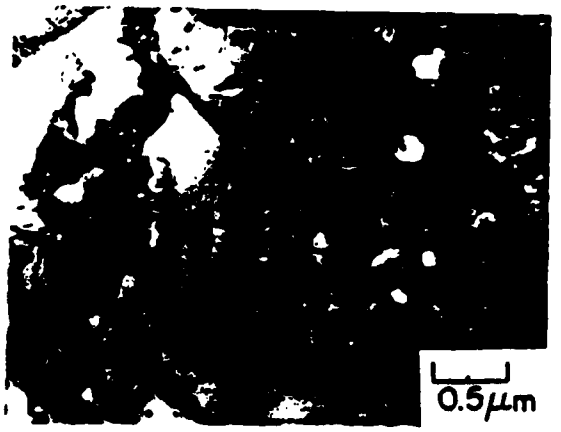

(b)

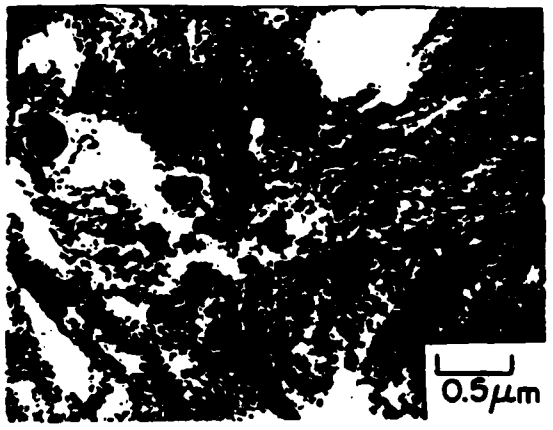

(c)

(d)

Fig. 6 Isothermal annealing of HIPed Ti-5Al-7.5Th at 900°C
(a) no annealing
(b) 25h
(c) 50h
(d) 75h

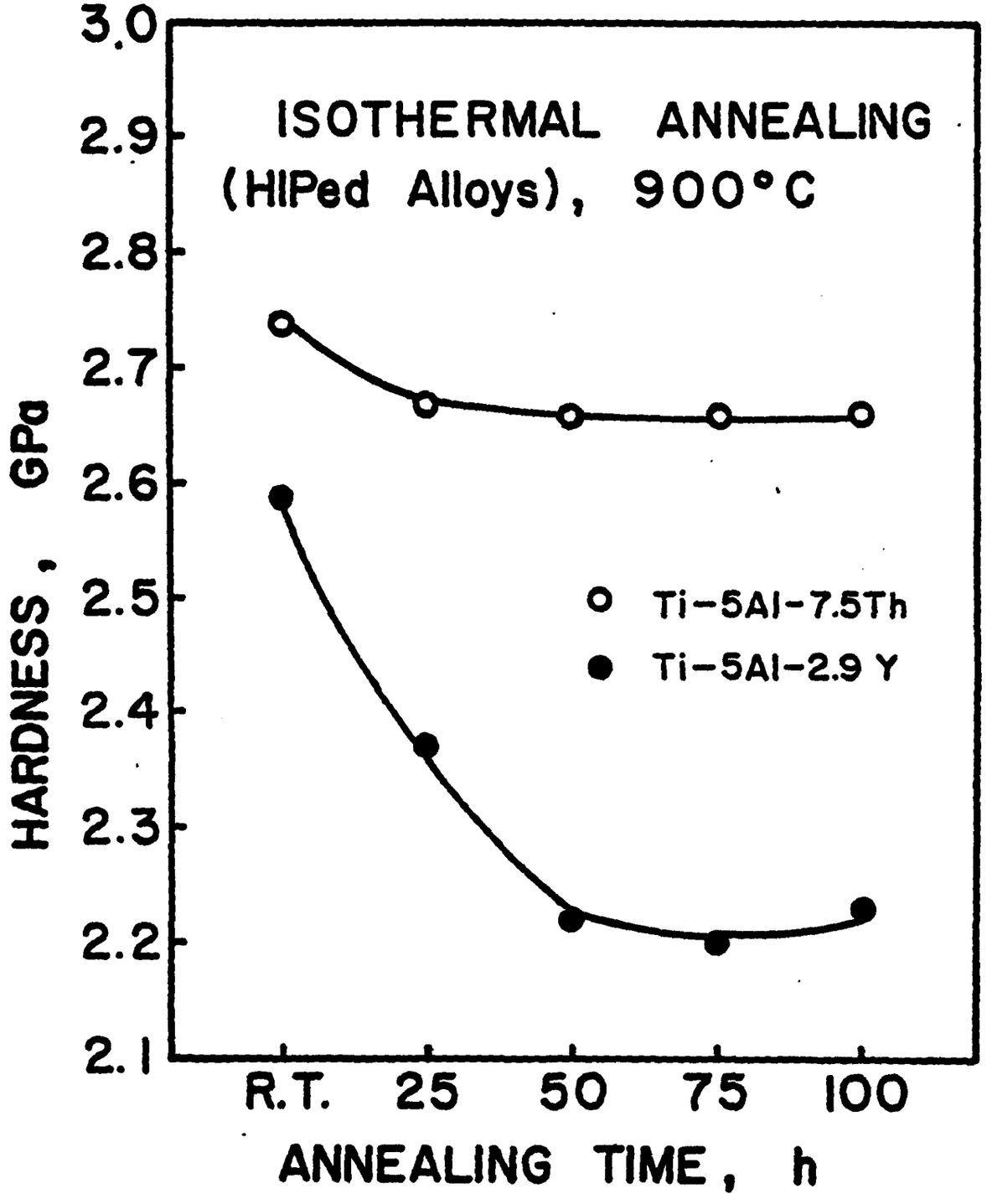
ISOTHERMAL ANNEALING
(HIPed Alloys), 900°C
HARDNESS, GPa
3.0
2.9
2.8
2.7
2.6
2.5
2.4
2.3
2.2
2.1
Ti-5Al-7.5Th
Ti-5Al-2.9 Y
R.T.
25
50
75
100
ANNEALING TIME, h

Fig. 7

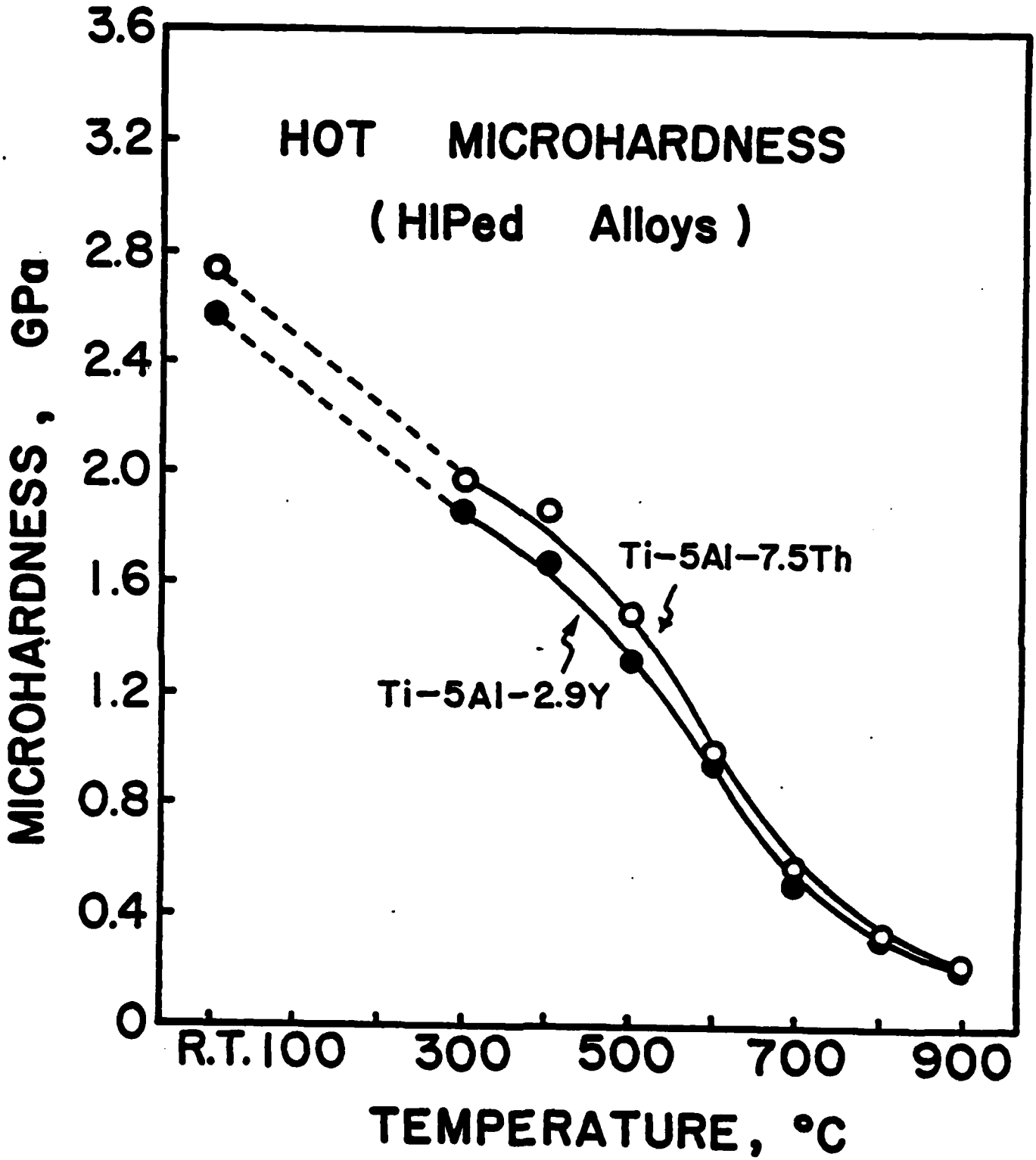
HOT MICROHARDNESS
(HIPed Alloys)
MICROHARDNESS, GPa
3.6
3.2
2.8
2.4
2.0
1.6
1.2
0.8
0.4
0
Ti-5Al-7.5Th
Ti-5Al-2.9Y
R.T.
100
300
500
700
900
TEMPERATURE, °C

Fig. 8

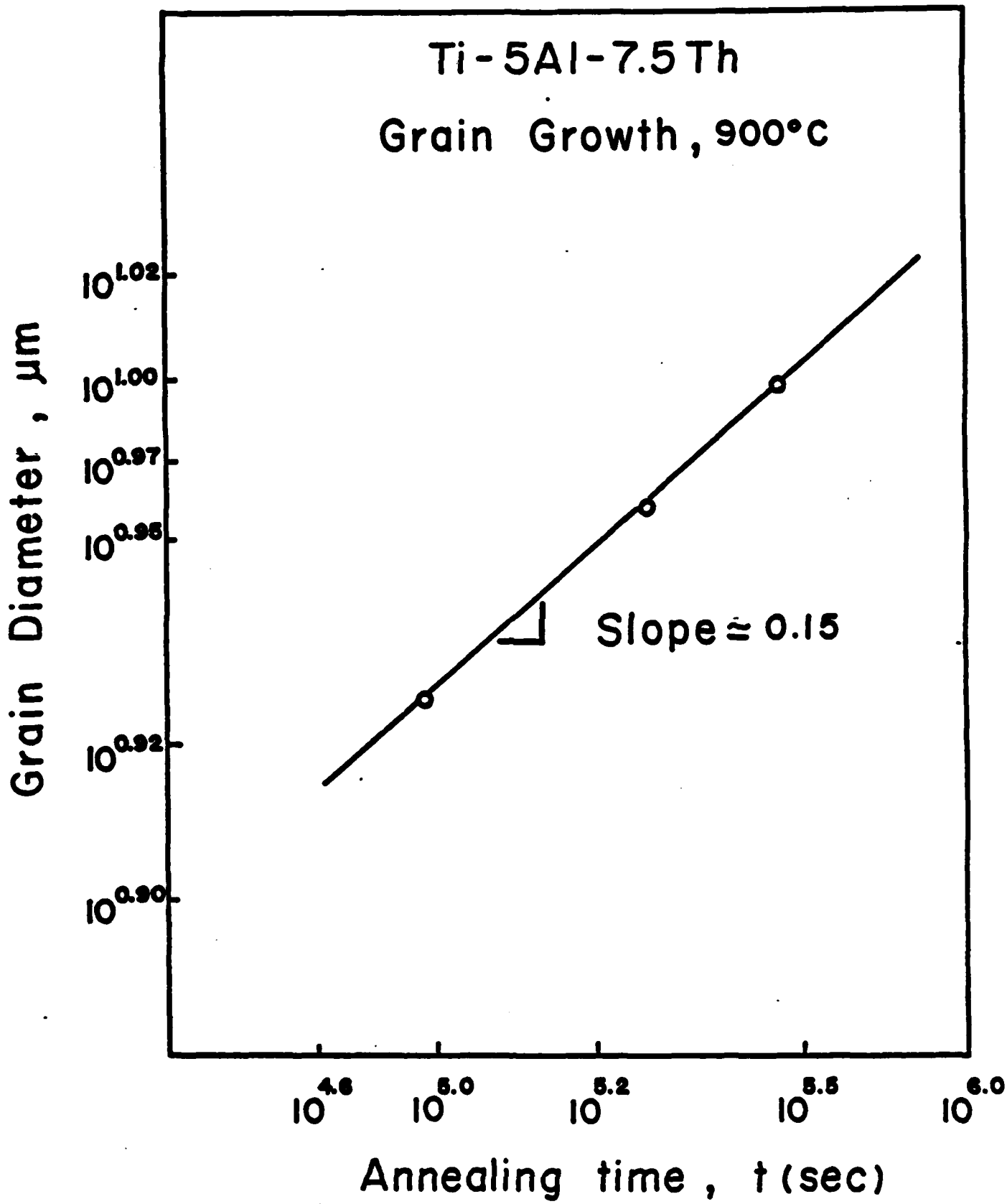
Ti-5Al-7.5Th
Grain Growth, 900°C
Grain Diameter, μm
$10^{1.02}$
$10^{1.00}$
$10^{0.97}$
$10^{0.95}$
$10^{0.92}$
$10^{0.90}$
Slope ≃ 0.15
$10^{4.8}$
$10^{5.0}$
$10^{5.2}$
$10^{5.5}$
$10^{6.0}$
Annealing time, t (sec)

Fig. 9

END

11-86

DTIC